Streamwater transit time distributions at the catchment scale: constraining uncertainties through identification of spatio-temporal controls

Michael Paul Stockinger

Energie & Umwelt / Energy & Environment
Band / Volume 313
ISBN 978-3-95806-131-6

JÜLICH
FORSCHUNGSZENTRUM

Member of the Helmholtz Association

Schriften des Forschungszentrums Jülich
Reihe Energie & Umwelt / Energy & Environment Band / Volume 313

Forschungszentrum Jülich GmbH
Institute of Bio- and Geosciences
Agrosphere (IBG-3)

Streamwater transit time distributions at the catchment scale: constraining uncertainties through identification of spatio-temporal controls

Michael Paul Stockinger

Schriften des Forschungszentrums Jülich
Reihe Energie & Umwelt / Energy & Environment Band / Volume 313

ISSN 1866-1793 ISBN 978-3-95806-131-6

Bibliographic information published by the Deutsche Nationalbibliothek.
The Deutsche Nationalbibliothek lists this publication in the Deutsche
Nationalbibliografie; detailed bibliographic data are available in the
Internet at http://dnb.d-nb.de.

Publisher and Distributor: Forschungszentrum Jülich GmbH
Zentralbibliothek
52425 Jülich
Tel: +49 2461 61-5368
Fax: +49 2461 61-6103
Email: zb-publikation@fz-juelich.de
www.fz-juelich.de/zb

Cover Design: Grafische Medien, Forschungszentrum Jülich GmbH

Printer: Grafische Medien, Forschungszentrum Jülich GmbH

Schriften des Forschungszentrums Jülich
Reihe Energie & Umwelt / Energy & Environment, Band / Volume 313

D 5 (Diss., Bonn, Univ., 2016)

ISSN 1866-1793
ISBN 978-3-95806-131-6

The complete volume is freely available on the Internet on the Jülicher Open Access Server (JuSER)
at www.fz-juelich.de/zb/openaccess.

Zusammenfassung

Niederschlagswasser nimmt auf dem Weg zum Auslass eines Einzugsgebiets sowohl schnelle als auch langsame Fließwege. Kenntnisse über die Verteilung der relevanten Fließwege und der zugehörigen Wassertransportzeiten ist wichtig, da Wasser das Hauptmedium des Schadstofftransports im Boden ist und anthropogene Einflüsse die Hydrologie eines natürlichen Systems drastisch ändern können. Jedoch sind die genauen Prozesse, die den Wassertransport durch ein Einzugsgebiet bestimmen, unbekannt, da derzeit keine Technologie existiert, um den gebietsweiten Wassertransport in-situ zu messen. Deshalb werden konservative Tracer, wie zum Beispiel die stabilen Isotope des Wassers ($\delta^{18}O$ und $\delta^{2}H$), zur Modellierung dieser Transportprozesse verwendet. Mit ihnen wird die Verteilung der Wasserreisezeiten (Transit Time Distribution, TTD) berechnet; eine Modellschätzung, die verschiedene Fließwege von Niederschlagswasser durch ein Einzugsgebiet integriert. Aufgrund unterschiedlicher Unsicherheiten, wie z.B. der Modellstruktur, sind Schätzungen von TTD mit Unsicherheiten behaftet. Deshalb sind die Ergebnisse aktueller Forschungsprojekte, die mit Hilfe der TTD die Hydrologie von Einzugsgebieten erforschen, diese vergleichen oder hydrologische Schätzungen für Einzugsgebiete ohne Abflussstation berechnen wollen, unweigerlich ebenfalls mit Unsicherheiten behaftet.

Das Ziel der vorliegenden Studie ist die Untersuchung raum-zeitlicher Einflüsse auf die Unsicherheiten von TTDs, um schlussendlich die Schätzungen von TTDs zu verbessern. Ein einfaches Konzeptmodell wurde in zwei humiden, klein- bis mittelgroßen Einzugsgebieten angewandt, um die folgenden drei Hypothesen zu untersuchen: (1) die Heterogenität von TTDs in einem kleinen Einzugsgebiet lässt sich mit Hilfe der vorhandenen Bodentypen erklären, (2) Änderungen im Isotopen-Tracersignal, die aufgrund von Interzeption im

Blätterdach hervorgerufen werden, beeinflussen TTD Schätzungen, und (3) eine höhere zeitliche Auflösung von Tracerdaten führt zu veränderten TTDs.

Die Ergebnisse dieser Studie deuten darauf hin, dass die Bodenart tatsächlich als Erklärung für räumliche Muster von TTDs in einem kleinen Einzugsgebiet dienen kann. Somit könnte man diese Information zur Begrenzung von Unsicherheiten z.B. in Einzugsgebieten ohne Abflussstation nutzen. Bei der Ermittlung von TTD in einem bewaldeten Gebiet muss die Interzeption berücksichtigt werden, da dadurch die Unsicherheit in TTDs verringert wird. Außerdem führt eine höhere zeitliche Auflösung der Tracerdaten zu drastisch anderen TTDs. Dies deutet darauf hin, dass die üblicherweise benutzte wöchentliche Auflösung nicht ausreicht, um Fließwege durch ein Einzugsgebiet verstehen zu können.

Die vorliegende Studie ist ein Schritt zur Reduktion der Unsicherheiten von TTD Schätzungen durch die Berücksichtigung von Interzeption und dem Argument für zeitlich höher aufgelöste Tracerdaten. Zukünftige Forschung muss sich auf die Automatisierung von zeitlich hochaufgelösten Probenahme-Systemen konzentrieren, um so die Datenbasis für eine Begrenzung der TTD Unsicherheiten zu schaffen.

Abstract

Precipitation water traveling through a catchment takes faster and slower flow paths to reach the outlet. The knowledge about the distribution of relevant flow paths in a catchment and their respective transit times of water is important when considering that water is the main transportation agent for pollutants and that anthropogenic impacts to natural systems can alter the hydrology dramatically, thus endangering water resources. However, the exact processes governing water transport through a catchment are unknown, as no measurement technology exists to capture them in situ. Tracers such as the stable isotopes of water ($\delta^{18}O$ and $\delta^{2}H$) are used to model these transport processes. The Transit Time Distribution (TTD) is a model estimate that integrates different flow paths of precipitation water through a catchment to the outlet. Due to different sources of uncertainties, e.g., the model structure, the estimates of TTDs are inherently uncertain. The conclusions of present day studies that want to elucidate the hydrological behavior of catchments, compare catchments or predict the hydrology of ungauged catchments from TTDs inherently suffer from these uncertainties.

The aim of this study was to investigate spatiotemporal influences on the uncertainty of TTDs with the overall goal to ensure better estimates of TTDs. A simple, conceptual model was applied to two humid, small to medium scale catchments to investigate three hypothesis: that (1) heterogeneities of TTDs of a small catchment stem from different soil types, (2) canopy-induced changes in the tracer signal of stable isotopes of water due to interception will influence TTD estimates, and (3) a higher temporal resolution of tracer data will lead to differences in TTDs.

The obtained results indicate that the soil types can indeed explain the spatial patterns of TTDs in a small scale catchment and could be used to limit uncertainty in e.g., ungauged

catchments. When calculating TTD for forested catchments, interception must be considered, as it decreases the uncertainty of TTD estimates. Furthermore, a higher temporal resolution of tracer data led to drastically different estimates of TTDs, indicating that the usually applied weekly data is not enough to understand faster flow paths through a catchment.

Thus, this study is a step forward in decreasing uncertainties in TTD estimates by considering canopy interception and arguing for higher resolution tracer data. Future work will have to concentrate on automatization of high-resolution measurements of tracer data to establish the data basis needed for less uncertain TTD estimates.

Contents

List of Figures

Figure II.2 (a) Daily mean runoff (log-transformed, base: 10) against *SWCm* for dry states (red dots) and wet states (blue dots), respectively (dates in Table II.1). Inset shows runoff against *SWCm*. Correlation and 95% confidence interval for dry states (red solid and dashed lines) with Log-Runoff = 0.110 *SWCm* - 5.597 with $R^2 = 0.53$, wet states (blue solid and dashed lines) with Log-Runoff = 0.223 *SWCm* - 9.525 with $R^2 = 0.81$ and both combined (gray solid and dashed lines) with Log-Runoff = 0.187 *SWCm* - 8.173 with $R^2 = 0.88$, all three with significance value $p<10^{-39}$. Outlier values are marked with a black circle. (b) Result of cluster analysis without outliers using the initial assumption of two clusters (red and blue dots).

Figure II.3 Time series (6 June 2009–31 March 2011) of (a) observed (gray line) and simulated runoff (black line) in logarithmic scale, precipitation (black bars from top), stream water sampling times (black crosses) for two summer and two winter seasons, (b) depth-weighted average soil water content *SWCm* and threshold of 35 vol % (dashed line), and (c) isotope data for all stream water locations (gray lines) and precipitation (black line). Black vertical lines in Figures II.3a and II.3b are hydrograph modeling periods based on *SWCm*. As isotope modeling has not been split up, no modeling periods are shown in Figure II.3c.

Figure II.4 Isotopic composition of precipitation (crosses) and Local Meteoric Water Line (LMWL) for the observation period (solid line) compared with the Global Meteoric Water Line [*Craig*, 1961] (GMWL, dashed line). LMWL has an R^2 of 0.98 with $\delta^2H = 7.549\ \delta^{18}O + 9.611$. Stream isotopes samples of all 15 stream locations are slightly shifted from the LMWL (red dots).

Figure II.5 Cumulative RTDs for the dry (black line) and the wet state (gray line) for the outlet of the Wüstebach catchment (location 14). Inset shows details from 0 to 25 days response time.

Figure II.6 Relation between simulation performance (RMSE) of hydrograph simulations for Summer_09 (solid) and Summer_10 (dashed) and variable assumed sizes of the riparian zone area in the Wüstebach catchment (hydrologically active catchment during dry state).

Figure II.7 Stream isotope simulations for (top) location 1 and (bottom) 14. Observed isotope values (gray line with error bars), simulation result with changing active catchment area (black line) and simulation results with 38.5 ha active catchment area throughout the whole modeling period (dashed line). Location 1 with VE = 0.9788 and NSE = 0.74; location 14 with VE = 0.9855 and NSE = 0.34. Mark that strong deviations between observed and simulated values in summer 2009 are most likely caused by missing resolution of precipitation input.

Figure II.8 (a) Cumulative TTDs of all sampling locations (numerals), without subcatchment 7. The red line represents location 14 (outlet). Labels ‘‘Faster than 14’’ and ‘‘Slower than 14’’ indicate two subcatchment groups with shorter (upper group) and longer (lower group) MTTs compared to the outlet. (b) NSE and VE of all model simulations. Subcatchments have been divided in main stream (crosses) with the catchment’s outlet highlighted (red cross), tributaries (triangles), and groundwater-dominated tributaries (circles). Regression line (solid line) with VE = -0.0103 * NSE + 0.989, R^2 of 0.63, significance $p<0.0004$ and the 95% confidence intervals (dashed lines).

Figure II.9 Fast reservoir contribution (ϕ) of the TPLR model for TTDs of all sampling locations (numerals) and the fraction of riparian soils of the respective subcatchments (Riparian), without subcatchment 7. Subcatchments have been divided in main stream (crosses) with the catchment’s outlet highlighted (red cross), tributaries (triangles), and groundwater-dominated tributaries (circles). Thick line is regression line with ϕ = 0.777 Riparian + 0.037, with R^2 = 0.71, significance $p<0.00008$ and the 95% confidence intervals (dashed lines).

Figure A5 a) $\delta^{18}O$ time series of δTF, δOP and δOPcorr used as precipitation isotope input data for estimating TTDs. b) $\delta^{2}H$ time series of δTF and δOP used as precipitation isotope input data for estimating TTDs. Several times samples were frozen (frozen samples).

Figure A6 Linear regression line (black, n = 35) of OP and TF volumes with TF = 0.7667 * OP – 2.976, $R^2 = 0.92$ and $p = 1.10 * 10^{-19}$. The deviation from the 1:1 line (red) is caused by interception evaporation.

Figure A7 Response Time Distributions of the 3 modeling periods (Winter 2012, Summer 2013 and Winter 2013) and, for reasons of comparison, the year before the modeling period of this study (Winter 2011 and Summer 2012).

Figure A8 (a) and (b) stream isotope simulation results for location 1 (spring) and location 14 (outlet) based on $\delta^{2}H$. Observed stream isotopes with grey errors bars compared to simulations using δOP and δTF. Uncertainty boundaries are shown as dashed lines.

Figure A9 TTDs derived by using δOP, δOP_{corr} and δTF isotope tracer data of $\delta^{18}O$ for (a) the spring (location 1) and (b) the outlet (location 14). Uncertainty boundaries are shown as dashed lines. Panel (c) shows absolute differences of cumulative TTDs as a function of transit time.

List of Tables

List of Abbreviations

^{1}H	hydrogen atom with 1 AMU	
^{16}O	oxygen atom with 16 AMU	
^{18}O	oxygen atom with 18 AMU	
^{2}H	hydrogen atom with 2 AMU	
ACO	ant colony optimization	
a_{eff}	effective contributing area	
AMU	atomic mass unit	
API	antecedent precipitation index	
asl	above sea level	
b2	precipitation weighing factor	
b3	initial API	
C	runoff coefficient	
C_{in}	precipitation tracer concentration at time *t*	[‰]
$\delta^{18}O$	ratio of ^{18}O to ^{16}O referenced to VSMOW	[‰]
$\delta^{2}H$	ratio of ^{2}H to ^{1}H referenced to VSMOW	[‰]
D	drying phase	
DM	dispersion model	

DEM	digital elevation model	
d_m	depth of hydrologically active soil	
δOP	isotopic composition of open precipitation	[‰]
δOPcorr	isotopic composition of corrected OP	[‰]
δTF	isotopic composition of throughfall	[‰]
DWD	Deutscher Wetterdienst	
E	exponential model	
EM	expectation-maximization	
EP	exponential piston-flow model	
ET	evapotranspiration	
ϕ	fast reservoir fraction	
FAO	Food and Agriculture Organization	
G	gamma distribution model	
GISP	Greenland ice sheet precipitation	
GMWL	global meteoric water line	
HDPE	high-density polyethylene	
IAEA	International Atomic Energy Agency	
IAHS	International Association of Hydrological Sciences	

IB	Im Brand	
IRMS	isotope-ratio mass spectrometry	
LMWL	local meteoric water line	
MC	Monte Carlo	
MRT	mean response time	[d]
MTT	mean transit time	[d] or [a]
NE	northeast	
NSE	Nash-Sutcliffe efficiency	
OP	open precipitation	
P	precipitation intensity	[mm/h]
p_{eff}	effective precipitation	[mm/h]
PUB	Predictions in Ungauged Basins	
Q	runoff	[mm/h]
RMSE	root mean square error	
RTD	response time distribution	
SLAP2	standard light Antarctic precipitation	
SWC	soil water content	[Vol.%]
$SWCm$	mean soil water content	[Vol.%]
TF	throughfall	

τ_f	residence time of the fast reservoir (TPLR)	[h] or [d]
τ_s	residence time of the slow reservoir (TPLR)	[h] or [d]
TERENO	Terrestrial Environmental Observatories	
TPLR	two parallel linear reservoirs model	
TRANSEP	transfer function hydrograph separation model	
TTD	transit time distribution	
UN	United Nations	
UoT	University of Trier	
VE	volumetric efficiency	
VSMOW	Vienna Standard Mean Ocean Water	
W	wetting-up phase	
WGS84	World Geodetic System 1948	
WU	Wüstebach	
WVER	Wasserverband Eifel-Rur	

I. General Introduction

I.0 Understanding Science

The foremost aim of this work is to communicate science to interested readers. It is not my intention as author to waste my time or the time of the reader with a text that is incomprehensible to non-hydrologists. Thus, it is my goal to explain scientific concepts and ideas in the simplest way possible, sometimes using metaphors. Even readers who are not hydrologists should hopefully be able to understand the basics of this work.

I.1 Catchment Water Transport

Catchments can principally be thought of as a kitchen sink: water from the faucet falling within the area of the sink will eventually reach the drain, while water falling outside of the sink area, i.e., on the floor or worktop, will not reach the drain. Water entering the catchment area of the sink will reach the outlet, which is the drain. Following the drain is a system of pipes designed to transport the water outside the flat to the sewer network. Similar, the outlet of a catchment forms part of a stream.

Leaving this metaphor, catchments are areas of land that route precipitation water (P) to a specific stream location: the outlet. A part of P falling on the catchment area will eventually reach the outlet and then be part of the stream. This part of P is called effective precipitation (p_{eff}) which will be discussed below. For every stream location a unique catchment area can be identified which is done with the underlying assumption that the bedrock is impermeable to P. Often, grid-cell based digital elevation models (DEM) are used and different algorithms applied to the DEM to delineate the catchment boundaries, e.g., *Jenson and Domingue* [1988]. However, this approach cannot detect possible subsurface flows that could cross the catchment boundary in the subsurface and deliver water from outside the surface-derived catchment area. Additional to this, water flowing out of the system as deep groundwater can flow in such a depth that it bypasses rivers [*Goderniaux et al*., 2013]. It is thus invisible to observation of a runoff gauging station of a specific catchment.

Generally, the catchment area grows in size when following the river downstream as more and more land surface area contributes to the stream. For example, the catchment area for the Danube at Vienna is about 103,000 km², while at the end of the stream at the Black Sea it is approximately 817,000 km² [*Rank et al*., 2005].

Not every drop of P falling on a catchment will become runoff (Q) at the outlet. p_{eff} is the part of P actually reaching the outlet to generate runoff. A dominant process in reducing P to *peff* is interception by tree canopies. P gets intercepted by e.g., leaves and subsequently a sometimes large portion of P evaporates, thus being lost to the atmosphere as water vapor [*Gerrits and Savenije*, 2011; *Peng et al.*, 2014]. In the context of this work, 'lost' is used in the sense of 'not generating runoff at the outlet'. Additionally to leaves, below-the-canopy interception occurs on rocks and other non-vegetation surfaces, while the formation of stagnant water pools additionally increases evaporative losses [*Savenije*, 2004].

The remaining p_{eff} then reaches the soil surface. To understand how water reaches the outlet, imagine the soil to be dishes and a sponge lying inside the kitchen sink. In this situation, water from the faucet does not directly hit the metal surface of the sink and flows to the drain. First, it must pass the dishes by using different flow paths that will depend on characteristics of the dishes (size, form, roughness, position and orientation in the sink). Similar to this, the soils of the catchment are not the same everywhere; they are heterogeneous [*Vuurens et al*., 2005]. There are soil areas where water can travel faster and areas that only allow slower water transport. Water must take different flow paths through the soil which consist of matrix and preferential flow, with the latter being orders of magnitude faster in water travel time [*Liu and Lin*, 2015; *Navar et al.*, 1995]. In terms of the kitchen sink, matrix flow relates to slower and faster water transport through the sponge and along dishes, while preferential flow can be expressed as a hole in the sponge. The hole allows for a very quick water transport within the sponge, bypassing the cellulose or plastic polymers sponges consist of. In soils, these holes are called macropores and are the product of roots, animals or the shrinkage of soils which results in cracks [*Beven and Germann*, 2013; *Jost et al*., 2004; *van Schaik et al*., 2014].

Some water of the kitchen sink might get confined in bowls or cups. New water added to the water in the cup mixes with it. From time to time, the water level in the cup reaches its maximum and mixed water gets released to the drain. Generally, however, the cup water is constantly present in the sink, although the degree of filling can vary in time. This part of the water in the soil is temporarily or constantly present and referred to as the passive storage, as it does not actively contribute to runoff generation [*Birkel et al.*, 2011a; *Hrachowitz et al*., 2013a].

Additionally to this, catchments are usually vegetated. Via their roots, plants access the soil water and use it for transpiration, transporting it out of the soil system into the plants transport veins. When compared to evaporation losses of e.g., standing water pools or wet soil surfaces, the transpiration flux dominates, although the exact proportion of transpiration to evaporation are still discussed in scientific literature [*Coenders-Gerrits et al*., 2014; *Jasechko et al*., 2013; *Jasechko et al*., 2014].This water is then additionally lost to the runoff generation process.

Thus, individual water parcels follow different flow paths through the soil or more seldom run off directly on the soil surface [*Horton*, 1933; *Miyata et al.*, 2009]. As the process of surface runoff is assumed to be negligible for the study sites of this work, it will not be further discussed.

The time it takes for a water parcel to reach the outlet, the transit time, depends on the catchment characteristics. These can be e.g., the distance to the outlet, the topography, hydraulic soil properties, groundwater recharge rates and others [*Goderniaux et al*., 2013; *Lyon et al.*, 2010; *Tetzlaff et al.*, 2009a].

Despite this general knowledge about what can potentially influence transit times of water through a catchment, the exact relationships are still unclear [*McDonnell et al.*, 2010]. However, it is important to understand how catchments transport water and what influences

and regulates the transport characteristics of a catchment. First, it should be considered that water transports pollutants through the soil where they could potentially reach the groundwater [*Bachmair et al*., 2009]. Ignoring soil heterogeneities could lead to over- or underpredictions of such solute transports through the soil [*Vuurens et al*., 2005]. Second, different types of land use were shown to have an effect on the provision of water resources [*Garmendia et al*., 2012]. Considering the growing global population and the emerging freshwater crisis [*Srinivasan et al*., 2012], the lack of understanding the effects of land use changes on the water transport properties of a catchment are concerning.

I.2 State of the Art

I.2.1 The Transit Time Distribution

Generally speaking, the transit time distribution (TTD) is a function which is incorporated into a model to mathematically transform water parcels of p_{eff} to become water parcels of Q. It integrates the different flow paths taken by the water parcels, thus characterizing the water transport properties of a catchment. Any mathematical function or model can be applied and many different functions are used in scientific literature, e.g., exponential, linear, piston-flow, dispersion, gamma or two-parallel linear reservoir models [*Timbe et al*., 2014]. It is the a priori choice of the modeler which function to use, although recent model developments are free from this choice by avoiding the concept of a fixed, time-invariant function in favor of a flexible, time-variant TTD [*Heidbüchel et al*., 2012; *Klaus et al*., 2015].

Three fundamentally different TTDs must be considered (Figure I.1, taken from *Botter et al*. [2011]): (a) TTDs conditional on injection time, (b) TTDs conditional on exit time, and (c) the residence time distribution [*Botter et al.*, 2011; *Hrachowitz et al.*, 2013a; *Rinaldo et al.*, 2011]. The TTD conditional on injection time describes the travel of individual P events through the

catchment to the outlet ($p_T(t_T,t_0)$ in Figure I.1). In terms of the kitchen sink, when activating the faucet (i.e., creating a *P* event) part of the water might be soaked up by the dry sponge, while other parts quickly runoff to the drain. Doing this again and creating a second *P* event changes the travel times as the sponge is now pre-wet and transport water more quickly. Thus, these TTDs are conditional on the injection time as they depend on when the *P* event was 'injected' into the catchment and the respective catchment conditions at this time.

The second kind of TTD is conditional on exit time and describes the transit times of water leaving the catchment at a certain point in time ($p'_T(t_R,t)$ in Figure I.1). If we can know the age composition of water at the drain of the kitchen sink, we might find very young water from a recent activation of the faucet, as well as medium age water from the sponge. Additionally, a cup that was filling up over the last days now spills over, delivering very old water to the drain. That is why similar to the first kind, this kind of TTD changes in time and depends on when the water in the stream is observed.

Lastly, the residence time distribution ($p_{RT}(t_R,t)$ in Figure I.1) describes the age distribution of water currently in store in the catchment. In the kitchen sink, it is the age of the water parcels that are currently on-route to the drain, that are stored in the sponge and that are trapped in the cup.

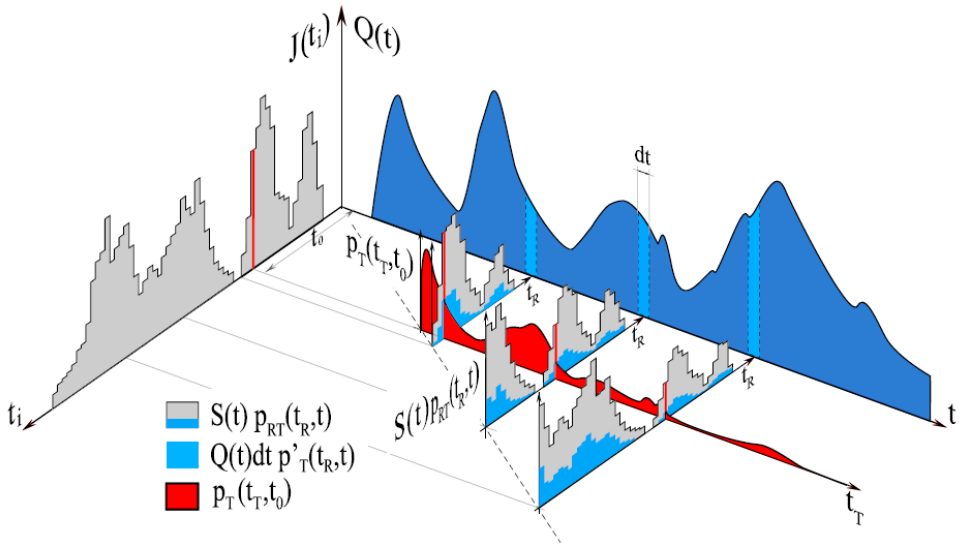

Figure I.1. The three different transit time distributions as described in the text: (1) A single *P* event injected into the catchment at time t_0 (red bar on the rainfall axis $J(t_i)$) and its TTD conditional on injection time $p_T(t_T,t_0)$ as a function of transit time t_T and t_0; (2) The three internal slices depict the water age distribution in the catchment storage at three different times t of the runoff axis Q(t). Each slice represents one instance of the residence time distribution $p_{RT}(t_R,t)$ which is dependent on the residence time t_R and t. Note that the *P* event injected at t_0 is part of the catchment storage (red bars in internal slices); (3) The composition of the water ages in runoff is displayed as cyan bars on the hydrograph of the Q(t) axis. These waters were taken out of the catchment storage S(t) and the respective age distribution is the TTD conditional on exit time $p'_T(t_R,t)$ which is displayed as the cyan part of the internal slices. Note that a certain fraction of *P* has become a part of runoff Q(t) as dictated by $p_T(t_T,t_0)$: the proportion of stored water taken out of the catchment (cyan bar in internal slices) is equal to the $p_T(t_T,t_0)$ for the *P* event for all three internal slices (Figure taken from [*Botter et al*., 2011], Caption according to [*Botter et al*., 2011]).

These distinctions are important as only in the case of a completely mixed and time-invariant system all three TTDs are equal [*Niemi*, 1977]. However, such conditions are rare in catchment hydrology [*Rinaldo et al.*, 2011]. In the context of this work, only the TTD

conditional on exit time will be considered and the term ‘streamwater transit time’ or just ‘TTD’ used for it.

Different in physical meaning but equal in function to a TTD is the response time distribution (RTD). It too describes the transformation of p_{eff} to Q and is a mathematical function incorporated into a model that can take any form. However, while the TTD integrates actual water particles following flow paths, the RTD just integrates the response of Q to P. This does not necessarily mean that the P water particles actually traveled to the stream when considering the RTD. Q could also increase due to a pressure wave propagating through the soil [*Roa-Garcia and Weiler*, 2010]. This can be conceptualized with a U-shape pipe, where one arm of the ‘U’ is longer than the other. The pipe is filled with water up to the brim of the shorter arm. When putting e.g., red-colored water on the side of the longer arm (similar to P), the water level of the shorter arm will overflow the brim, spilling water out of the system (similar to Q). The spilled water will not be the red water, as it cannot travel so fast through the pipe; the increase in Q was triggered by the pressure wave due to the P event of red water. The concept of differently colored water will be useful in the following chapter when discussing the application of tracers to hydrological studies.

A fundamental problem with TTDs is that catchment-wide water transport cannot be measured with current technology [*Rinaldo et al.*, 2011]. The TTDs reported in literature are estimates and not model simulations, as there is no observed TTD to simulate in the first place. These estimates are acquired by inverse modeling, i.e., simulating an observed tracer concentration in the stream [*McGuire and McDonnell*, 2006]. Because of this, TTDs as products of inverse modeling can currently not be verified. There even is a lack of clear concepts in the hydrological community on what to measure to properly characterize flow paths [*McDonnell and Beven*, 2014].

I.2.2 Applying Isotope Hydrology to Estimate TTDs

The stable isotopes of water ($\delta^{18}O$ and $\delta^{2}H$) are a commonly used tracer in estimating TTDs [*Kendall and McDonnell*, 1998]. Isotopes are atoms of the same element but with different atomic mass units (AMU) due to different amounts of neutrons in their nucleus. For example, hydrogen has two stable isotopes: ^{1}H with an AMU of 1 and ^{2}H or Deuterium with an AMU of 2. They are considered stable, as they do not show radioactive decay. Contrary to this, Tritium or ^{3}H is a radioactive isotope of hydrogen.

Isotope hydrology often applies the ratios of the stable isotopes of water $^{2}H/^{1}H$ ($\delta^{2}H$) and $^{18}O/^{16}O$ ($\delta^{18}O$) to study hydrological processes as they are considered conservative tracers. This means that the tracer signal does not change while traveling through the catchment.

Using mass spectrometry [*Gat*, 2010] or laser-based technology [*Gupta and Berman*, 2013], the ratio of heavy to light isotopes is measured and reported as $\delta^{18}O$ and $\delta^{2}H$. These 'δ values' are defined as deviation from an international standard, the Vienna Standard Mean Ocean Water (VSMOW), which was officially defined by the International Atomic Energy Agency (IAEA) of the United Nations (UN) [*Gonfiantini*, 1978].

However, the stable isotopes of water are not fully conservative tracers. During evaporation of water, the remaining water gets enriched (meaning an increase in isotopic value) while the water vapor is depleted. This is due to the differences in mass resulting in a slightly different physical behavior. This is called isotopic fractionation [*Cappa et al.*, 2003].

To estimate TTDs, the stable isotopes of water are used as tracers as they naturally appear in *P* as part of the water molecule H_2O. A commonly used equation to do this is the convolution integral [*Leibundgut et al.*, 1999]. By modeling the observed streamwater isotopes based on the precipitation isotopes, the TTD is estimated:

$$C(t) = \frac{\int_0^t C_{in}(t-\tau)p_{eff}(t-\tau)h(\tau)d\tau}{\int_0^t p_{eff}(t-\tau)h(\tau)d\tau} \quad \text{(I.1)}$$

where $C(t)$ is the streamwater isotope value at time t, $C_{in}(t-\tau)$ the precipitation isotope value at time t with travel time τ and $h(\tau)$ the chosen function for the TTD.

These concepts can be thought of in terms of differently colored water, as mentioned in the previous chapter. If the streamwater would be yellow and blue rain would fall on the catchment, the stream would gradually turn green over time. The speed of this change is determined on how fast *P* travels through the catchment to become *Q*. Similar to this, when the streamwater has a lower isotope value than a *P* event and then it quickly increases, it would indicate a fast transport of *P* water to the stream. The convolution integral estimates what percentage of a *P* event arrives at which time at the outlet, thus estimating the shape of the TTD. The TTD itself is nothing else than a function defining the portions of a *P* event that can be found in the stream at specific transit times.

I.2.3 Uncertainties in TTD Estimation

As already mentioned, TTDs are estimates and cannot be verified currently. They are based on model simulations of observed tracers and are uncertain for several reasons: First, the models themselves are mathematical representations of complex real world systems that were designed based on the modelers understanding of essential system functions. *Beven* [2012] termed the understanding of a modeler about a real world system the 'perceptual model'. The simplification of a real world system inherently carries uncertainties stemming from the structure of the model itself and possible misconceptions about how the real world system works. It was shown that TTDs react sensitive to model assumptions [*Dunn et al.*, 2010]. Thus, the mismatch of complex reality and model simplification induces uncertainty of TTD estimates.

Second, all measured data that are necessary to run the model are imperfect. For example, in rainfall-runoff modeling *P* is an important input variable. However, regionalization and measurement uncertainties affect the runoff simulation and water balance [*Graf et al.*, 2014; *Yoo et al.*, 2012]. Error models of precipitation data can only partly account for this [*McMillan et al.*, 2011]. Knowledge about the individual error sources and their overall influence on modeling results is scarce at best [*Beven*, 2009].

The uncertainty about the validity of TTD estimates and the current lack of technology to measure it are problems for hydrologists trying to understand the still unclear internal catchment processes that govern water transport. For example, *Hrachowitz et al*. [2013a] investigated residence times of different water storages and the age distribution of different flux components of three Scottish catchments. They came to the conclusion that customized model structures have the potential to elucidate catchment transport dynamics. Recently, a study of *Evaristo et al*. [2015] suggested a fundamental change in the hydrological understanding of catchment functioning. Instead of a *P* infiltration front replacing old soil water, thus replenishing the groundwater reservoir, they suggest that groundwater and streamwater stem from a different water storage in the soil than the water used by plants for transpiration. TTDs can only offer insights into the internal mechanisms of a catchment and help clarify these questions if they are as correctly estimated as possible, meaning that uncertainties are kept to a minimum.

I.3 Objectives

This work focuses on investigating spatiotemporal controls of uncertainties in streamwater TTD estimation. In the first study, the small scale heterogeneities of TTDs from several main stream and tributary locations were compared to the in scientific literature usually reported TTD of the outlet only. The spatial controls of the heterogeneous TTDs were investigated.

The aim of the second study was to investigate the effect of in-canopy changes of stable isotope values on the estimation of TTDs. The third and final study investigated TTDs derived from different temporal resolutions of isotope tracer data. The first two studies were conducted in the forested Wüstebach catchment, while the third study was conducted in the higher order Erkensruhr catchment (see appropriate chapters for site descriptions).

The different studies investigated the following hypotheses:

(i) **A headwater catchment will show heterogeneities in TTDs along its stream network. As most catchment characteristics are homogeneous for the study site, the spatially differing soil types are the source of the varying TTDs.**

Weekly stable isotope measurements of 15 stream and tributary locations were used to estimate TTDs for these locations. The necessity of knowing effective precipitation for all these locations to estimate TTDs was negligible due to the small catchment size and uniform land cover with spruce trees. Thus, a uniform p_{eff} distribution was assumed. The ratio of well-saturated to less saturated soils and the subcatchment area were used to elucidate the spatial control of soil types on the respective subcatchment TTDs.

(ii) **The estimates of TTDs of forested catchments are affected by canopy-induced stable isotope tracer changes. Open precipitation or above canopy isotope data is not sufficient to properly characterize these TTDs.**

Water samples of open precipitation and throughfall from a coniferous forest were collected and analyzed for stable isotopes. They were used as model input data for TTDs estimation and differences were evaluated by comparison of TTD quantiles of $\delta^{18}O$ and $\delta^{2}H$.

(iii) The estimates of TTDs are affected by the temporal resolution of stable isotope data.

Two temporal resolutions (weekly and daily to subdaily) for both streamwater and precipitation stable isotope tracer data were applied to estimate TTDs. The effect of using a higher temporal resolution was evaluated by comparison of (a) streamwater isotope simulation results, and (b) estimated TTDs.

II. Seasonal soil moisture patterns: Controlling transit time distributions in a forested headwater catchment

Modified on the basis of

Stockinger, M. P., H. R. Bogena, A. Lücke, B. Diekkrüger, M. Weiler, and H. Vereecken (2014), Seasonal soil moisture patterns: Controlling transit time distributions in a forested headwater catchment, Water Resour Res, 50(6), 5270-5289.

II.1 Introduction

The distribution of transit times of precipitation (Transit Time Distribution, TTD) and its average travel time (Mean Transit Time, MTT) through a catchment to the outlet have been used in hydrological studies to investigate catchments in terms of e.g. flow paths [*Pearce et al.*, 1986] and storage [*Maloszewski et al.*, 1992; *Soulsby et al.*, 2009]. Since the TTD integrates different water transport mechanisms (e.g. overland flow, preferential flow, laminar sub-surface flow, and ground water flow) that are controlled by catchment characteristics such as geology, land-use, soil properties, and topography, dominant characteristics controlling runoff generation can theoretically be identified by comparison of respective TTDs. Such knowledge of the specific relation between the TTD and catchment characteristics becomes important when considering that catchment-wide water transport to the outlet has important implications for the catchment's sensitivity to anthropogenic influences, such as surface and groundwater pollution or land use change [*McGuire and McDonnell*, 2006]. However, the relation between catchment properties and TTDs is difficult to define because of catchment-specific heterogeneities and the lack of observational data with a high spatial and temporal resolution [*Tetzlaff et al.*, 2008]. Furthermore, no method exists to directly measure catchment-wide water transport, making it difficult to verify or falsify results gained from inversely modeled TTDs.

Often the stable isotopes of water (δ^2H and $\delta^{18}O$) are used as tracers in precipitation and runoff to derive TTDs. Usually, a highly-variable precipitation tracer signal is time-shifted and attenuated by a transformation function (the TTD) to a less-variable runoff tracer signal.

In recent years, many studies have investigated the relationship between TTDs and catchment characteristics via different modeling approaches in several geographic and climatological settings. For instance, *Herrmann et al.* [1999] found that low permeability of bedrock and

assumed average flow path lengths influence MTTs, with smaller subcatchments showing shorter transit times in a deep-soiled, wet mountainous catchment. For catchments with well-drained, shallow soils, *McGuire et al.* [2005] found no direct relationship between catchment size and MTT and indicated that rather flow path characteristics than catchment size have a significant influence on TTDs. They found a decrease of transit times with increasing flow path gradient and an increase in transit times with increasing flow path length. In similar conditions, *Asano and Uchida* [2012] were able to link spatial differences in base flow MTTs to the depth of the hydrologically active soil (d_m) and bedrock for mountainous catchments with shallow soils. They argue that contrasting relationships of topographic indices and MTT found in previous studies (e.g. *McGuire et al.* [2005], *Rodgers et al.* [2005], *Tetzlaff et al.* [2009b]) could be a result of d_m being not always linked to topography. Even at sites where topography and d_m are related to each other, they argue that the relationship should vary across different sites.

The relationship between the ratio of riparian to hillslope zone surface area and water and solute transport have been investigated by *McGlynn and Seibert* [2003] in headwater catchments. They argue that headwater catchments are influenced by riparian zones, because they can efficiently buffer hillslope-generated runoff. However, the capacity of the riparian zone to buffer water and solute transport may become negligible in case of large catchments. To compare different geographical regions and their effects on the control of topography on TTDs, *Tetzlaff et al.* [2009b] investigated 55 catchments in different geographical settings by comparing topographic indices such as distance from stream or average gradient derived from a Digital Elevation Model (DEM) to a proxy of TTD (ratio of standard deviation of a tracer signal in stream water to the standard deviation of the tracer signal in precipitation). They found that the controls of the investigated topographic indices on TTDs vary among different geomorphological regions, including glaciated steep mountainous and hilly, forested

catchments. These studies demonstrate that transferring knowledge from one catchment to another catchment as well as hydrological catchment classification are complex tasks that sometimes require detailed knowledge of a catchment's characteristics. Further complications in finding controlling factors for TTDs may arise due to the assumptions of linearity and stationarity of TTDs [*Rinaldo et al.*, 2011] and uncertainties in input data and models.

Identifying links between TTDs and changes in catchment characteristics is even more challenging, e.g. in case of catchments which are strongly influenced by groundwater and as a consequence, usually are characterized by longer transit times, e.g. *Stewart and Fahey* [2010]. They showed that shallow aquifers and deep aquifers within the bedrock were controlling the TTDs, while the afforestation of the modeled catchment in the 1980s had not yet affected deep storage flow in 2009.

The difficulties and ambiguities in identifying the relative effect of catchment characteristic on TTDs of catchments of a wide variety of geographical and climatological conditions were summarized by *Hrachowitz et al.* [2009a]. They used long-term data sets in 20 different headwater-catchments, ranging from <1 to 35 km² in size, and found that no single dominant catchment characteristic controlled TTDs. Rather an ensemble of soil cover, precipitation patterns, stream structure and topography worked well in estimating TTDs in a multiple regression model.

This and previous studies focused either on topography-derived measures or spatiotemporally limited measurements to explain possible mechanisms that had influenced obtained TTD results. What is currently lacking in hydrology are studies that allow hypothesis about the relation of catchment characteristics and TTDs based on high-resolution spatiotemporal measurements, constraining possible solutions to the question why these results have been obtained *McDonnell et al.* [2010].

In this study, we used data from a high-resolution spatiotemporal measurement network to investigate the spatial pattern of TTDs of ungauged subcatchments of the mountainous, forested Wüstebach headwater catchment (38.5 ha) and one tributary catchment (11 ha). We then compared the TTDs to subcatchment characteristics (size and riparian zone area). Therefore, the objectives of this study were

(1) to derive an approach to determine subcatchment TTDs of ungauged stream locations,
(2) to investigate spatial variability of TTDs within the catchment,
(3) to use the available dense soil moisture measurement network to explain spatial patterns of TTDs.

II.2 Study Site

II.2.1 The Wüstebach Headwater Catchment

The Wüstebach headwater catchment (38.5 ha) is located in the humid temperate climatic zone with a mean annual precipitation of 1107 mm (1961–1990) and a mean annual temperature of 7°C [*Zacharias et al*., 2011]. Note that in *Bogena et al.* [2010] and subsequent publications, e.g. [*Rosenbaum et al.*, 2012], the catchment size is given as 27 ha. This difference is the result of using a new DEM in this study, with a resolution of 1 m (before: 10 m). Based on this new DEM, we added an area south of a federal road as part of the catchment, increasing its size to 38.5 ha (see also *Graf et al.* [2014]).

The catchment is located in the low mountain reaches of Western Germany (50° 30´ 16´´N, 6° 20´ 00´´E, WGS84) at about 595 to 628 m above sea level (asl.). The Wüstebach site is part of the Lower Rhine/Eifel Observatory of the Terrestrial Environmental Observatories (TERENO) network [*Zacharias et al.*, 2011]. It belongs to the Eifel national park and is dominantly covered by Norway spruce (*Picea abies*) and Sitka spruce (*Picea sitchensis*) [*Etmann*, 2009].

The bedrock consists of Devonian shales with sporadic inclusions of sandstone [*Richter*, 2008]. It is covered by two periglacial layers: a 'top layer' with a mean depth of about 50 cm throughout most of the catchment [*Borchardt*, 2012] and a 'base layer' of varying depths (50 – 150 cm). The base layer has a higher bulk density and thus lower hydraulic conductivity than the top layer [*Borchardt*, 2012]. Soil depths in these periglacial layers range from less than one meter to a maximum of 2 meters with an average depth of 1.6 m [*Graf et al.*, 2014]. Food and Agriculture Organization (FAO) soil types of cambisol and planosol/cambisol are dominantly found on the hillslopes while gleysols, histosols and planosols are found in the riparian zone.

We additionally investigated a smaller tributary-catchment (11 ha, not included in the 38.5 ha) situated north-east of the Wüstebach test site, which is also part of the weekly sampling campaign described in Section II.2.2. This subcatchment drains into the Wüstebach a few meters downstream of the catchment's outlet (Figure II.1).

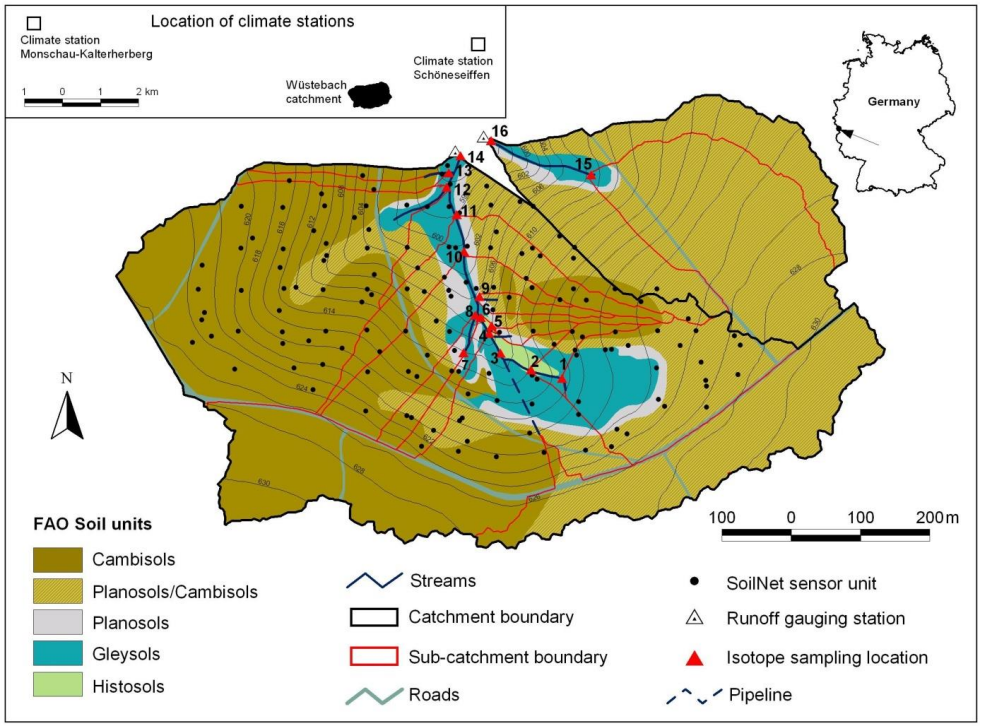

Figure II.1. Map of the 38.5 ha Wüstebach headwater catchment (outlet: location 14), with the smaller 11 ha tributary catchment (outlet: location 16) adjacent to the north-east. Displayed are FAO soil units, isolines and stream/tributary locations for water sampling (numerals). Due to constantly low-water levels, we were not able to use location 7 for this study. Runoff gauging stations are marked with open triangles. Black dots mark SoilNet sensor units for soil moisture measurements. Subcatchments of each measurement location are given as red outlines. Note that subcatchment 3 receives water from a pipe, originating from an artificial water catchment system south of location 3. The inset shows the location of the meteorological stations used.

II.2.2 Measured Data

For this study hydrological and isotopic measurements from 6th June 2009 to 31st March 2011 were used. Discharge was measured at the catchment's outlet equipped with a V-notch weir for low flow measurements and a Parshall flume to measure medium to high flows. The precipitation time series with a temporal resolution of 1 hour and a 0.1 mm measurement increment was acquired from the meteorological station Kalterherberg (German Weather

Service, station number 80115, 535 m asl.) located approx. 5 km west of the Wüstebach catchment. Daily snow height data with 1 cm resolution from Kalterherberg station was used with a simple snow model to account for snow storage retardation effects (see Section II.3.2).

The acquisition of weekly stream and tributary water grab samples for analysis of stable isotopes of water started on 18th May 2009. We sampled 50 ml of stream water from each of the 15 different locations along the Wüstebach main stream and its tributaries (see Figure II.1). Due to infrequent water flow, sampling location 7 was not included in this study. Weekly precipitation samples for isotopic analysis were collected since 8th June 2009 from a wet deposition collector at the close-by TERENO meteorological station Schöneseiffen (620 m asl., approximately 3.5 km to the NE), as there is no rainfall sampler at Kalterherberg station. The precipitation water was collected by a funnel (200 cm²) connected to a 2.3 liter high-density polyethylene (HDPE) bottle via plastic tubing. The samples were cooled in-situ to 4°C in a standard refrigerator. As the collection funnel was not heated, it is unknown if all snowfall eventually melted into the collection funnel or if losses occurred due to snow cover build-up. In the beginning of 2010 we were not able to gather precipitation isotope samples for almost 3 months, leading to a very coarse bulk sample during this time. Nevertheless, we used this 3 month bulk sample, as during this 3 month sampling gap evaporation was limited (winter with low ambient air temperatures) and the accumulated precipitation amounts did not exceed the maximum storage capacity of the collection bottle.

The isotopic analysis of water samples was carried out using Isotope-Ratio Mass Spectrometry (IRMS) with high-temperature pyrolysis to analyze $\delta^{18}O$ and $\delta^{2}H$. Isotope values are given as δ values and are reported on the Vienna Standard Mean Ocean Water (VSMOW) scale [*Gonfiantini*, 1978]. Several in-house laboratory standards calibrated against VSMOW, Standard Light Antarctic Precipitation (SLAP2) and Greenland Ice Sheet

Precipitation (GISP) where used to calibrate the measurements and to guarantee long-term stability of our analyses during the investigation period. The analytical accuracy of our IRMS is ≤ 0.1 ‰ for $\delta^{18}O$ and ≤ 1.0 ‰ for $\delta^{2}H$.

Hourly soil water content data at three depths (5, 20 and 50 cm) used in this study stem from the wireless sensor network SoilNet installed in the Wüstebach test site (Figure II.1) [*Bogena et al.*, 2010].

II.3 Methods

II.3.1 Data Preparation

We combined runoff data of the two gauges by using V-notch values for water levels below 5 cm (equal to 2.9 m³/h), Parshall flume values for water levels greater than 10 cm (equal to 56.9 m³/h) and a weighted mean value in between those water levels (all water levels refer to measurements at the V-notch weir). V-notch discharge was calculated from the Thomson weir equation and Parshall flume discharge (uncertainty of about 3%) from a rating curve provided by its manufacturer. We then averaged the discharge measurements to hourly resolution.

The precipitation time series from the Kalterherberg station was checked for consistency by comparison to the Schöneseiffen station. One large rainfall event (3rd July 2009 12:00 PM) with an intensity of 27.7 mm/h did not show any corresponding reaction in the hydrograph or in soil water content. We therefore assumed that a convective storm cell had passed over the Kalterherberg station but did not cross the Wüstebach catchment. Consequently, we substituted this measurement with data from the Schöneseiffen station that recorded only 1.8 mm/h. The measured Kalterherberg precipitation data series was corrected for losses due to evaporation and wind drift according to *Richter* [1995]. The correction resulted in an overall increase of the total rainfall during the modeling period by 13 % (from 2209.7 to 2508.4 mm),

and in an improved closure of the catchment's water balance [*Cornelissen et al.*, 2014; *Graf et al.*, 2014].

We selected 111 SoilNet locations from the total number of 150 sensor nodes in order to have a continuous time series. The three depths (5, 20 and 50 cm) were summed up to calculate the weighted mean soil water content (*SWCm)* for a 1.6 m soil column. The 5 cm and 20 cm SWC measurements were given weights of 0.1 and 0.2, representing the depths from 0 – 0.1 m and 0.1 – 0.3 m respectively, with the 50 cm measurement receiving a weight of 1.3, representing the remaining depth from 0.3 – 1.6 m.

II.3.2 Snow Melt Model

We used a simple snow melt model to account for the delay of precipitation input due to storage as snow. During times of snow cover build-up, precipitation is accumulated in a snow storage component. In case of partial melt of the snow cover, defined as decrease in measured snow cover height and expressed in percent, a corresponding percent of melt water is uniformly released over an arbitrarily chosen time period of six hours. A sensitivity analysis with snow melt periods between 3 and 6 hours showed negligible impact on the results. We are aware of the fact that compaction of the snow cover can account for decreasing snow cover height. In this study, we assumed that compaction accounts for markedly smaller changes than partial melt, keeping possible errors due to this simplification to a minimum. In the case of complete melt of the entire snow cover, all stored water was uniformly released over a time period of six hours. We acknowledge the simplicity of the snow model and that six hours might be too short for complete snow cover meltdown in some cases. However, the use of our snow melt model in rainfall-runoff simulations showed no major hydrograph simulation misfits owing to this approach, as the eventual release of snow cover stored rainfall inputs coincided well with observed runoff events. As snow accumulation and melting

happens only a few times during the two year modeling period, we assume that a more advanced snow model would not lead to a significant increase in the runoff simulation performance.

II.3.3 Determination of the Transit Time Distributions

For hydrograph simulation we used the conceptual rainfall-runoff transfer function hydrograph separation model (TRANSEP) [*Weiler et al.*, 2003], which inversely solves Equations II.1 and II.2 on the basis of observed runoff time series, to calibrate the effective precipitation time series p_{eff}. Determination of p_{eff} is based on a non-linear Antecedent Precipitation Index (API) approach [*Jakeman and Hornberger*, 1993]:

$$p_{eff} = p(t)s(t) \tag{II.1a}$$

$$s(t) = b_1 p(t) + (1 - b_2^{-1})s(t - \Delta t) \tag{II.1b}$$

with $p(t)$ the measured precipitation, $s(t)$ the API, Δt the calculation time step of 1 h, b_1 a scaling factor to match the amount of total simulated runoff to the amount of total effective precipitation and b_2 weighing each precipitation event backward in time. An additional parameter, b_3, sets the initial API conditions for time step $t = 0$.

The hydrograph is calculated using:

$$Q(t) = \int_0^t g(\tau) p_{eff}(t - \tau) d\tau \tag{II.2}$$

with $Q(t)$ being the calculated runoff, $g(\tau)$ the Response Time Distribution (RTD), τ is the response time and $p_{eff}(t - \tau)$ the effective precipitation for time step t - τ. The RTD is the hydrological response of the catchment to a unit rainfall input (similar to the unit hydrograph). While the RTD incorporates travel times of water molecules and celerities of hydraulic pressure waves propagating through the soil, the TTD only captures travel times of water

molecules. As hydraulic pressure wave celerities can exceed travel times of water molecules by far, response times of a catchment are typically shorter compared to actual particle travel times [*Rinaldo et al.*, 2011; *Roa-Garcia and Weiler*, 2010; *Williams et al.*, 2002]. In TRANSEP several model types for the RTD and TTD are available: exponential model (E), exponential piston flow model (EP), dispersion model (DM), gamma distribution (G), two parallel linear reservoirs (TPLR). Previous studies showed that the TPLR model produced good results in modeling TTDs [*Hrachowitz et al.*, 2009b; *Weiler et al.*, 2003]. In this study we used two 3-parameter TPLR models, each consisting of a fast and a slow responding reservoir, for both RTD ($g(\tau)$) and TTD ($h(\tau)$) simulation:

$$g(\tau) = h(\tau) = \frac{\phi}{\tau_f}\exp\left(-\frac{\tau}{\tau_f}\right) + \frac{1-\phi}{\tau_s}\exp(-\frac{\tau}{\tau_s}) \quad \text{(II.3)}$$

with ϕ a fractionation factor between 0 and 1, partitioning a certain fraction of a unit precipitation input into the fast reservoir, τ_f and τ_s being the mean residence times of the fast and the slow reservoir, respectively. Mean Response Times (MRTs) and Mean Transit Times (MTTs) are calculated as the 50 percent quantile of the respective cumulative RTD and TTD.

The parameters of the TPLR model (ϕ, τ_f, τ_s) and for the API calculation (b_1, b_2, b_3) were simultaneously optimized by the Ant Colony Optimization algorithm (ACO) [*Abbaspour et al.*, 2001]. The ACO algorithm efficiently found the optimum solution in previous studies that also used TRANSEP [*Roa-Garcia and Weiler*, 2010; *Weiler et al.*, 2003]. We chose the Volumetric Efficiency (VE) as the objective function [*Criss and Winston*, 2008]:

$$VE = 1 - \frac{\sum|Q_{sim} - Q_{obs}|}{\sum Q_{obs}} \quad \text{(II.4)}$$

with Q_{sim} calculated and Q_{obs} observed runoff. Contrary to the commonly used Nash-Sutcliffe Efficiency [*Nash and Sutcliffe*, 1970], the VE has the advantage that it equally weighs the

residuals between observed and modeled runoff and does not put an emphasis on peak runoff. Since for this study weekly isotope samples taken mostly during low to moderate runoff conditions were available, VE is more appropriate for our runoff data.

The TTDs of gauged and ungauged stream and tributary isotope measurement locations can be modeled by using $p_{eff.}$ Due to the small size of the Wüstebach catchment and its homogeneous land cover, we assumed the p_{eff} time series to be spatially representative for the whole catchment:

$$C(t) = \frac{\int_0^t C_{in}(t-\tau) p_{eff}(t-\tau) h(\tau) d\tau}{\int_0^t p_{eff}(t-\tau) h(\tau) d\tau} \quad \text{(II.5)}$$

with $C(t)$ stream water isotope values at time t, $C_{in}(t-\tau)$ precipitation isotope values at time t with travel time τ and $h(\tau)$ the TTD. We used $\delta^{18}O$ and $\delta^{2}H$ to model several locations; as the results were similar, we solely used $\delta^{18}O$ data for modeling of all sampling locations. As we used a spin-up period of 2 years in isotope modeling, initial TTD results had to be rescaled to the modeling time frame of 665 days by leaving out the 2 years of spin-up. To do this, we summed the initial results corresponding to the time frame of 0 to 665 days transit time and divided each by the sum of these values, so that their final cumulative sum equaled unity. This implicitly assumes that 100% of the tracer leaves the catchment within 665 days. As the conductivity of the shale bedrock at the Wüstebach catchment is extremely low (10^{-7} to 10^{-9} m/sec [*Graf et al.*, 2014]), we assumed that the contribution of deep groundwater to total runoff with transit times longer than 665 days is negligible. Furthermore, we assumed that the contribution from the shallow soil water reservoir and the riparian zone in the Wüstebach catchment has a turnover time shorter than 665 days.

To optimize the TTD simulation, we used the ACO algorithm and the NSE measure, as we modeled the complete isotope tracer time series with an emphasis on dynamics in the time series (i.e. isotope peaks in the time series). The NSE is given as:

$$NSE = 1 - \frac{\sum(C_{obs} - C_{sim})^2}{\sum(C_{obs} - \overline{C_{obs}})^2} \quad \text{(II.6)}$$

with C_{sim} the simulated isotope concentration in the stream, C_{obs} the observed isotopic concentration in the stream and $\overline{C_{obs}}$ the mean value of all observations. Additionally, we computed the VE for the optimized isotope results (with absolute values in the denominator of Equation II.4 to account for negative $\delta^{18}O$) to compare NSE and VE values for each location.

For analysis of correlations between catchment characteristics and spatial TTDs patterns we derived the subcatchment areas of all stream isotope sampling locations using the single flow direction algorithm as described in *Jenson and Dominique* [1988] of the software ArcView (ESRI, Redlands, CA).

II.3.4 Splitting the hydrograph into sub-modeling periods

At an early stage of hydrograph simulation, we simulated the entire study period and found that the model overestimated runoff in summer and underestimated it in winter (not shown). It was not possible to capture the annual variability of the catchment's hydrological behavior using a single optimized parameter set. Thus, we had to derive a method to split the hydrograph into distinct sub-modeling periods where the catchment's hydrological behavior would be quasi-constant, allowing for hydrograph simulation with one single parameter set for each period.

In accordance with *Graf et al.* [2014], we found that at a *SWCm* value of about 35 Vol.% the relation between daily mean runoff and soil water storage changes. In winter, when *SWCm* is

generally higher than 35 Vol.%, we found a higher slope between *SWCm* and runoff than during summer, when *SWCm* is generally lower than 35 Vol.% (Figure II.2a). Based on this, we divided the two-year time series into four sub-modeling time series, splitting the hydrograph at points where *SWCm* values of 35 Vol.% were exceeded for a longer period of time. We did not split the hydrograph at a) short-term exceedances of a few days and b) an approximately 10-day exceedance in mid-May 2010, where before and after values dominantly stayed below 35 Vol.%. The divisions of the complete hydrograph time series fall almost exactly on hydrological half year dates with 1st November 2009, 1st May 2010 and the exception of 15th August 2010. Accordingly, the four periods are indicated as: 'Summer_09', 'Winter_09', 'Summer_10' and 'Winter_10', respectively, and the Wüstebach's dry (*SWCm* < 35 Vol.%) and wet state (*SWCm* > 35 Vol.%) are simply referred to in the following as 'dry state' and 'wet state'.

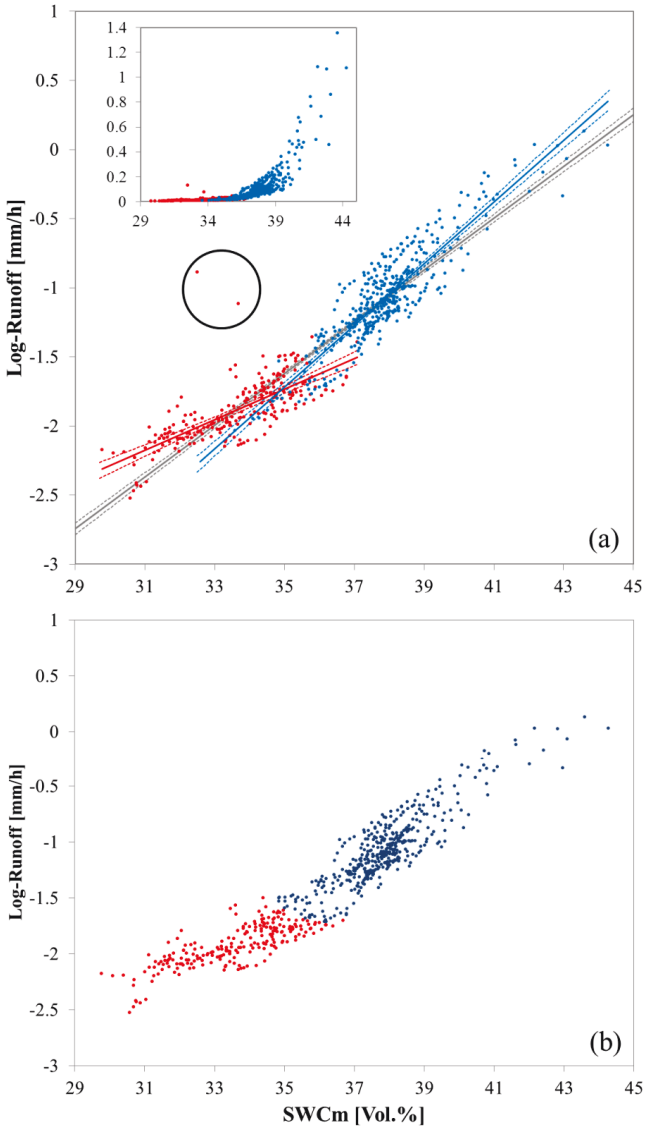

Figure II.2. (a) Daily mean runoff (log-transformed, base: 10) against *SWCm* for dry states (red dots) and wet states (blue dots), respectively (dates in Table II.1). Inset shows runoff against *SWCm*. Correlation and 95% confidence interval for dry states (red solid and dashed lines) with Log-Runoff = 0.110 *SWCm* - 5.597 with $R^2 = 0.53$, wet states (blue solid and dashed lines) with Log-Runoff = 0.223 *SWCm* - 9.525 with $R^2 = 0.81$ and both combined (gray solid and dashed lines) with Log-Runoff = 0.187 *SWCm* - 8.173 with $R^2 = 0.88$, all three with significance value $p<10^{-39}$. Outlier values are

marked with a black circle. (b) Result of cluster analysis without outliers using the initial assumption of two clusters (red and blue dots).

To test the validity of the subjectively chosen *SWCm* value for splitting the hydrograph, we used an expectation-maximization (EM) algorithm to objectively find data clusters in the relationship between runoff and *SWCm* [*Fraley and Raftery*, 2002]. We tested 1 to 4 clusters and compared their maximum likelihood value, leaving out two outlier runoff events during summer months. The likelihood for two clusters was higher than for one cluster, with the algorithm splitting the data points in a range from 35 to 37 Vol.% (Figure II.2b). Higher order cluster analysis (i.e. using 3 or 4 clusters) were rejected because they resulted in a similar cluster split compared to the two cluster analysis.

The p_{eff} of the high-intensity (31 mm/h) event of 3rd July 2010 was estimated separately as it met dry topsoil conditions and resulted in preferential subsurface flow, leading to a rapid runoff response (see *Rosenbaum et al.* [2012]). This would result in a unique RTD compared to the rest of this summer's modeling period. To derive the p_{eff} of this event, we used the sum of the first two hours of the event runoff as they showed a fast and markedly increase compared to the situation prior and subsequent these two hours. We then subtracted the mean runoff of the three days prior to this event (low flow conditions and thus, we assumed, base flow) to calculate the event fraction of the runoff reaction. We assumed this event fraction to be p_{eff} for the 3rd July 2010 storm event.

For further analysis of the individual modeling periods, we additionally calculated the runoff coefficient *C* as the ratio of precipitation to runoff amounts for each period.

II.3.5 Adaption of stable isotopes in precipitation

Catchment-scale lumped parameter models utilizing tracers are based on the assumption that representative model inputs are used [*McGuire and McDonnell*, 2006]. Our study catchment

is forested while we used precipitation isotope data from open land. Precipitation passing through canopy generally increases in isotope values compared to open land precipitation [*Allen et al*., 2013; *Saxena*, 1986]. Due to the uncertainties of the canopy-influence on rainfall isotope values, we used the simple approach of adding an overall mean change to all isotope rain values.

We acknowledge the simplicity of this approach and the unknown uncertainties it introduced into the TTD modeling process and are currently conducting an experiment designed to further investigate this issue.

II.4 Results

Overall, there were no long-term hydrological extremes in precipitation or runoff (Figure II.3), with neither of the investigated years being too dry or too wet compared the long term precipitation mean (1107 mm, without approximately 13% increase due to correction for evaporation and wind drift, *Richter* [1995]). This is reflected in total precipitation and runoff, which amounted to 2508.4 mm and 1266.9 mm, respectively, indicating 49% evapotranspiration (ET) losses and storage change. Only one extreme storm event occurred, leading to a pronounced recharge response in *SWCm* (refer to Figure II.3a and II.3b, 'Summer_10'). During both winters, base flow water levels rose to the approximately same level, with multiple event hydrographs sharing similarities in behavior. The *SWCm* reacted very similar to the hydrograph (Figure II.3b). Isotopically, the modeling period also did not show any unexpected extremes. $\delta^{18}O$ in precipitation had a typical seasonal variation with enriched isotope values during summer and depleted values during winter months. In comparison, stream isotope values were heavily attenuated compared to the amplitudes observed in precipitation, (Figure II.3c). Stream isotope observations ranged from approximately -9.0 to -7.0 $\delta^{18}O$, with precipitation samples ranging from approximately -14.0

to -2.5 $\delta^{18}O$. Plotting isotope values of precipitation in the delta space plot ($\delta^{18}O$ vs. $\delta^{2}H$), we determined the Local Meteoric Water Line. We found that the stream isotope values were slightly shifted from the LMWL (Figure II.4). However, the average of all stream isotope values ($\delta^{18}O$ = -8.37, $\delta^{2}H$ = -52.23) almost matched with the LMWL.

II.4.1 Hydrograph Simulation

Hydrograph simulation results are shown in Figure II.3a, while Table II.1 lists the six optimized parameters, the VE, the runoff coefficient *C* and the MRT for each period. The model was able to fit all periods equally well, with VE values of 0.76, 0.55, 0.65 and 0.64 respectively. We found p_{eff} for the 3rd July 2010 event to be 19.8 mm/h, meaning that 64% of gross precipitation appeared as immediate event runoff.

Table II.1. Optimized parameters of the rainfall runoff model for the four modeling seasons

	Summer_09 6/6/2009 - 10/31/2009	**Winter_09** 11/1/2009 - 4/30/2010	**Summer_10** 5/1/2010 - 8/15/2010	**Winter_10** 8/15/2010 - 3/31/2011
C	1.08	1.67	0.98	1.34
b_1	0.39	0.08	0.50	0.11
b_2	1.37	10.00	10.00	7.00
b_3	0.83	0.00	0.65	0.00
τ_f [d]	4	7	4	7
τ_s [d]	13	72	13	72
ϕ [-]	0.00	0.70	0.00	0.70
MRT [d]	9	7	9	7
VE	0.76	0.55	0.65	0.64

C, runoff coefficient; b_1, scaling parameter; b_2, precipitation weighing parameter; b_3, API at t=0; τ_f, fast reservoir mean residence time in days for RTD $g(\tau)$; τ_s, slow reservoir mean residence time in days for RTD $g(\tau)$; ϕ, fast reservoir contribution for RTD $g(\tau)$; MRT, mean response time; VE, volumetric efficiency.

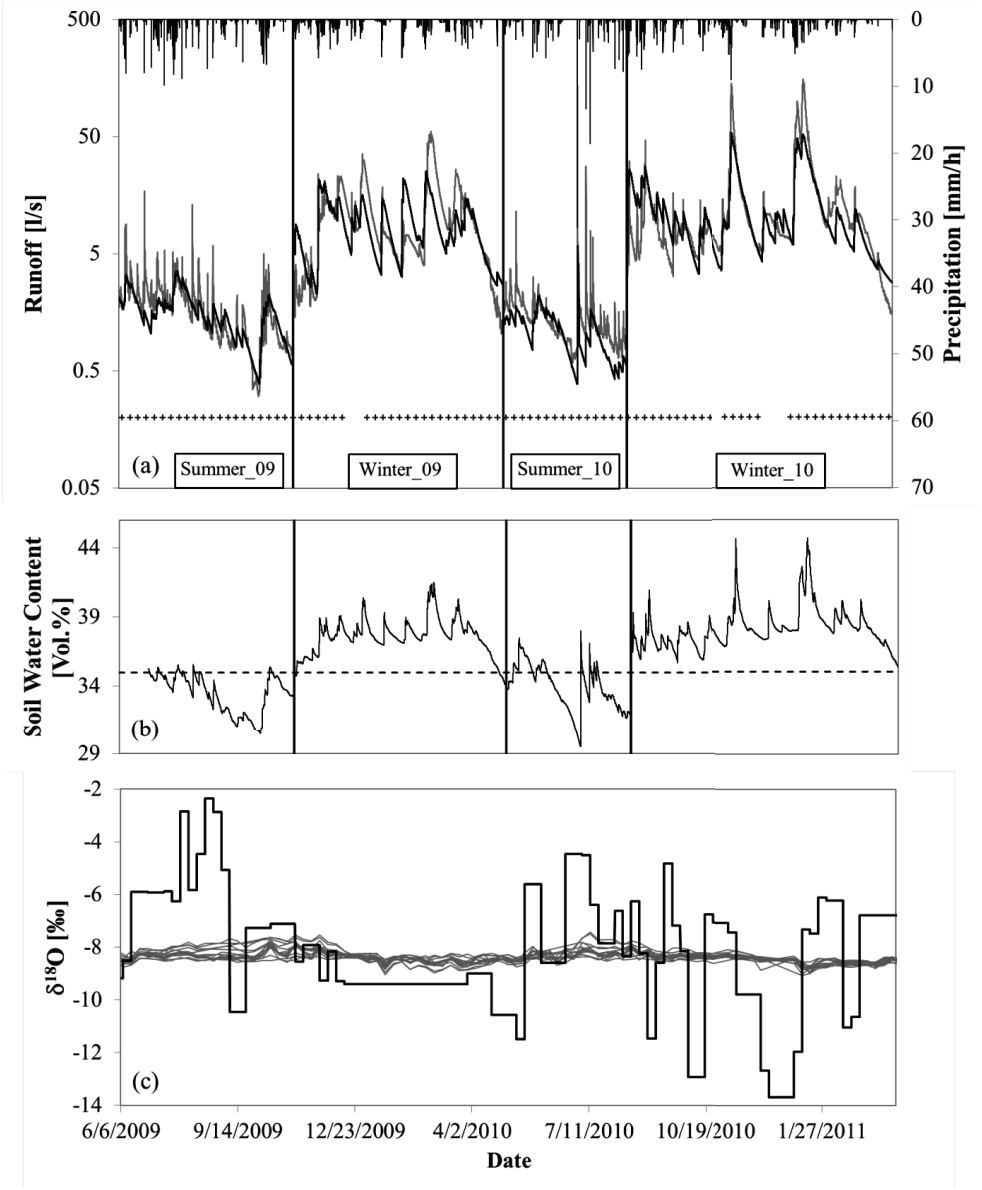

Figure II.3. Time series (6 June 2009–31 March 2011) of (a) observed (gray line) and simulated runoff (black line) in logarithmic scale, precipitation (black bars from top), stream water sampling times (black crosses) for two summer and two winter seasons, (b) depth-weighted average soil water content *SWCm* and threshold of 35 vol % (dashed line), and (c) isotope data for all stream water locations (gray lines) and precipitation (black line). Black vertical lines in Figures II.3a and II.3b are

hydrograph modeling periods based on *SWCm*. As isotope modeling has not been split up, no modeling periods are shown in Figure II.3c.

Cumulative RTDs for the dry and the wet state are shown in Figure II.5. We initially calculated parameter sets for each modeling period separately. As the two dry states showed negligible differences in parameters, with the same being true for both wet states, we assumed that the catchment's hydrological reaction in both dry and wet states did not change significantly during the modeling period. Therefore, based on model performance we decided to use one parameter set (Summer_09) for both dry states and one (Winter_10) for both wet states. The RTD of the dry state first shows a slower reaction than that of the wet state, but then reacts much faster beginning at 13 days response time. Although hydrograph modeling during dry state is focusing on low to medium flows only, the dry state periods lacked a slow component in comparison to the wet states, with 99.5% of response times within 66 days during dry state and 205 days during wet state respectively. Contrary to this, the wet state periods have both a fast and a slow component. This indicates that water following slower flow paths does not reach the outlet during dry state. Due to these RTD results, we had to recalculate p_{eff} for the dry state periods. In doing so, we postulate that the obtained RTDs indicate that during the wet state the whole Wüstebach catchment is hydrologically active, while during the dry state only the riparian zone contributes to runoff. The reduction in runoff contributing area increases the precipitation-equivalent runoff, which directly affects dry state p_{eff} and thus stream isotope simulations and their respective TTDs (see Equation II.5).

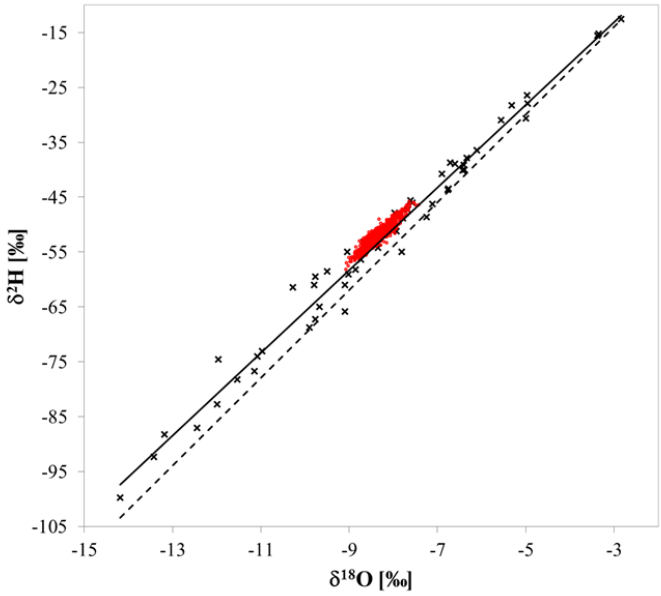

Figure II.4. Isotopic composition of precipitation (crosses) and Local Meteoric Water Line (LMWL) for the observation period (solid line) compared with the Global Meteoric Water Line [*Craig*, 1961] (GMWL, dashed line). LMWL has an R^2 of 0.98 with $\delta^2H = 7.549\ \delta^{18}O + 9.611$. Stream isotopes samples of all 15 stream locations are slightly shifted from the LMWL (red dots).

In the course of recalculating p_{eff} for dry state, we tested if the increased runoff amounts (in mm) would not exceed total precipitation amounts (in mm). We, therefore, used the already obtained RTD to simulate runoff for both dry states separately with varying contributing areas ranging from 1 ha (corresponding to runoff amount increase of 3700%) to 8 ha (increase of 375%). We found that from 1 to 4 ha there was not enough rain to match runoff amounts, which led to very poor model performances. Starting with 5 ha, precipitation amounts sufficed and the Root Mean Square Error (RMSE) reached a low plateau (Figure II.6, also see runoff coefficients of Table II.1). This value corresponds well with the extent of the riparian zone in the soil map (Figure II.1). Using 5 ha catchment-area for dry state conditions resulted in an increase of precipitation-equivalent runoff by 770% compared to the 38.5 ha catchment. Corresponding runoff coefficients C are 1.08 and 0.98 for both dry states (5 ha) and 1.67 and

1.34 during wet state (38.5 ha) periods (Table II.1). The low *C* in each dry state is attributable to only the riparian zone generating runoff, in which nearly all of precipitation creates a runoff response.

Thus, the final p_{eff} time series is a composite of four modeling periods with alternating runoff contributing areas. Total p_{eff} was 1607 mm, which is 64% of the total precipitation. The remaining 36% of total precipitation are either lost to ET and storage changes or appear as runoff in the not simulated hydrograph parts (e.g. rainfall-runoff events during dry state).

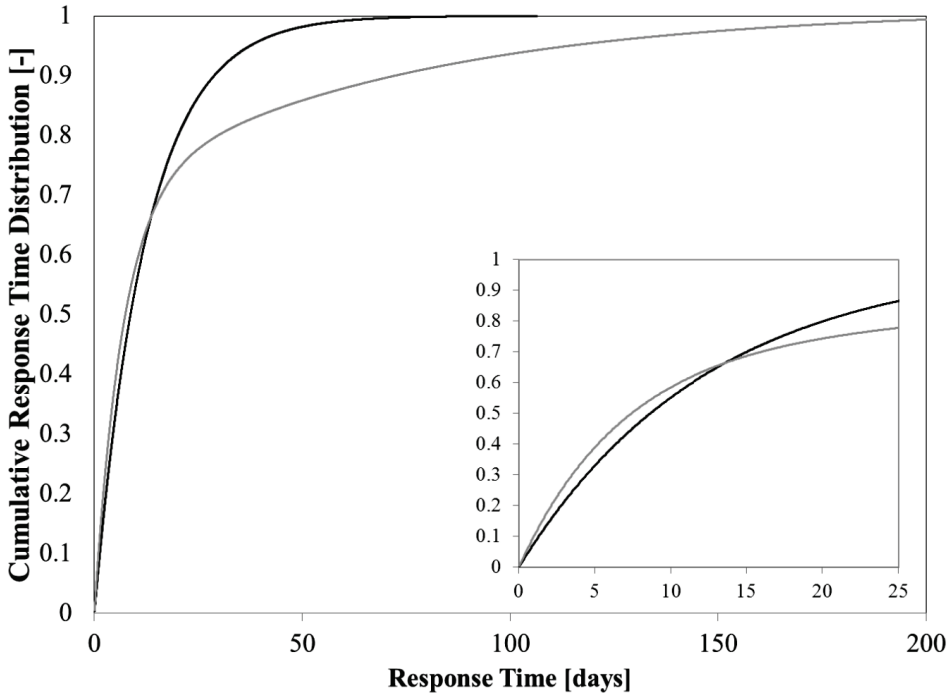

Figure II.5. Cumulative RTDs for the dry (black line) and the wet state (gray line) for the outlet of the Wüstebach catchment (location 14). Inset shows details from 0 to 25 days response time.

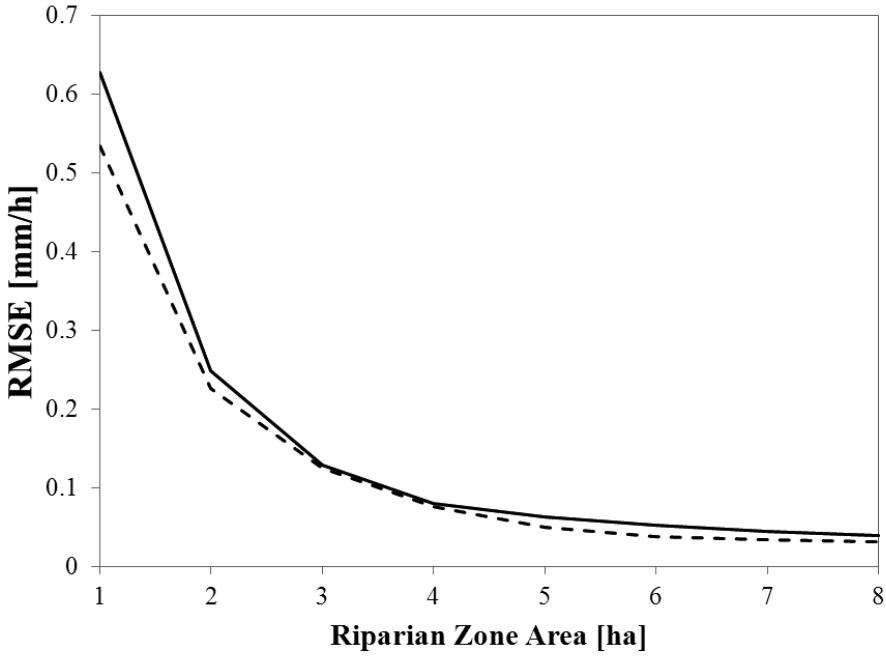

Figure II.6. Relation between simulation performance (RMSE) of hydrograph simulations for Summer_09 (solid) and Summer_10 (dashed) and variable assumed sizes of the riparian zone area in the Wüstebach catchment (hydrologically active catchment during dry state).

II.4.2 Stream Isotope Modeling

We found the overall mean change in isotope values from open land precipitation to throughfall to be 0.5 ‰ in $\delta^{18}O$ after calibration. The simulation performance increased by 0.11 in NSE, exemplary for a stream location near the spring of Wüstebach (location 1, see Figure II.1). In general, the precipitation isotope time series showed a higher variability than the stream isotope time series, as transport through the catchment delays and attenuates the precipitation isotope signal. However, only a few stream locations showed similar, but attenuated, seasonal variations, with some locations showing almost none at all (e.g. location 3, 12, 15).

To further test the hypothesis of a partial contributing area of 5 ha during dry state, we simulated stream $\delta^{18}O$ values at measurement locations 1 and 14 with two approaches. First, we assumed a constant active catchment area of 38.5 ha in the derivation of p_{eff} and second we used a season-dependent active catchment area approach with 38.5 ha during wet state and 5 ha during dry state. The comparison of both approaches (see Figure II.7) showed that a catchment area of 38.5 ha for the whole period resulted in poorer simulation result (NSE = 0.45) than using 38.5 ha during wet and 5 ha during dry state periods (NSE = 0.74) for location 1. In the case of location 14, the model performance slightly decreased from the 38.5 ha only (NSE = 0.37) to the 38.5 and 5 ha simulation (NSE = 0.34).

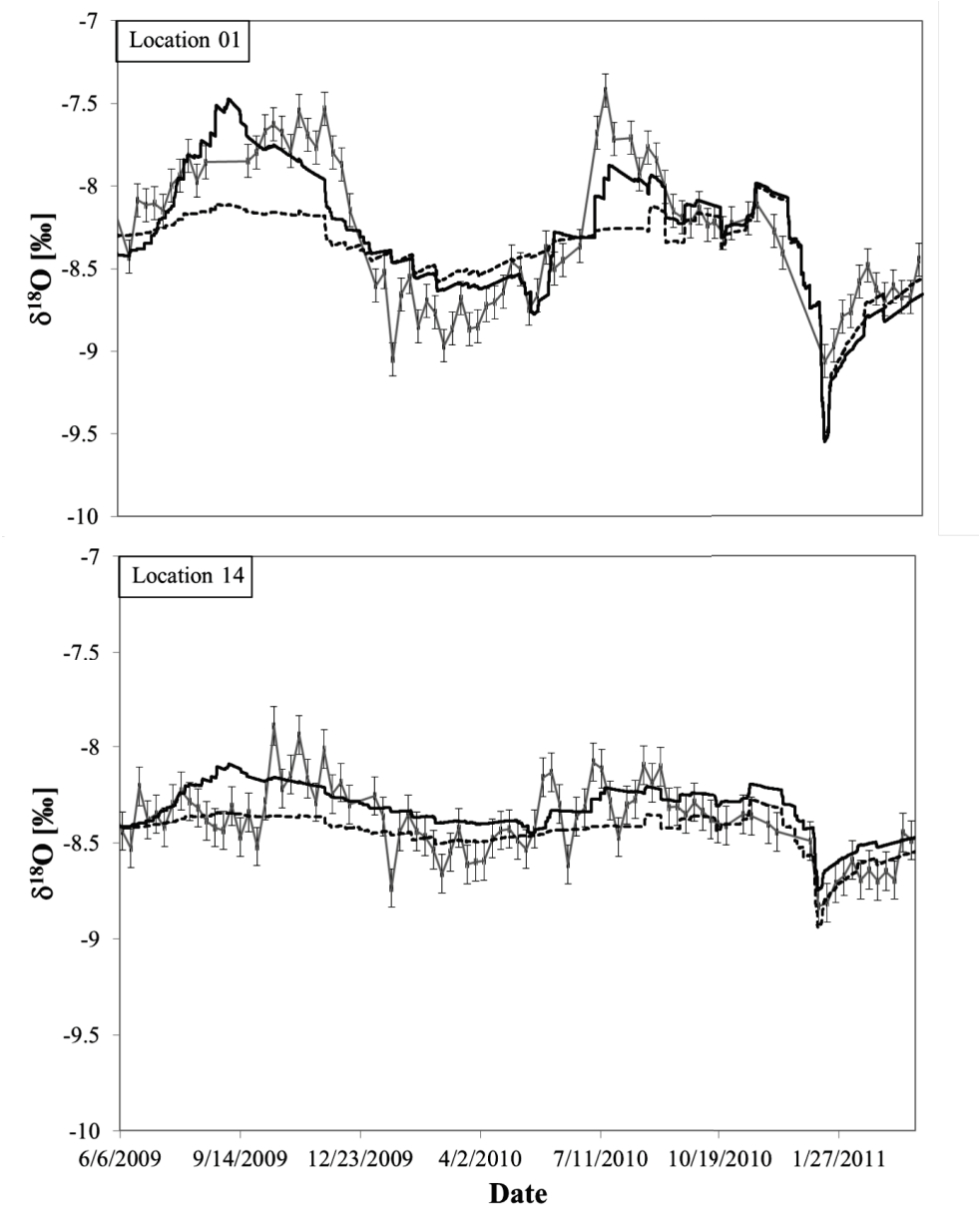

Figure II.7. Stream isotope simulations for (top) location 1 and (bottom) 14. Observed isotope values (gray line with error bars), simulation result with changing active catchment area (black line) and simulation results with 38.5 ha active catchment area throughout the whole modeling period (dashed line). Location 1 with VE = 0.9788 and NSE = 0.74; location 14 with VE = 0.9855 and NSE = 0.34.

Mark that strong deviations between observed and simulated values in summer 2009 are most likely caused by missing resolution of precipitation input.

Isotope simulation results are shown exemplary for locations 1 and 14 in Figure II.7, while all TTD results are summarized in Figure II.8a. Table II.2 lists the objective function values, parameters and subcatchment characteristics for each location respectively. Comparison of all TTDs in Figure II.8a revealed that the outlet (Location 14) is indeed an integration of the catchment's spatially different response to precipitation input, integrating shorter and longer transit times [*Shaman et al.*, 2004]. The NSE for all 15 stream locations ranged between -0.09 and 0.74, with VE values ranging between 0.9788 and 0.9897. Note that the small variability of the VE values is due to the reformulation of Equation II.4 with $\delta^{18}O$ values instead of runoff, leading to more subtle differences. We found that locations that have a high NSE usually have a low VE and show more dynamics in their isotope time series (not shown) with shorter MTTs compared to locations with a low NSE and high VE that have less dynamic isotope time series and longer MTTs (Figure II.8b, Table II.2). The outlet (location 14) integrated different NSE and VE values comparable to its integration of the different TTDs.

From location 1 (near the spring) downstream to the outlet (location 14) we generally found increasing MTTs for main stream locations (Figure II.8a, Table II.2, see Figure II.1 for locations). Exceptions to this rule were locations 10 and 11, in which location 10 showed a shorter MTT than the upstream location 6, and 11 showed a longer MTT than the downstream outlet 14. Comparison of the TTDs of locations 10 and 11 revealed two different TTDs, sharing little similarity in MTTs (120 and 169 days). As location 10 is nested in location 11, with both locations having a similar subcatchment area and percentage of riparian zone, we would have expected similar TTDs. Tributaries mostly showed shorter MTTs than the mainstream location where they discharge. Exceptions to this rule were location 3, 5 and 12 (Table II.2).

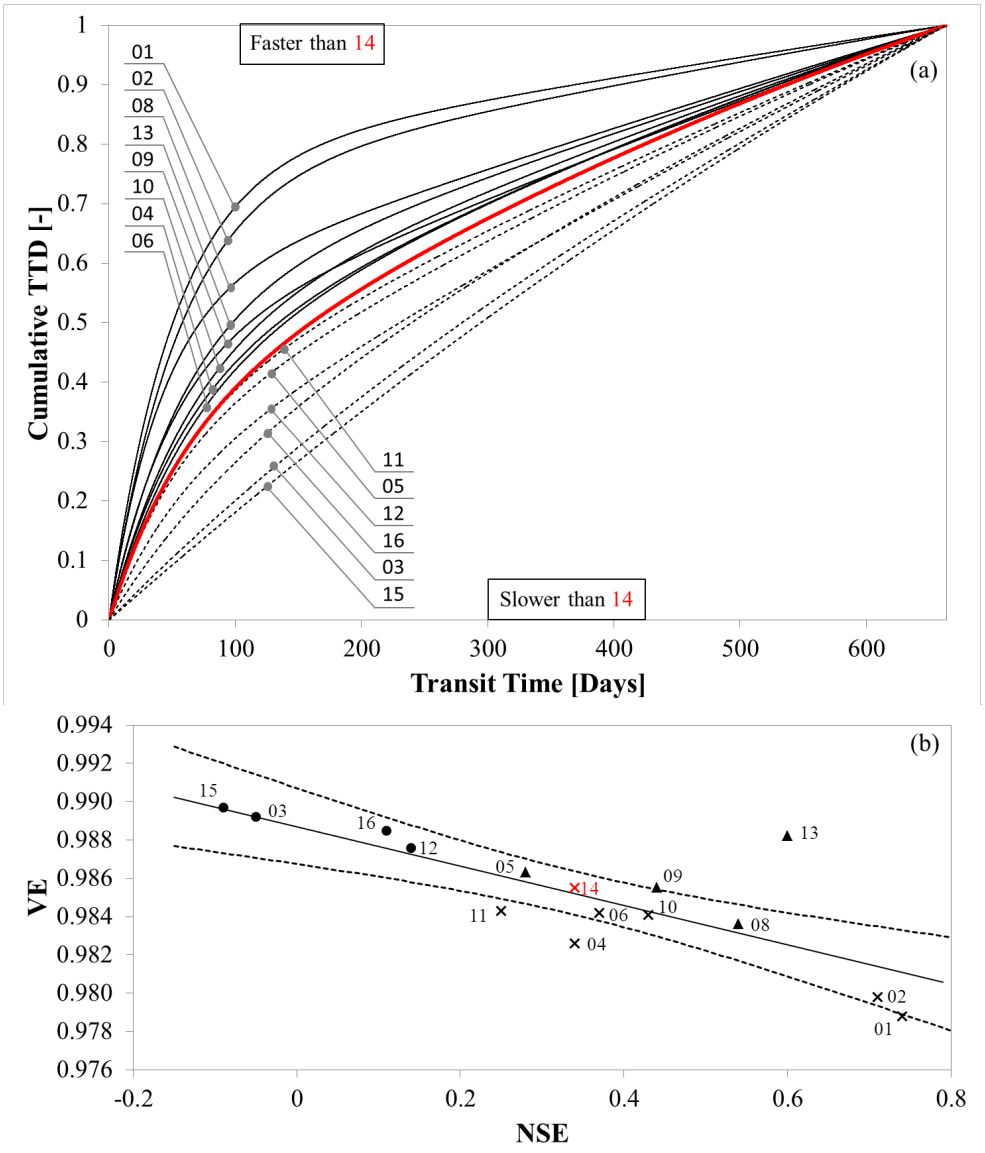

Figure II.8. (a) Cumulative TTDs of all sampling locations (numerals), without subcatchment 7. The red line represents location 14 (outlet). Labels ‘‘Faster than 14’’ and ‘‘Slower than 14’’ indicate two subcatchment groups with shorter (upper group) and longer (lower group) MTTs compared to the outlet. (b) NSE and VE of all model simulations. Subcatchments have been divided in main stream (crosses) with the catchment’s outlet highlighted (red cross), tributaries (triangles), and groundwater-dominated tributaries (circles). Regression line (solid line) with VE = -0.0103 * NSE + 0.989, R^2 of 0.63, significance $p<0.0004$ and the 95% confidence intervals (dashed lines).

Table II.2. TTD modeling parameters and sub-catchment characteristics.

Pos.	VE [-]	NSE [-]	MTT [d]	τ_f [d]	τ_s [d]	ϕ [-]	Riparian [-]	Diff [-]	Area [ha]
1	0.9788	0.74	51	51	3226	0.37	0.32	0.05	3.9
2	0.9798	0.71	58	55	3209	0.33	0.35	0.02	4.6
3	0.9892	-0.05	280	278	5693	0.04	0.00	0.04	5.2
4	0.9826	0.34	134	56	1252	0.20	0.17	0.03	18.6
5	0.9863	0.28	186	49	1607	0.11	0.27	0.16	0.2
6	0.9842	0.37	140	63	1319	0.20	0.17	0.03	19.4
8	0.9836	0.54	72	41	4164	0.15	0.21	0.06	0.6
9	0.9855	0.44	111	48	3267	0.13	0.08	0.05	0.3
10	0.9841	0.43	120	63	2070	0.19	0.17	0.02	23.1
11	0.9843	0.25	169	54	1919	0.12	0.17	0.05	25.3
12	0.9876	0.14	231	54	2819	0.05	0.02	0.03	10.0
13	0.9882	0.60	98	58	4814	0.12	0.04	0.08	0.5
14	0.9855	0.34	160	57	1026	0.18	0.13	0.05	38.5
15	0.9897	-0.09	295	123	1472	0.00	0.02	0.02	6.3
16	0.9885	0.11	240	83	1472	0.07	0.06	0.01	11.4

Pos., measurement location (Figure II.1); VE, volumetric efficiency; NSE, Nash-Sutcliffe efficiency; MTT, mean transit time; τ_f, fast reservoir mean residence time for TTD $h(\tau)$; τ_s, slow reservoir mean residence time for TTD $h(\tau)$; ϕ, fast reservoir contribution for TTD $h(\tau)$; Riparian, percentage of riparian zone of total subcatchment area; Diff, absolute difference between fraction of riparian zone and ϕ; Area, total subcatchment area

As shown before, the RTD in the Wüstebach catchment was strongly affected by the riparian zone, because during the dry state only the riparian zone contributed to runoff. Therefore, we assumed that also the TTDs were highly influenced by the riparian zone. If the three optimized parameters of the TPLR model were not random combinations, the constantly well-saturated riparian zone should have been represented by the fast and the remaining part of the catchment by the slow reservoir of the TPLR model, as water conductance increases with increasing soil water content. The fast reservoir fraction (ϕ) should correspond to the proportion of the riparian zone within the subcatchment of each sampling location. A direct comparison revealed that the absolute differences were mostly less or equal to 10% (see Figure II.9 and column 'Diff' in Table II.2). This indicated that the parameter sets were not physically meaningless and that the TTDs and their order can be explained by the influence of the riparian zone. The only exception was location 5, which showed an absolute difference of

16% for its relatively small subcatchment. Additionally comparing the residence time of water in the fast and the slow reservoir, τ_f and τ_s, revealed that the model consistently chose very similar τ_f values, with larger variation in τ_s (Table II.2). Although the model is conceptual, it appears that it was still able to find at least one explainable parameter.

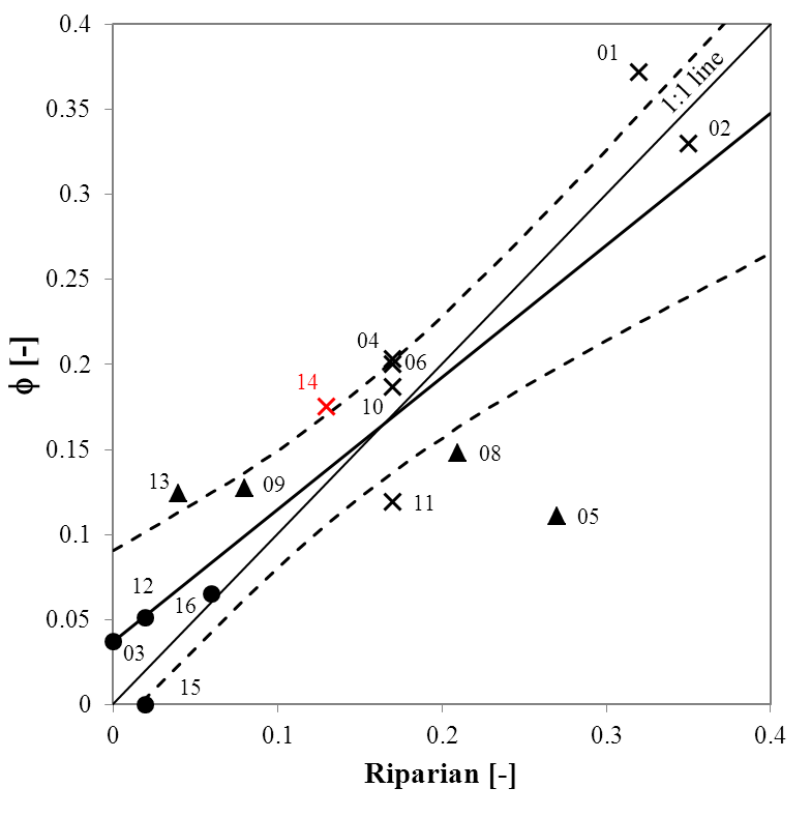

Figure II.9. Fast reservoir contribution (ϕ) of the TPLR model for TTDs of all sampling locations (numerals) and the fraction of riparian soils of the respective subcatchments (Riparian), without subcatchment 7. Subcatchments have been divided in main stream (crosses) with the catchment's outlet highlighted (red cross), tributaries (triangles), and groundwater-dominated tributaries (circles). Thick line is regression line with $\phi = 0.777$ Riparian + 0.037, with $R^2 = 0.71$, significance $p<0.00008$ and the 95% confidence intervals (dashed lines).

Comparing the fraction of the riparian zone in each subcatchment to the respective MTT, we found higher proportions of riparian zone corresponding with shorter MTTs (Figure II.10a). Main stream locations plotted relatively close together, with approximately the same percentage of riparian zone area. The exceptions to this are locations 1 and 2 near the spring of Wüstebach with a higher proportion of riparian zone. Locations 3, 12, 15 and 16 also group together, have low percentages of riparian zone and the longest MTTs. Most tributary streams to the Wüstebach main stream (5, 8, 9, and 13) showed a variety of ranges of riparian zone fractions and MTTs. The linear regression between MTT and riparian zone area showed an R^2 of 0.50 with significance $p < 0.03$, indicating statistical significance. Comparing this to the TTDs in Figure II.8a, it is apparent that locations with faster reacting TTDs than the outlet usually have a higher percentage of riparian zone (with the outlet having 13%); conversely, slower reacting TTDs have a smaller riparian zone fraction.

In contrast, no clear relationship between all subcatchment sizes and MTTs was found (Figure II.10b). However, our data indicated a weak positive relationship between MTT and catchment size for the main stream locations. Additionally, tributaries and locations with long MTTs (possible groundwater influence, see Discussion) seem to group together.

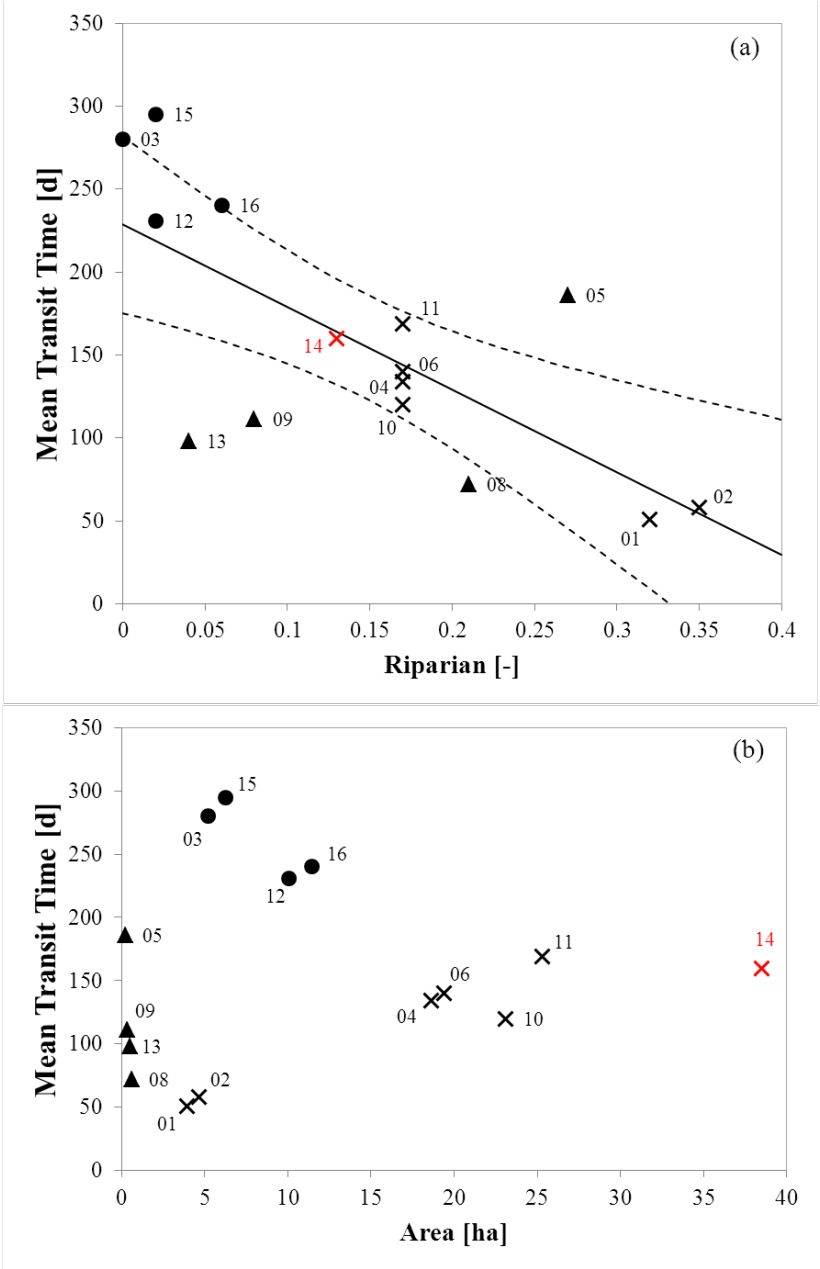

Figure II.10. (a) Mean Transit Time (MTT) in days as a function of percentage of riparian zone area (Riparian) in each subcatchment (numerals) without subcatchment 7. Subcatchments have been divided in main stream (crosses) with the catchment's outlet highlighted (red cross), tributaries (triangles), and groundwater-dominated tributaries (circles). Solid line is a linear regression line for

MTT = -497.82 Riparian + 228.68 with R^2 = 0.50, significance $p<0.03$ and the 95% confidence intervals (dashed lines). (b) MTT in days as a function of subcatchment area. Subcatchment locations are divided in different locations as described for Figure II.10a.

II.5 Discussion

Water balance results based on the whole modeling period and complete catchment area indicated an ET loss and storage change of 49%, which compares well with the Wüstebach catchment's 44% annual mean actual ET found by *Graf et al.* [2014]. The final p_{eff} sum used for TTD modeling indicated an ET loss of only 36%, explainable by the reduced active catchment area during the dry state, where less p_{eff} is lost in the well-saturated riparian zone.

Results of the cluster analysis showed that the split between dry and wet state occurred at a range between 35 and 37 Vol.% *SWCm*. Comparable seasonality in catchment behavior was also found in previous studies [*Birkel et al.*, 2012; *Heidbüchel et al.*, 2012]. Threshold-driven non-linearities in a catchment's response, governed by soil moisture states, can be observed for many hydrological processes [*Zehe et al.*, 2007].

There are several possible physical explanations for the dry state's RTD lacking a slow component. We ruled out consistent infiltration-excess overland flow due to hydrophobicity and constant activation of preferential flow paths, as only one precipitation event (3rd July 2010, 31 mm/h) showed clear signs of preferential flow in *Rosenbaum et al.* [2012]. Another explanation would be that the hydrological reaction of the Wüstebach catchment is controlled by partial-area contributions (*Dunne and Black* [1970]). According to *Dunne and Black* [1970], well-drained soils of the riparian zone were primarily responsible for fast infiltration-excess overland-flow during summer storms in a small headwater catchment. At the same time, they observed that hillslopes did not produce significant subsurface flow during dry states and that precipitation was mainly stored in the soil. However, during wet states in

winter, lateral hillslope subsurface flow (interflow) contributed to storm runoff generation. This concept of fast-reacting, well-saturated riparian zones and slow-reacting, unsaturated hillslopes has also been observed in other studies [*Rodgers et al.*, 2005; *Tetzlaff et al.*, 2009a]. We take this concept a step further by extending it from the event scale to the seasonal scale. In a similar way, *Beven and Freer* [2001] acknowledged the seasonality in the dynamics of the effective contributing area (a_{eff}) as an important control on the catchment response by including a variable a_{eff} in their dynamic TOPMODEL approach.

In our study, we argue that during the dry state the connectivity of hillslopes and the riparian zone is lost due to drying of the soil, while during the wet state it recovers. Thus, during winter months, with *SWCm* being typically larger than 35 Vol.%, both riparian zone and hillslopes are contributing to runoff, where the riparian zone contributes mainly the fast and the hillslopes mainly the slow reacting parts of the winter RTD. During summer, the hillslope zones become hydrologically disconnected. Precipitation falling on the hillslopes is being stored in the soil, evaporated and/or withdrawn by the spruce forest through transpiration. A hydrological disconnection of hillslopes from riparian zones has also been observed in *Jencso et al.* [2009] and *Detty and McGuire* [2010].

Bogena et al. [2013] used the one-dimensional soil hydraulic model HYDRUS 1-D [*Simunek et al.*, 2008] to simulate spatially average soil moisture dynamics in the Wüstebach catchment neglecting lateral flow processes. They found that soil moisture dynamics could be successfully modelled using a no-flux lower boundary condition as long as the pressure head at the soil–bedrock interface is negative and using zero pressure head as soon as the bottom of the profile becomes saturated. This procedure mimicked drainage by bedrock fissures acting as preferential pathways, laterally transporting water to the outlet. We complement this conceptual model of *Bogena et al.* [2013] for lateral flow processes using results of a field

study of *Borchardt* [2012] to physically explain the hydrological disconnection of hillslopes. *Borchardt* [2012] found a distinct decrease in measured vertical hydraulic conductivities with soil depth and argued that this results in partial waterlogging at the top layer–base layer interface. The accumulated water preferentially flows laterally along this interface, with only minor percolation into the base layer. At locations where water gathers in depressions in the interface, percolation into the base layer is locally facilitated.

We postulate that during the dry state the lateral transport of soil water along this interface is negligible for the hillslope areas, as soil water is mainly consumed by forest transpiration. Additionally, no runoff is generated by the base layer of the hillslopes by lateral flow paths, as the bottom of the soil profile will be predominantly unsaturated. We argue the existence of a capillary barrier in the form of weathered bedrock, located at the transition zone between soil and solid bedrock. Under unsaturated conditions, this prevents vertical water movement to the bedrock fissures and lateral flow is also negligible. Thus, during dry states vertical flow paths dominate within the soil column, lateral water transport being negligible and the hillslopes becoming hydrologically disconnected from the stream. This general dry condition can be different during extreme rainfall events, where lateral flow may occur. During the wet state the reduced ET demand, and thus higher soil water content, could result in the activation of lateral transport mechanisms, connecting the hillslopes to the stream: (1) lateral transport along the top layer-base layer interface through the soil matrix, accounting for slow transport, (2) saturation of the bottom of the soil profile and breakthrough of the capillary barrier, eventually with lateral water transport in the weathered bedrock layer, i.e. another slow transport mechanism, and (3) fast vertical water transport through the soil via macropores [*Wiekenkamp*, personal communication, 2014]. The subsequent activation of bedrock fissures as lateral flow pathways, as modeled by *Bogena et al.* [2013], could account for the fast reaction of hillslope areas to precipitation in the wet state. They either react by transporting

water to the stream delivering new water or by a pressure wave pushing out old water. Our conceptual model explains how soil water content could control the hydrological connectivity of hillslopes in the Wüstebach catchment. This dominance of vertical water transport during dry states and lateral water transport during wet states was also found in previous studies (e.g., [*Grayson et al.*, 1997]). With the available data we are, however, not able to analyze the lateral transport processes in the Wüstebach in more detail.

II.5.1 Can we determine subcatchment TTDs of ungauged stream locations?

We found that stream isotope simulation markedly improved when applying the variable contributing catchment area approach. Additionally, we found that the stream isotope simulation performance increased when applying a correction of adding 0.5 ‰ to $\delta^{18}O$ C_{in} data, accounting for isotopic enrichment due to canopy interception processes. Previous studies found the increase in isotopic concentration to be inconsistent, showing a temporally non-stable, spatial pattern [*Allen et al.*, 2013] or varying increases with rare decreases in isotope values [*Saxena*, 1986]. However, although the mean increase in $\delta^{18}O$ values for spruce stands of about 0.3 ‰ in *Saxena* [1986] and 0.3 ‰ for Douglas fir in *Allen et al.* [2013] do not coincide with our added 0.5 ‰, it compares well to the mean increase for spruce of 0.56 ‰ of *Dewalle and Swistock* [1994].

Although we considered the seasonally changing active catchment area as well as the isotope signal changes due to throughfall, it was not possible to constrain all 15 TTD results. For example, locations 3, 11, 12, 15 and 16 showed comparatively low NSE values, which might be the result of the strong influence of deep groundwater (see Section II.5.2), resulting in relatively stable isotope concentrations. *Stewart et al.* [2010] pointed out that stable isotopes cannot determine MTTs of greater than 4 years, as the variability in stream flow isotopes is lost with longer time frames. Generally, the model was able to constrain more dynamic

isotope time series better than rather stable time series. An additional factor to consider is the low precipitation and stream water sampling frequency (weekly). *Birkel et al.* [2012] pointed out that weekly isotope observations will produce less certain TTDs estimates compared to shorter sampling intervals because information of temporal dynamics in the time series is lost. In our study, this happened due to averaging (precipitation) and due to time gaps (stream). Therefore, the already low isotope dynamics in the groundwater-influenced time series were further reduced due to the low sampling rate. The stream isotope simulation results generally showed less variability than the observed isotope time series (Figure II.7). This can be explained by a missing dominant process in our model, accounting for e.g. surface-runoff. However, we believe that the loss of temporal information due to the weekly sampling interval and the difference between average (precipitation) and grab (discharge) samples is the main reason for reduced variability in our simulation results.

The model parameter responsible for routing a certain percentage of precipitation through the fast reservoir (ϕ) showed good agreement with the percentage of riparian zone in each subcatchment, with the exception of location 5. We therefore assumed the TPLR's fast reservoir to be a good conceptualization of the riparian zone and that the slow reservoir represents the hillslopes. A possible explanation for the bigger deviation in location 5 is that the subsurface extent of its subcatchment could actually be larger than the topography derived subcatchment area. The difference could also be explained by the fact that we used a single flow direction algorithm for catchment boundary delineation. This algorithm assumes that subsurface flow only occurs in the steepest downslope direction, while a multiple flow direction algorithm allows for subsurface flow in all downslope directions [*Jenson and Domingue*, 1988]. Nonetheless, the good agreement between ϕ and a measurable catchment characteristic indicates, if not necessarily quantitatively, but qualitatively correct results. Thus,

we conclude that we were able to determine TTDs of ungauged stream locations to a mostly satisfying degree.

II.5.2 Spatial variability of TTDs

Calculation of the 15 different TTDs yielded spatial information about the Wüstebach catchment, revealing possible sources of stream water. Overall, the outlet integrated the different TTDs observed in the Wüstebach catchment. Similar findings for the RTDs of nested catchments (ranging in size from 0.09 to 62.42 km²) have been found in *McGuire et al.* [2005]. Locations that showed short MTTs and stronger dynamics in their seasonal stream isotope signal were most likely influenced by younger water. These locations usually had higher contributions of riparian zone in their respective subcatchments (e.g. locations 1, 2 and 8) as water can be routed fast through constantly saturated or near-saturated soil. Contrary to this, locations with longer MTTs (e.g. locations 3, 12 and 15) had less riparian zone contribution and less dynamics in their stream isotope signal. As location 3 receives its water from an old, artificial groundwater catchment system, we surmise that the sources of water of the other less dynamic time series locations are most likely groundwater too. The relationship between topographic indices and MTTs found in previous studies (e.g. [*Tetzlaff et al*., 2009b]) can be explained by the fact that topography is often a major influence on the distribution of saturated zones and thus the distribution of riparian zones and hillslopes [*Grabs et al*., 2009]. Comparing the TTDs of the main stream locations (1, 2, 4, 6, 10, 11 and 14) and tributaries we found that most main stream locations TTDs plotted quite close to each other (the exception being locations 1 and 2, see Figure II.8a). The reason could be that the subcatchments of the main stream are nested, with major parts of downstream subcatchments consisting of upstream subcatchments, and thus not independent from each other. The tributary TTDs on the other hand are more divergent from each other, as their subcatchments

are more distinct and separate. This can also be seen in the percentage of riparian zone of each tributary, where we found more variation than for main stream locations (Figure II.10a).

II.5.3 Can we explain the spatial variability of TTDs with catchment characteristics?

We found a negative correlation between the percentage of riparian zone and the MTT, as was already shown for mesoscale catchments [*Tetzlaff et al.*, 2009a]. Similar to *McGuire et al.* [2005], we could not find a correlation between TTDs and the subcatchment size. What becomes apparent, however, is a relationship between subcatchment area and MTT for the main stream locations (Figure II.10b). As already mentioned above, in the case of mainstream locations major parts of downstream subcatchments consist of upstream subcatchments, which could explain the observed relation between subcatchment size and MTT. Also, the tributaries and groundwater-influenced locations seemed to group together individually. However, it generally becomes apparent that at the small catchment scale it is also not the catchment size that has an influence on TTDs but flow path distributions governed by topography and soil cover, as has already been shown for mesoscale catchments before [*Asano and Uchida*, 2012; *Tetzlaff et al.*, 2009a].

The shorter transit times in the riparian zone and the longer transit times in hillslope regions could be an explanation for the 'old water phenomenon', where it was shown that most storm flow events mainly consist of old water, although the storm events deliver considerable runoff amounts [*Pearce et al.*, 1986]. Fast transport mechanisms of storm water volumes are still under debate, for example immobile water increasing the water age of the mobile phase in *Duffy* [2010]. *Kirchner* [2003] summarized the old water phenomenon together with a chemical phenomenon by asking (a) how a catchment can store old water for a long time and then quickly release it during a storm and (b) how at the same time the chemistry of base flow and storm flow differ, although they both are mostly comprised of old water. As it was

suggested in other studies (e.g. [*Inamdar and Mitchell,* 2007; *Jencso et al.*, 2010; *McGlynn and Seibert* [2003]; *Ranalli and Macalady*, 2010]) we also hypothesize that the riparian zone in the Wüstebach catchment is buffering water that stems from the hillslopes. We see from the TTDs that the transport through the soil matrix of the hillslopes is slow and leads to attenuated isotope signals. Therefore, the water has time to age before it reaches the saturated riparian zone via lateral flow pathways. During rainfall events, the resulting pressure wave (RTD) pushes the old water out of the riparian zone, creating the event hydrograph reaction. Thus, old water gets activated fast during an event as it does not need to travel far. A certain amount of event water will also discharge along more direct flow paths (overland flow, lateral preferential flow). This event water creates different chemical compositions in the stream. The remaining portion of event rainfall that follows slow flow paths (e.g. soil matrix) is at first new water that will eventually become old water over the course of its travel. When it eventually reaches the riparian zone, it will be stored and activated at the next event.

Alternative explanations of the 'old water phenomenon' suggested in previous studies include activation of pre-event water as overland and subsurface storm flow [*Kienzler and Naef*, 2008] and rapidly rising groundwater reaching soil horizons of high lateral conductance [*Bishop et al.*, 2004]. We ruled out both hypotheses in the case of the Wüstebach catchment, as there was no significant overland flow during the simulation period, while recently available, preliminary observations of groundwater levels do not indicate a rise to soil layers of significant lateral transport capabilities.

Indications of the riparian zone's soil water being old water from the hillslopes were found in a comparison of the main stream isotope time series of the individual stream locations (not shown). In the scenario of the riparian zone's water actually being relatively young water, every main stream location should show higher amplitudes in their isotope signal during the

dry state, taking into account that only the fast-reacting riparian zone remains hydrologically connected. However, we observed diminishing amplitudes in the stream isotope signals downstream from the spring, with location 1 and 2 showing high amplitudes and subsequent locations lower ones. This indicates the existence of old water in the riparian zone. The riparian zone fraction to the respective catchment area decreases downstream from 32% (location 1, spring) to 13% (location 14, outlet), and consequently the potential contributions of old water from hillslopes to the riparian zone via slow pathways originating from wet states increases. This explains the decrease in the amplitudes of the isotope tracer signals during the dry states observed at downstream locations, as each downstream location's riparian zone collects water from a larger fraction of hillslope. This also implies that the isotopic composition of the riparian zone is not spatially uniform, but that there is a gradient downstream towards more groundwater-like isotopic signatures.

II.5.4 Limitations

A limitation of our proposed method is the assumption that p_{eff} is spatially homogeneous for a small scale catchment. Small catchments with different land use types, e.g. forest and bare soil, would have spatially heterogeneous evapotranspiration characteristics and thus not a uniform p_{eff}. We assume that a small number of deviations in the p_{eff} time series, e.g. due to localized storm cells, will have minimal effect on a weekly stream isotope time series where simulation results tend to focus on long-term trends. In our study there was only one event in two years which we assumed to be a localized convective storm cell. However, in case of systematic deviations we expect a non-negligible error in TTDs estimates. The catchment also needs to be sufficiently small to justify this assumption. We suggest a range of maximum catchment sizes between 1 to 5 km², keeping in mind that this may depend on climate and other factors, e.g. the extent of uniform vegetation cover.

Judging by the good NSE values, we saw that the p_{eff} time series derived from the outlet seemed to work for location 1, which is one of the furthest locations from the outlet (Figure II.1). Thus, it seems that for the small and comparably homogeneous Wüstebach catchment the assumption of p_{eff} is valid.

II.6 Conclusions

We have presented a method to calculate TTDs for gauged and ungauged stream locations using the conceptual model TRANSEP, given that p_{eff} is spatially uniform. The modeling of the isotope time series was only possible with information gained by the dense measurement network available at this study site. We found a critical mean soil water content of 35 Vol.% where the catchment switches between two different hydrological behaviors. This closely resembles the partial-area contribution concept by *Dunne and Black* [1970], who observed such a behavior for single storm events. TTDs modeling results were generally solid, with exceptions though, and supported by comparing the model parameter of fast reservoir contribution to the measurable proportion of the riparian zone in each subcatchment. Results suggested that fast flow paths are more often activated in the riparian zone compared to hillslopes, as the riparian zone is more often well saturated. RTDs indicated that hillslopes become hydrologically disconnected during dry states. We found that even in small catchments like the Wüstebach (38.5 ha) the MTTs were closely linked to the surface area of riparian zone and not to the size of its subcatchments. The different hydrological behavior of riparian and hillslope areas may prove to be instrumental in explaining the amount of old water that gets activated during storm events, which is often observable in tracer studies.

III. Interception effects on stable isotope driven streamwater transit time estimates

Modified on the basis of

Stockinger, M. P., A. Lücke, J. J. McDonnell, B. Diekkrüger, H. Vereecken, and H. R. Bogena (2015), Interception effects on stable isotope driven streamwater transit time estimates, Geophys Res Lett, 42(13), 5299-5308.

III.1 Introduction

The stable isotopes of water (δ^2H and $\delta^{18}O$) are conservative tracers of water movement. Many studies have used them for estimating the mean transit time (MTT) of precipitation through a catchment and the respective streamwater transit time distribution (TTD) [*McGuire and McDonnell*, 2006]. Recently, much work focused on the relation between the TTD and catchment characteristics [*Hrachowitz et al*., 2009a; *Tetzlaff et al*., 2009b], on the time-varying nature of transit times [*Heidbüchel et al*., 2012; *Rinaldo et al*., 2011], on incomplete mixing of tracer signals in the soil [*Brooks et al*., 2010] and on differences in transit times of precipitation, resident soil water, groundwater and streamwater [*Botter et al*., 2011; *Hrachowitz et al*., 2013a].

Most studies of TTD to date have assumed that precipitation δ^2H and $\delta^{18}O$ is unaffected by passage through the vegetation canopy to the soil surface. However, forest canopies affect precipitation by interception, reducing the total volume of precipitation by evaporation, thus generating throughfall (TF). Interception, canopy evaporation and drip occur mainly on leaves and can change the stable isotope tracer signal of water reaching the forest floor via isotopic fractionation [*Cappa et al*., 2003]. The infiltrating TF can therefore be isotopically enriched compared to open precipitation (OP) [*Dewalle and Swistock*, 1994].

Previous studies that have investigated the differences between TF isotope composition (δTF) and OP isotope composition (δOP) have focused on (a) isotopic enrichment during canopy evaporation and subsequent canopy drip [*Saxena*, 1986]; (b) complete evaporation of residual interception water after the secession of rainfall, taking into account the temporally non-uniform isotope signal of single precipitation events [*Berman et al*., 2009; *Celle-Jeanton et al*., 2004; *Saxena*, 1986]; (c) isotopic exchange with ambient air vapor [*Brodersen et al*., 2000];

(d) rainfall partitioning processes within the canopy [*Kato et al*., 2013] and (e) mixing with residual canopy water of a prior rainfall event [*Allen et al*., 2014].

In a hydrograph separation study *Kubota and Tsuboyama* [2003] measured δTF and found a difference of up to 10% in the estimation of 'old water' in runoff when compared to δOP. *Asano et al*. [2002] used δTF for the study of MTT in a forested catchment in Japan. However, no studies have yet compared the streamwater TTD model estimates when using δTF instead of δOP as tracer input.

Here we investigate the differences in streamwater TTD estimates emerging with δTF versus δOP as input to the TTD model. We focus on the well-studied forested Wüstebach catchment, Germany. Specifically, we address the following research questions: (1) How and to what extent are TTDs altered by using δTF instead of δOP? (2) How does spruce forest canopy influence precipitation water volume and isotope composition of water that makes its way to the forest floor? (3) Is a simple correction factor for δOP able to adequately represent canopy influence in a TTD model?

III.2 Methods

III.2.1 Study Site

The Wüstebach headwater catchment (38.5 ha) is located in Germany (50° 30′ 16′′N, 6° 20′ 00′′E, WGS84) at 595 to 628 m above sea level (asl.). The climate is humid temperate with mean annual precipitation of 1107 mm (1961–1990) and a mean annual temperature of 7°C [*Zacharias et al*., 2011]. The Wüstebach test site is part of the Lower Rhine/Eifel Observatory of the Terrestrial Environmental Observatories (TERENO) network. The catchment is located in the Eifel national park and was homogeneously afforested after World War II with Norway spruce (*Picea abies*) and Sitka spruce (*Picea sitchensis*) [*Etmann*, 2009]. The bedrock

consists of Devonian shale with sporadic inclusions of sandstone [*Richter*, 2008]. Soils are up to 2 m deep with an average depth of 1.6 m [*Graf et al.*, 2014]. Food and Agriculture Organization (FAO) soil types of cambisol and planosol/cambisol are found on hillslopes, while gleysols, histosols and planosols are found in the riparian zone. The catchment had a manmade structure (since World War II) that consisted of a pipe that routed groundwater from a groundwater spring located in the catchment directly downstream to the stream, enabling a portion of catchment groundwater to bypass the soil matrix. This pipe was shut down in Spring 2011. In September 2013, 9 ha were clear-cut as part of the national park development [*Bogena et al.*, 2015] (Figure III.1).

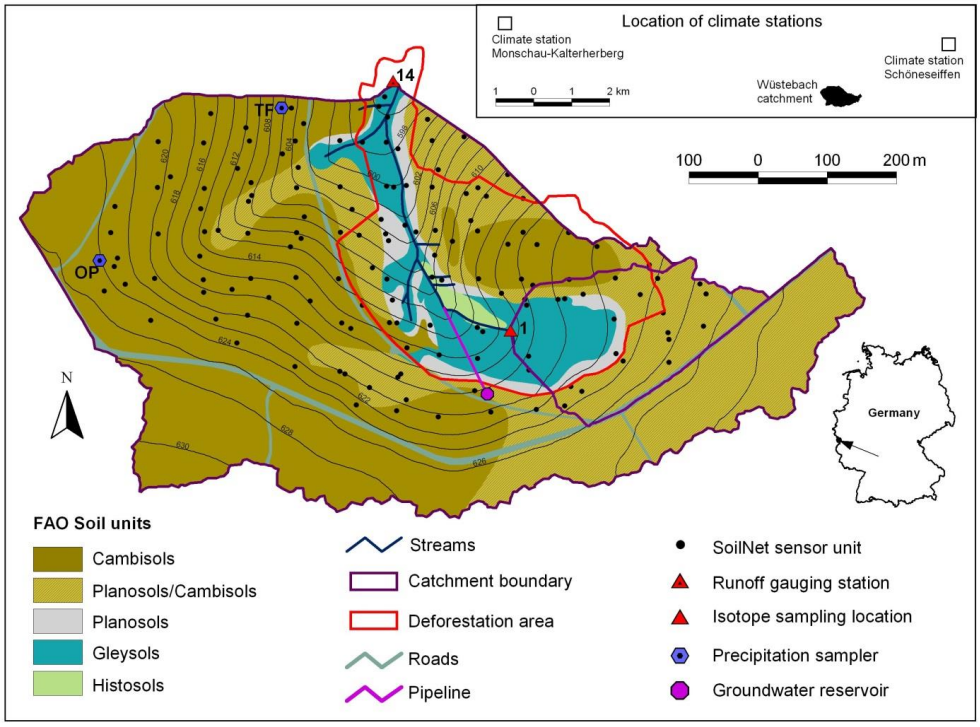

Figure III.1. The Wüstebach test site (38.5 ha) with soil types and contour lines. Also shown are the subcatchment area of location 1 (violet, thick outline), the deforestation area (red outline), the groundwater reservoir and transport pipeline and the location of the TF and on-site OP samplers. Inset displays relative location of the test site to the climate stations Kalterherberg and Schöneseiffen.

III.2.2 Measured Data

We used hydrological measurements and isotope data from 3rd October 2012 to 21st April 2014. TF was measured with six TF samplers (RS200, UMS GmbH, Germany). The TF sampling approach followed World Meteorological Organization [*WMO*, 2008] specifications. Each sampler consisted of a 50 cm pipe (diameter: 20 cm) buried in the forest soil (30 cm), and a 100 cm pipe with a collection funnel (area: 314 cm²) inserted on top (Appendix Figure A1). To protect against litterfall, a metal mesh with 5 mm diameter holes was placed in the funnel. TF was led via a plastic hose (inner diameter: 4 mm) to a sample bottle inside the buried pipe to prevent evaporation losses. The funnel outlet was covered by a table tennis ball as an additional barrier against evaporation. The samplers were placed 2 m from tree trunks at a 2 m spacing (Appendix Figure A1). The spatial representativeness of the sampled TF volumes was tested by comparing them to TF volumes of a second TF sampling system operated by the University of Trier in a distance of 50 m. However, due to a lack of protective measures against evaporation this system was inappropriate for isotope sampling and thus no further data of it was used in this study (Appendix Figure A2).

In May 2013, two OP samplers were installed in a small clearing in the Wüstebach catchment, measuring OP on-site for 11 months. Due to the shortness of this time series, we did not use them for TTD estimation, but only for the calculation of interception loss (difference of OP to TF) and the differences between δTF and δOP.

OP volume used as model input was acquired at 1 hour intervals in 0.1 mm increments from the Kalterherberg meteorological station (German Weather Service, station number 80115, 535 m asl.) located 9 km northwest of Wüstebach. The Kalterherberg data was validated for Wüstebach by regression to the on-site OP measurements of the clearing and to precipitation data from a rain gauge (Pluvio^2, Ott, Kempten, Germany) installed in the clear-cut area of

Wüstebach (available from January 2014 onwards). Model input δOP was acquired from a site 3 km to the NE at the Schöneseiffen meteorological station (620 m asl.). This site has a time series of weekly isotope samples available from 2009 to the present.

δTF and δOP (onsite, Figure III.1) were collected in weekly intervals. Due to organizational and technical issues, deviations from routine sampling occurred leading to shortest and longest intervals being 4 and 35 days, respectively. We measured water volumes of all TF and OP samplers (6 under canopy, 2 in clearing) in 10 ml increments (50 ml increments from 18th December 2012 to 1st August 2013) and took samples for isotope analyses in 50 ml HDPE bottles. Field experiments with the TF samplers using water of known isotopic value showed no significant evaporative enrichment of isotope values over a 21 day period (see Appendix for details). To calculate precipitation volume (mm) we used the arithmetic mean of all TF and OP samplers, respectively, while the volume-weighed mean was calculated for isotope values. During four sampling weeks needle litter blocked the TF system, which led to standing water pools in the funnels. Consequently, these weeks were not considered in the further analyses.

Water isotopic analysis was carried out using an Isotope-Ratio Mass Spectrometer (IRMS, Delta V Advantage, Thermo Scientific) coupled with a high temperature pyrolysis furnace (HT-O, HEKAtech). Results are reported as δ-values relative to Vienna Standard Mean Ocean Water (VSMOW) [*Gonfiantini*, 1978]. Internal standards calibrated against VSMOW, Standard Light Antarctic Precipitation (SLAP2) and Greenland Ice Sheet Precipitation (GISP) were used to ensure long-term stability of analyses. The precision of the analytical system was ≤ 0.1 ‰ for $\delta^{18}O$ and ≤ 1.0 ‰ for $\delta^{2}H$.

III.2.3 TTD calculation

We used the conceptual model TRANSEP [*Weiler et al.*, 2003] for TTD estimation. TRANSEP uses the convolution integral to calibrate effective precipitation p_{eff} by simulating the outlet's hydrograph:

$$Q(t) = \int_0^t g(\tau_R) p_{eff}(t - \tau_R) d\tau_R \quad \text{(III.1)}$$

where $Q(t)$ is the simulated runoff, $g(\tau_R)$ is the Response Time Distribution (RTD), τ_R is the response time and $p_{eff}(t - \tau_R)$ the effective precipitation for time step t - τ_R. According to catchment-wide wetness conditions the hydrograph was split into three modeling periods (Winter 2012, Summer 2013 and Winter 2013). The winter periods represent the catchment's wet state, whereas the summer period represents the dry state. Calculation of p_{eff} during dry state was based on a reduced runoff-generating area, representing hydrological disconnection of the Wüstebach's hillslopes from the runoff generation process (for more details see *Stockinger et al*. [2014]). Using p_{eff} and a 2-year spin-up with mean values of all model input variables, TTDs were inferred by simulation of observed streamwater isotope composition using the convolution integral:

$$C(t) = \frac{\int_0^t C_{in}(t-\tau_T) p_{eff}(t-\tau_T) h(\tau_T) d\tau_T}{\int_0^t p_{eff}(t-\tau_T) h(\tau_T) d\tau_T} \quad \text{(III.2)}$$

where $C(t)$ is the stream water isotope concentration at time t, $C_{in}(t-\tau_T)$ is the precipitation isotope concentration at time t with travel time τ_T and $h(\tau_T)$ is the TTD.

RTD and TTD were estimated using the Two Parallel Linear Reservoir (TPLR) method, as it produced good results of TTD estimates for the Wüstebach (*Stockinger et al*. [2014]):

$$g(\tau_R) = \frac{\phi}{\tau_f} \exp\left(-\frac{\tau_R}{\tau_f}\right) + \frac{1-\phi}{\tau_s} \exp\left(-\frac{\tau_R}{\tau_s}\right) \quad \text{(III.3)}$$

$$h(\tau_T) = \frac{\phi}{\tau_f}\exp\left(-\frac{\tau_T}{\tau_f}\right) + \frac{1-\phi}{\tau_s}\exp(-\frac{\tau_T}{\tau_s}) \quad \text{(III.4)}$$

where ϕ is a partitioning factor (between 0 and 1) and τ_f and τ_s are the mean transit times of the fast and slow reservoir, respectively.

We used the Volumetric Efficiency (VE) ranging from 0 to 1 (1 indicating a perfect fit) as an objective function for hydrograph simulation, as it equally weighs the simulation quality of baseflow and storm event conditions. In addition, the Nash-Sutcliffe Efficiency (NSE) was used to ensure that temporal stream isotope dynamics are adequately captured [*Criss and Winston*, 2008; *Nash and Sutcliffe*, 1970]:

$$VE = 1 - \frac{\sum|Q_{sim} - Q_{obs}|}{\sum Q_{obs}} \quad \text{(III.5)}$$

$$NSE = 1 - \frac{\sum(C_{obs} - C_{sim})^2}{\sum(C_{obs} - \overline{C_{obs}})^2} \quad \text{(III.6)}$$

The parameter space was searched using the Ant-Colony Optimization (ACO) algorithm [*Abbaspour et al.*, 2001]. Parameter uncertainties for stream isotope simulation results and TTD estimates were obtained by using the 95%-confidence limits of the posterior parameter distribution based on the last third of parameter sets used by ACO. The obtained 95%-confidence limits were then used as parameter boundaries for 1000 Monte Carlo (MC) simulations (MATLAB toolbox "MCAT v.3) and we plot the minimum and maximum stream isotope and TTD values found by all 1000 MC runs. The given stream isotope uncertainties are the measurement precision of the IRMS.

As the outlet (location 14, Figure III.1) showed an attenuated isotope signal, we additionally simulated *C(t)* of the isotopically more dynamic spring (location 1) to further explore differences in simulation results when using δOP or δTF. To do this, we used the outlet-calibrated p_{eff} with stream isotope data of the spring with Equation III.2. TTDs were compared

by evaluating the absolute and relative changes in transit time at 10-, 25-, 50-, 75- and 90-quantiles, respectively, as well as identifying the maximum change in TTD. This was done to compare the behavior of both TTD curves for shorter and longer transit times.

To test if missing δTF data in TTD estimation can be approximated with an ordinary δOP correction approach, we used a general factor of 0.5‰ added to the measured $\delta^{18}O$ values of δOP as a means to account for canopy influence (δOP_{corr}). This factor was already used for isotope modeling of the Wüstebach catchment by *Stockinger et al*. [2014] for a period where no δTF data was available. Its value was found empirically through inverse modeling and it produced a better fit of observed stream isotope values than δOP.

III.3 Results & Discussion

Comparison of OP volume from the Kalterherberg rain gauge with the two on-site measured precipitation time series showed strong agreement (R^2 = 0.96 with 95%-significance p = $1.8*10^{-9}$ and R^2 = 0.92 with p = $4.3*10^{-21}$). Both regressions were close to the 1:1 line (slopes = 0.95 and 1.06), indicating that the Kalterherberg station represents reliable OP input data for hydrological modeling of the Wüstebach. This was further supported by the almost complete closure (>97 %) of the Wüstebach catchment water balance for a period of 3 years when using Kalterherberg station data [*Graf et al.*, 2014].

III.3.1 Interception effects on throughfall

The time series of model input δOP and δTF showed a typical seasonal isotope signal (Appendix Figure A5), with measured $\delta^{18}O$ variations ranging from -16.40 to -2.77 ‰ in δOP and from -14.27 to -3.04 ‰ in δTF. The absolute difference between δOP and δTF ranged between –0.98 and +1.29 ‰ $\delta^{18}O$ and –8.20 and +11.50 ‰ $\delta^{2}H$. These differences are comparable to those found in a similar study by *Dewalle and Swistock* [1994].

TF volume increased with increasing OP volume with a slope of 0.77 and $R^2 = 0.92$ (n = 35, Appendix Figure A6). *Peng et al*. [2014] found similar results in a Qinghai spruce forest and argued that the deviation from a slope of 1 was indicative of evaporative influence in the canopy. During the observation period, the measured average interception loss due to canopy evaporation was 41% with a standard deviation of 19%. This is consistent with *Brodersen et al*. [2000] who observed approx. 40% interception loss for a 130-170 year old spruce stand in the Black Forest, Germany. Similar to their study, no clear seasonal variations in interception loss or in isotopic changes between δOP and δTF were found in the present study. This can be explained by the different processes that induce isotopic changes (e.g., evaporation, mixing with residual canopy storage water) and by the weekly bulk samples, which aggregate different events.

III.3.2 How did throughfall isotope composition affect stream isotope simulation?

TRANSEP simulations using $\delta^{18}O$ of δOP as input (results for $\delta^{2}H$ as well as details on hydrograph simulation are shown in the Appendix) were not able to adequately reproduce observed stream isotope values (Figure III.2b, c) as indicated by low NSE values (0.44 for location 1 and 0.22 for location 14, respectively). When using δOP_{corr}, NSE values increased to 0.67 (location 1) and 0.33 (location 14), and for δTF simulations NSE values reached 0.61 (location 1) and 0.33 (location 14).

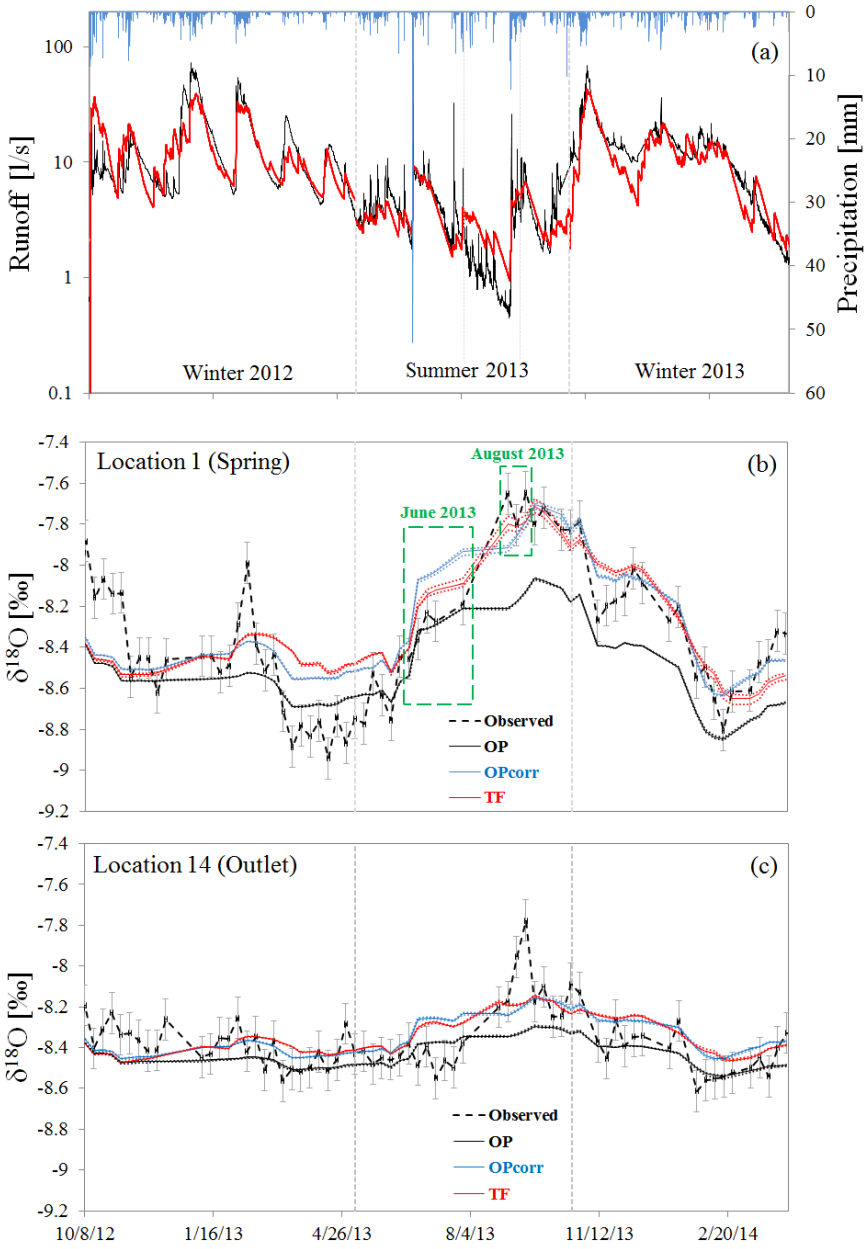

Figure III.2. (a) Rainfall (blue bars from top) and observed runoff (black) together with simulated (red) runoff from hydrograph simulation in logarithmic scale for the three modeling periods. (b) and (c) Stream isotope simulation results for location 1 (spring) and location 14 (outlet) based on $\delta^{18}O$. Observed stream isotopes with grey error bars compared to simulations using δOP, δOPcorr, and δTF.

Uncertainty boundaries are shown as dashed lines. Vertical, light grey dashed lines in all panels separate the three modeling periods, with thinner lines in Figure III.2a delineating the deforestation period. Green rectangles in Figure III.2b are discussed in the main text.

Generally, the obtained NSE values are similar to results of previous studies simulating $\delta^{18}O$ and $\delta^{2}H$ for stream ([*Birkel et al*., 2010]; [*Birkel et al*., 2011b]) and soil water ([*Windhorst et al.*, 2014]). While an NSE value of 0.33 is certainly low, it can be attributed to the emphasis of the NSE to time series peaks [*Criss and Winston*, 2008] and the attenuated tracer signal of location 14. For location 1 it can be observed that the second half of the time series was better modeled (NSE = 0.84) than the beginning (NSE = 0.05). The worse performance during the first half can be attributed to the incorrect input data of the spin-up, i.e., using mean values for all input variables. This also explains the almost non-existent parameter uncertainty bands in the first half of the time series. The second half of the time series does not have this issue as can be seen in the drastically increased model performance and the widening of the parameter uncertainty bands.

The difference between δOP and δTF results is especially prominent for location 1 (Figure III.2b). Here, the simulation result of δOP mostly underestimated observed isotope values in the second half of the time series. In contrast, δTF results simulated this part considerably better. We attribute the deviation of δOP results from observed values to its inadequacy as an input variable for a forested catchment.

Comparing results for δOP_{corr} and δTF, we found most pronounced differences for the Summer 2013 seasonal isotope peak of location 1 (Figure III.2b). Isotope simulation results based on δOP_{corr} showed higher isotope values in June 2013 as compared to results derived with δTF. δOP_{corr} overestimated observed values while δTF performed better (Figure III.2b, green rectangle “June 2013”). Another example of the overall better performance of δTF is

the August 2013 peak (Figure III.2b, green rectangle "August 2013"). This peak was only reproduced by the isotope simulation using δTF, but not using δOP_{corr}. In both cases, results based on δTF were closer to observed isotope values. However, the similar NSE values of both inputs indicate that δOP_{corr} can produce comparable stream isotope results.

Thus, regarding the stream isotope simulation, δOP_{corr} may serve as a plausible surrogate for missing δTF data. We note that the correction factor depends on site specifics such as climate conditions or vegetation type. For instance, *Calderon and Uhlenbrook* [2014] accounted for δTF enrichment in a tropical forest by adding 1.4‰ to isotope values, while *Stockinger et al*. [2014] applied a simple correction factor of adding 0.5‰ for the humid Wüstebach site.

Since no seasonal trend in isotopic changes was found for the Wüstebach catchment, a constant correction factor for δOP_{corr} seems appropriate. However, for locations showing strong seasonal trends, a time-varying correction factor might be necessary. Further studies investigating the need for a time-varying correction factor are needed to address this issue.

III.3.3 How did throughfall isotope composition affect estimated TTD?

We found generally decreasing transit times for most quantiles when using δTF instead of δOP (Figure III.3, Table III.1). These changes were much more pronounced for δ^2H results, while $\delta^{18}O$ results showed only minor changes or no changes at all in the case of location 1. The maximum absolute difference in cumulative TTDs were observed when using δ^2H with 7.5% occurring at 208 days transit time for location 1, while for location 14 it was 7.3% occurring at 145 days transit time (Figure III.3c). The corresponding change in transit time was 119 days for location 1, and 85 days for location 14, respectively. Thus, for the Wüstebach differences of approximately 2-4 months in transit times are possible. Similar results were found in a Cl^--tracer study of *Hrachowitz et al*. [2013a]. The differences in their

study were caused by evaporative removal of young water from the interception storage leading to a change in tracer signal by evapoconcentration [*Harman*, 2015]. Given the overall differences between the obtained TTDs, the behavior of the catchment would be poorly characterized when using δOP.

While $\delta^{18}O$ and $\delta^{2}H$ gave different results for δOP, the TTDs from both isotopes converge for δTF for both locations. For location 1, the uncertainty bounds of the δTF-TTDs overlap with δOP-TTDs diverging from each other, while for location 14 δTF-TTDs plot closer together than for δOP. Considering that isotopic fractionation during evaporation is more pronounced for $\delta^{2}H$ than for $\delta^{18}O$, we hypothesize that the lack of accounting for canopy evaporation could be the reason for the spread of δOP-TTDs. This effect would also explain differences in hydrograph separation observed by *Lyon et al*. [2009] for oxygen and hydrogen stable isotopes [*Birkel et al*., 2012]. Thus, when using incorrect input data for a forested catchment (δOP), the choice of isotopic tracer strongly influences TTD results. Only δTF converges to approximately the same solution.

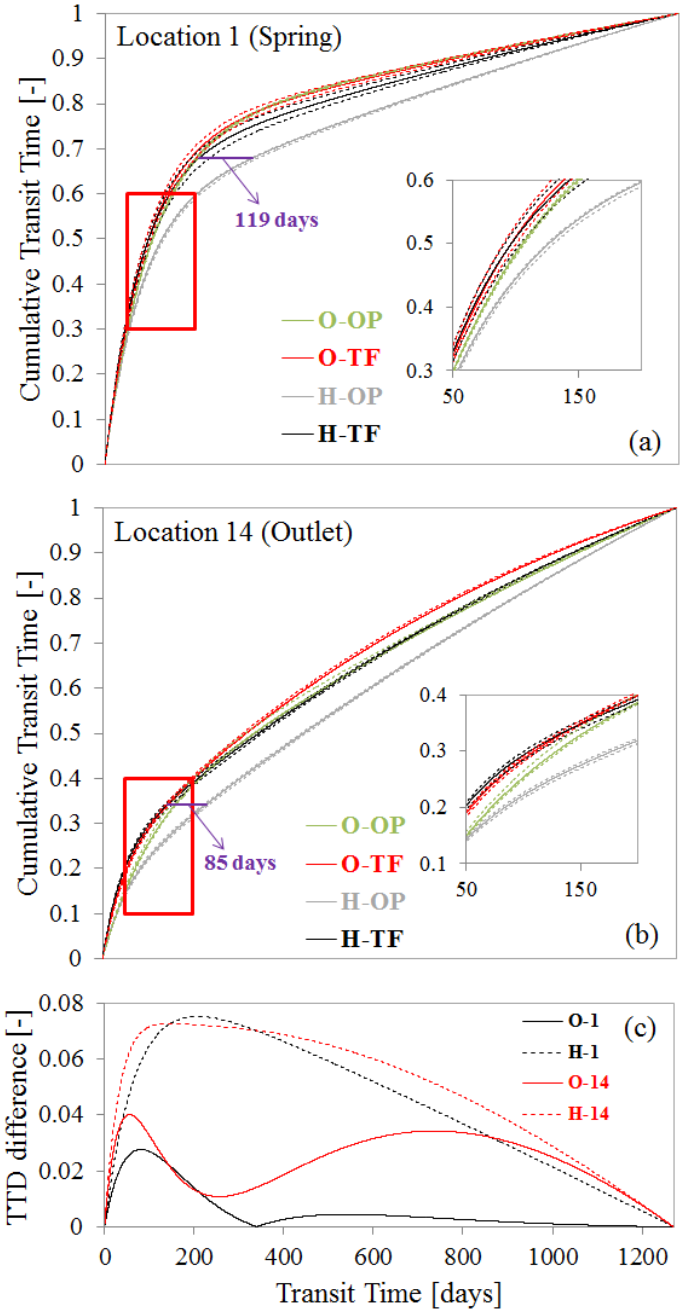

Figure III.3. TTDs derived by using δOP and δTF and isotope tracer data of either $\delta^{18}O$ (O-OP and O-TF) or $\delta^{2}H$ (H-OP and H-TF) for (a) the spring (location 1) and (b) the outlet (location 14).

Uncertainty boundaries are displayed as dashed lines. The violet line shows maximum change in transit time, and the insets highlight details of areas marked with red rectangles. (c) Absolute differences of cumulative TTDs (δOP-δTF) as a function of transit time.

Table III.1. Quantile transit times of the cumulative TTDs for location 1 and 14 using δOP, δOP_{corr} and δTF. Differences in transit time and percentage change (in brackets) shown for comparison of δOP with δOP_{corr} ($\Delta\delta OP_{corr}$) and of δOP with δTF (ΔδTF).

$\delta^{18}O$	**Quantile Transit Time of Cumulative TTD [days]**				
	10%	**25%**	**50%**	**75%**	**90%**
	Location 1				
δOP	14	40	106	280	761
δOP_{corr}	13	37	94	209	486
δTF	13	36	96	273	774
	Location 14				
δOP	31	98	336	755	1053
δOP_{corr}	23	76	256	590	917
δTF	22	78	318	692	1001
	Location 1				
$\Delta\delta OP_{corr}$	-1 (-7)	-3 (-8)	-12 (-11)	-71 (-25)	-275 (-36)
ΔδTF	-1 (-7)	-4 (-10)	-10 (-9)	-7 (-3)	13 (2)
	Location 14				
$\Delta\delta OP_{corr}$	-8 (-26)	-22 (-22)	-80 (-24)	-165 (-22)	-136 (-13)
ΔδTF	-9 (-29)	-20 (-20)	-18 (-5)	-63 (-8)	-52 (-5)
$\delta^{2}H$	**Quantile Transit Time of Cumulative TTD [days]**				
	10%	**25%**	**50%**	**75%**	**90%**
	Location 1				
δOP	14	42	127	501	944
δTF	12	35	97	327	839
	Location 14				
δOP	31	126	445	827	1084
δTF	19	72	346	745	1040
	Location 1				
ΔδTF	-2 (-14)	-7 (-17)	-30 (-24)	-174 (-35)	-105 (-11)
	Location 14				
ΔδTF	-12 (-39)	-54 (-43)	-99 (-22)	-82 (-10)	-44 (-4)

We found variations in TTD quantiles ranging from 1 to 275 days transit time for both locations (Table III.1, Figure III.3a and b, Appendix Figure A9 for δOP_{corr}-TTD). Using δOP_{corr} resulted in vastly different TTDs compared to δTF results. This affects the interpretation of e.g., the relationships between catchment characteristics and TTDs. Thus, contrary to stream isotope simulation, the applied simple TF correction factor is not sufficient for streamwater transit time estimates. Undoubtedly, measurement of δTF is necessary to improve TTD estimates of forested catchments (e.g., for the TTD studies of *Timbe et al*. [2014] and *Heidbüchel et al*. [2012], conducted in forested or partly-forested catchments).

The TTD is not directly measurable with current technologies. Thus it is necessary to ensure that TTD estimates are as correct as possible. Our results show that the TTD is more reliable when using δTF instead of δOP. As the hydrological community currently faces the challenge of predicting the hydrology of ungauged catchments by e.g., utilizing catchment characteristics to estimate MTTs [*Hrachowitz et al*., 2013b], it is very important to use TF in forested catchments. Therefore, we recommend using δTF instead of δOP to derive improved TTD estimates in forest hydrological studies. However, if δTF measurement is not possible, stable isotope driven TTD studies might benefit from an empirical calibration of δOP_{corr} with the initial assumption of an overall enrichment in the isotopic composition of δOP in temperate forests.

Our findings are relevant for forested catchments where isotopic fractionation due to interception occurs and is not implicitly considered in the model. This is regardless of catchment size when using spatially uniform input data, as is often done in the convolution integral approach [*McGuire and McDonnell*, 2006]. In the case of partially forested catchments, land cover information could be used to weigh TF and OP.

III.4 Conclusions

We compared δTF and δOP in TTD modeling for the spruce covered Wüstebach catchment in Germany. Calculated transit times were reduced when using TF for both tracers $\delta^{18}O$ and $\delta^{2}H$ by up to four months (119 days). The difference in cumulative TTD was 7.5%. While the quality of the stream isotope simulations varied significantly within TRANSEP, the results were always weaker when using δOP. We conclude that consideration of the effects of interception on δOP is important for accurate TTD estimation of forested catchments. This demands the inclusion of TF measurements in the design of hydrological sampling campaigns in forested catchments. Our results further suggest that if no TF measurements are available, a simple correction of precipitation data could lead to improved isotope modeling results. More studies are needed that investigate the actual effects of canopy-induced changes on δOP on hydrological modeling results, e.g., under different vegetation types or climatic conditions, and for different temporal resolutions.

IV. Influence of temporal resolution of tracer data on estimates of streamwater transit time distributions

On the basis of the manuscript

Stockinger, M. P., H. R. Bogena, A. Lücke, B. Diekkrüger, T. Cornelissen and H. Vereecken

manuscript in preparation

IV.1 Introduction

Many studies of transit time distributions (TTDs) of a catchment used weekly sampling intervals for chemical [*Hrachowitz et al*., 2009a; *Tetzlaff et al*., 2007] and isotopic tracer data [*Rodgers et al*., 2005; *Stockinger et al*., 2014; *Viville et al*., 2006]. Only few studies applied data with a higher temporal resolution [*Kirchner et al*., 2000; *Roa-Garcia and Weiler*, 2010]. Using high resolution data for event modeling only, *Roa-Garcia and Weiler* [2010] found evidence of time-variable Mean Transit Times (MTTs) when looking at event and base flow conditions. *Birkel et al*. [2012] refined this knowledge by estimating TTDs of a one year long time series applying daily $\delta^{18}O$ and $\delta^{2}H$ precipitation and weekly, daily and 4h (during two events) stream flow data, respectively. They found evidence for time-variable TTDs with summer and winter runoff events differing in MTTs. Consequently, *Birkel et al*. [2012] argue for the value of high-frequency sampling and that it can help to evaluate the feasibility of MTTs derived with data sets of e.g., weekly sampling intervals. This argument is supported by findings of *Berman et al*. [2009], who found fine-scale changes in the isotopic composition of precipitation measuring up to 90 samples per day. Additionally, the need for high-resolution tracer data to move forward in the hydrological sciences was recently emphasized [*McDonnell and Beven*, 2014].

Studying a tropical catchment, *Timbe et al*. [2015] compared different sampling resolutions of stable isotope data ranging from daily to bimonthly and found that it affected estimates of TTDs for soil and stream water. However, in their study the case of daily sampling intervals was based on daily precipitation data only, while the stream was sampled weekly. Additionally, modeling focused on baseflow conditions, as samples of several rainfall-runoff events were discarded.

The effect of tracer data resolution on estimates of MTTs was further investigated by *Hrachowitz et al*. [2011]. They used weekly precipitation and stream isotope data to estimate MTTs of a Scottish catchment and found increasing errors in MTTs with increasing sampling intervals up to 8 weeks. They argue that internal catchment processes will be misrepresented with a reduced sampling frequency.

Up to now, no study consistently used daily or higher resolution tracer data for a longer time frame to study the effects that different tracer data resolution have on the estimates of TTDs and MTTs. Considering the call for action for high-resolution data of *McDonnell and Beven* [2014] and the argument of *Hrachowitz et al*. [2011] that high-resolution data can potentially better represent internal catchment processes, the hydrological community faces the danger of acquiring a wrong understanding of catchment runoff generation processes when using low temporal resolution data.

In this study, we investigated the hypothesis that (1) shorter temporal time scales improve the quality of stable isotope modeling of stream water in terms of an objective function metric, and (2) the TTD of a higher temporal resolution will show considerable differences to the TTD derived from the lower resolution data. To this end, we estimated TTDs of a 1.5 year time series of a humid mesoscale catchment in Germany. We used stable isotope data ($\delta^{18}O$) with a temporal resolution of 0.5 day for precipitation and daily and 4h for stream flow under low and high flow conditions.

IV.2 Methods

IV.2.1 Study Site

The Erkensruhr catchment (approximately 42 km²) is located in the western part of Germany at an altitude of 286 m asl in the northern to 631 m asl in the southern part (Figure IV.1). The

catchment's climate is humid with a precipitation gradient with mean annual amount of 740 mm in the eastern part and 1150 mm in the western part. The mean annual temperature ranges from 7.6 °C for higher to 10 °C for lower altitudes. The catchment is part of the national park Eifel and dominantly covered by coniferous forest in the south and deciduous forest and grassland in the north (Figure IV.2, Table IV.1). Soils in the catchment are dominantly cambisols with the exception of river valleys where gleysols and planosols can be found. The base rock is Devonian clay shale with sandstone intrusions [*Stoltidis and Krapp*, 1980].

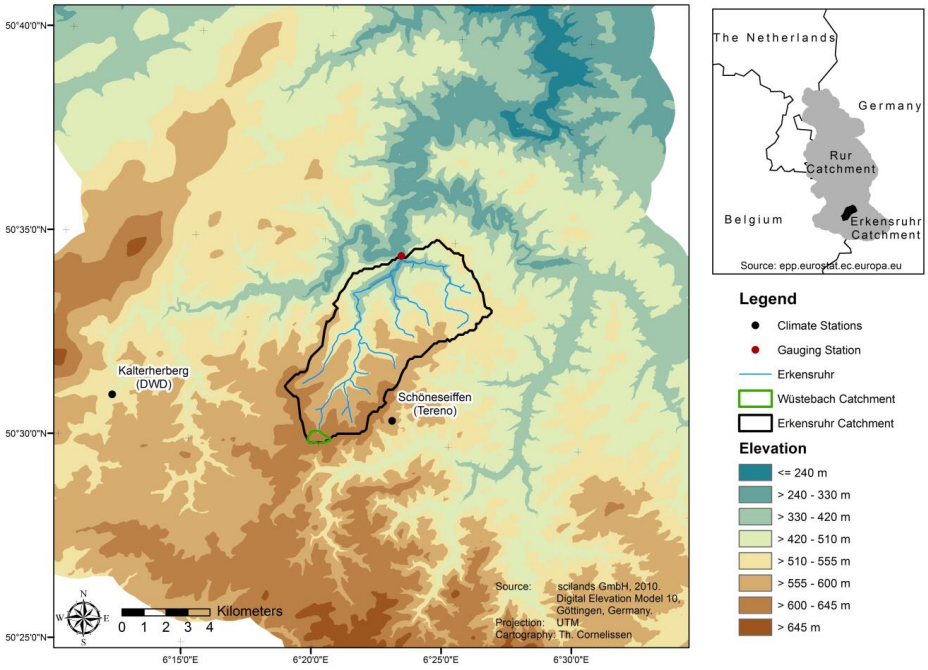

Figure IV.1. Location and elevation map of the Erkensruhr and the Wüstebach catchment.

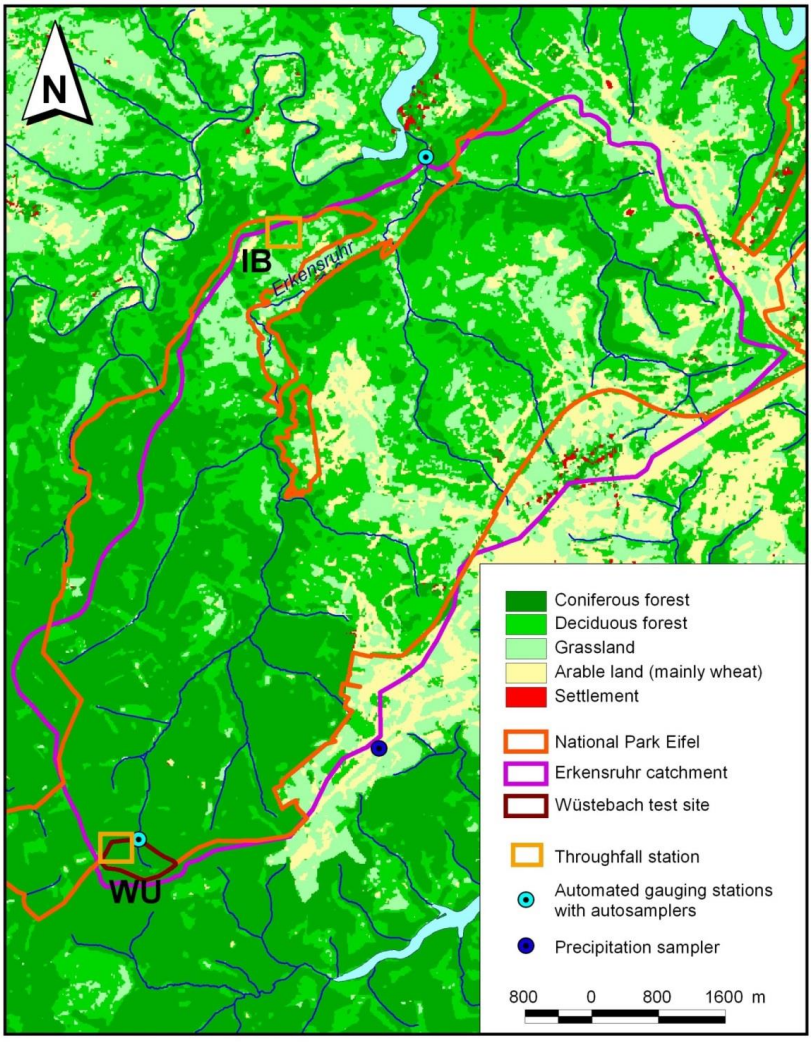

Figure IV.2. Land use and measurement network of the Erkensruhr catchment with the locations "Im Brand" (IB) and "Wüstebach" (WU).

Table IV.1. Percentage land use of the Erkensruhr catchment.

Land Use	Fraction [%]
Grassland	36
Coniferous Forest	33
Deciduous Forest	22
Heath	3
Agriculture	2
Copse	2
Settlement	2

Situated in the south of the catchment lies the well-studied sub-catchment 'Wüstebach' which is one of the Terrestrial Environmental Observatories (TERENO) sites [*Bogena et al*., 2015; *Zacharias et al*., 2011]. Data was used from this location to aid in modeling TTDs of the Erkensruhr.

IV.2.2 Measured Data

We used hydrological and isotopic data to estimate TTDs for the time period of 3rd October 2012 to 8th March 2014. Additionally, data from 24th November 2010 to 2nd October 2012 was used to spin up the model (Figure IV.3).

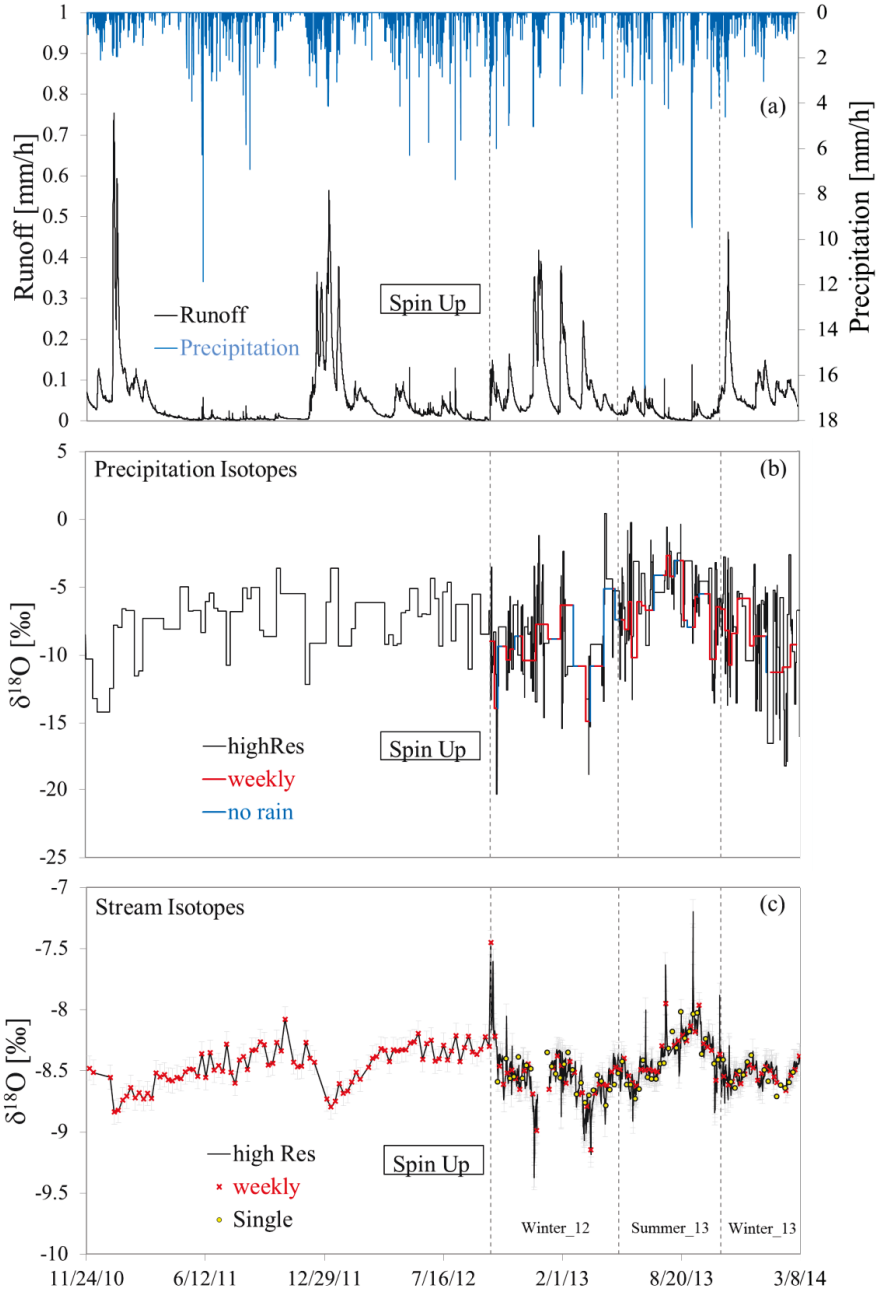

Figure IV.3. Measured and calculated data of the Erkensruhr catchment used for TTD estimation: (a) runoff and precipitation, (b) precipitation isotopes and (c) stream isotopes. Isotopes were measured in high resolution (high Res) and calculated for weekly resolution (weekly), with manually taken stream

samples for validation (Single, Panel c). Spin up phase (Spin Up) followed by the three modeling periods (grey, dashed lines).

Precipitation amount data (1 hour resolution, 0.1 mm increment) was acquired from the Schöneseiffen meteorological station (620 m asl.) located at the southeastern border of the catchment (Figure IV.1, Figure IV.2). To account for the catchment's precipitation gradient we used precipitation radar data from the Neuheilenbach station (585 m asl., German Weather Service, DWD). Pixel sizes varied between 0.95 and 2.1 km^2 and precipitation was determined in 5 minute intervals. A global rescaling factor was applied to the precipitation amounts of each pixel so that the value of the pixel to which the Schöneseiffen station belongs equals '1'. We then calculated the mean value of the other pixels to represent the areal precipitation and multiplied the Schöneseiffen precipitation amounts with it.

Stream stage data (15 minute resolution, 0.1 cm increment) is available from 2001 to the present (WVER) and was converted to runoff volumes using a polynomial regression to the 4^{th} power ($R^2 = 0.99$, not shown).

As about 55% of the catchment is forest-covered and canopy interception influences the estimates of TTDs [*Stockinger et al*., 2015], precipitation $\delta^{18}O$ samples were taken at three different locations throughout the catchment: (1) throughfall (TF) samples of a deciduous forest ('Im Brand', IB) in weekly resolution; (2) TF samples of a coniferous forest ('Wüstebach', WU) in weekly resolution; and (3) open land (OP) samples at the Schöneseiffen meteorological station in 0.5 day resolution. We could not sample IB from 6^{th} November 2012 to 17^{th} May 2013 due to administrative issues. While TF was sampled using RS200 samplers (see Chapter III), OP was sampled by a cooled, automatic sampler (NSA 181/KS-16, Eigenbrodt).

To create a single high resolution precipitation time series necessary for modeling, we first amount-weighed the high resolution OP data to create weekly OP data according to the sampling dates of the TF samples. Then we calculated the weekly isotopic differences of the weighed OP to the TF stations of WU and IB, respectively. This was done in such a way that a positive difference indicates enrichment in isotope values of TF when compared to OP, as can often be observed [*Dewalle and Swistock*, 1994]. To create high resolution IB data, the weekly differences of IB to OP were added to the respective high resolution OP values for these weeks. The same procedure was done for the calculation of high resolution WU data with WU to OP differences, respectively. Finally, the three high resolution time series of OP, IB and WU were unified into a single high resolution time series by weighing them according to the Erkensruhr land use percentages of coniferous forest (WU), deciduous forest (IB) and the remaining land uses (OP).

The amount-weighed, weekly OP was further used to verify OP data against (a) an independent measurement of weekly bulk samples refrigerated in-situ at Schöneseiffen; and (b) TF from IB in the north of the catchment (Figure IV.2) to investigate a possible intra-catchment gradient in precipitation isotopes.

Stream samples for stable isotope analysis were taken in daily time steps during low flow conditions and 4h time steps during high flow conditions using a cooled, automatic sampler (Liquistation CSF48, Endress+Hauser). The threshold for switching between low and high flow conditions was adjusted at irregular intervals and chosen to guarantee isotopic characterization of several runoff events. The sampler stream isotope data was verified against manually taken samples (weekly grab).

As only the stream stage data was available for the spin up phase, the other necessary data was acquired from different sources as the ones used for the modeling phase. Precipitation

amounts were acquired from the Kalterherberg station (1 hour resolution, 0.1 mm increment, DWD) located 6 km to the west of the catchment (Figure IV.1) and correlated to Schöneseiffen precipitation amounts. We then calculated the spin up precipitation amounts by multiplying the Kalterherberg data with the regression slope value and the global rescaling factor obtained by the precipitation radar. We used precipitation $\delta^{18}O$ from the weekly bulk samples taken at Schöneseiffen. For stream $\delta^{18}O$ we correlated the available Erkensruhr $\delta^{18}O$ time series to the Wüstebach sub-catchment's which extends to the necessary time period. The resulting regression equation was used to create weekly Erkensruhr stream isotope data.

Due to the high correlation of Wüstebach and Erkensruhr runoff values ($R^2 = 0.88$, not shown) and the lack of a catchment-wide soil water content (*SWC*) measurement network in the Erkensruhr catchment, we used the Wüstebach SoilNet data to estimate the overall wetness of the catchment (see Chapter II).

Water isotopic analysis was carried out using two measurement systems: (1) an Isotope-Ratio Mass Spectrometer (IRMS, Delta V Advantage, Thermo Scientific) coupled with a high temperature pyrolysis furnace (HT-O, HEKAtech), and (2) laser-based cavity ringdown spectrometers (models L2120-i and L2130-i, Picarro). Results are reported as δ-values relative to Vienna Standard Mean Ocean Water (VSMOW) [*Gonfiantini*, 1978]. Internal standards calibrated against VSMOW, Standard Light Antarctic Precipitation (SLAP2) and Greenland Ice Sheet Precipitation (GISP) were used to ensure long-term stability of analyses. The precision of the analytical system was ≤ 0.1 ‰ for $\delta^{18}O$.

IV.2.3 TTD Calculation

TTDs were estimated with the conceptual model TRANSEP [*Weiler et al*., 2003] by modeling effective precipitation (p_{eff}) including a simple snow model and subsequently simulating the observed stream isotope values in hourly time steps (for details see Chapter II).

Similar to the Wüstebach catchment (see Chapter II and III) the hydrograph of the Erkensruhr was split into individual modeling periods to estimate p_{eff} using *SWC*. These modeling periods describe the catchment's wet and dry state in terms of overall catchment wetness. However, during early modeling it became apparent that the standard approach applied at the Wüstebach (approximately 0.385 km²) was not sufficient for the hundredfold larger Erkensruhr (approximately 42 km²). Peak runoff situations were not modeled adequately (not shown) which could pose a problem with the high resolution isotope stream data that captured many peak runoff situations. Thus, to better simulate these situations and to better characterize the catchment's response to precipitation, several steps had to be taken.

First, we identified extreme runoff situations (i.e., events) during the wet and dry states and modeled them individually. For the wet states, we defined the start of an event as the exceedance of the 97.5% confidence band of the daily hydrograph gradient. Events ended when the falling limb has stopped its decline. These wet state events were modeled individually by subtraction of the base flow, which was identified as the lowest observed runoff value during this time period. To compare the response of the catchment (expressed as the Response Time Distribution (RTD)), we combined the RTDs of the non-event and the event modeling periods by weighing them according to their temporal proportion of the hydrograph. Contrary to this, dry state events had a much shorter duration and it was necessary to use the hourly hydrograph gradient to identify events. We estimated p_{eff} for three dominant events by first subtracting the mean runoff volumes of the three days prior an event

from the runoff volumes of the first two event hours. The ratio of the resulting value of this subtraction to the peak runoff was multiplied with OP amounts to estimate p_{eff} (also see Chapter II and the event of 3rd July 2010).

Second, even after separate p_{eff} calculation for events the modeling of the dry state resulted in a non-realistic hydrograph simulation (Figure IV.4). Thus, this modeling period was further separated into a main phase that is preceded by a drying phase and followed by a wetting-up phase. The main phase was characterized by a linear regression equation fitting a major part of the log-transformed hydrograph. As this regression equation did not encompass the whole modeling period, the beginning and end of the dry state were assumed to be a drying ('D' in Figure IV.4) and a wetting-up ('W' in Figure IV.4) phase. All three phases were also modeled individually.

We used the two-parallel linear reservoir (TPLR) model for the RTDs and TTDs. The corresponding mean response time (MRT) and MTT were calculated from the TPLR parameters as

$$MRT\ or\ MTT = \tau_f * \phi + \tau_s * (1 - \phi) \quad \text{(IV.1)}$$

with τ_f the residence time of the fast reservoir, τ_s the residence time of the slow reservoir and ϕ the fraction of water passing the fast reservoir. To objectively judge the hydrograph simulation we used the Volumetric Efficiency (VE), while we used the Nash-Sutcliffe Efficiency (NSE) for the stream isotope simulation [*Criss and Winston*, 2008; *Nash and Sutcliffe*, 1970]. The parameter space was searched using the Ant Colony Optimization algorithm [*Abbaspour et al.*, 2001].

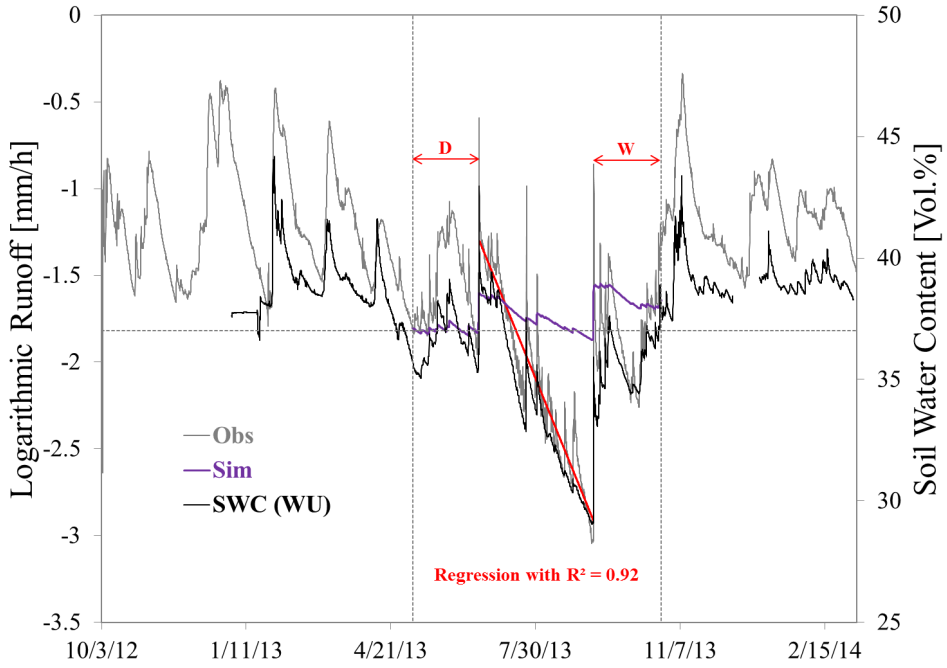

Figure IV.4. Logarithmic runoff (Obs) plotted against SWC measured at the sub-catchment Wüstebach (SWC (WU)). First simulation of Summer_13 resulted in an unrealistic solution (Sim). Thus, identifying a main phase using a regression with $R^2 = 0.92$ (red line), Summer_13 was split into this main phase, preceded by a drying (D) and followed by a wetting-up phase (W). Also shown is the separation of the complete time series into the three modeling periods (vertical, grey dashed lines) and SWC limit for splitting the hydrograph based on SWC data (horizontal, grey dashed line).

IV.3 Results

Measured high resolution OP isotopes varied between -21.4 to 1.1‰, while calculated high resolution TF isotopes varied between -19.4 to 0.7‰ for IB and -20.4 to -0.5‰ for WU. Regarding the weekly resolution, calculated OP isotopes varied between -15.0 to -1.8‰, while measured TF isotopes varied between -11.8 to -3.5‰ for IB and -14.3 to -3.0‰ for WU.

The precipitation isotope data showed a seasonal trend with enriched values in summer and depleted ones in winter. This seasonal trend was also reflected in the stream isotope data

(Figures IV.3b and IV.3c). $\delta^{18}O$ of the amount-weighed OP was highly correlated with the weekly Schöneseiffen bulk samples and the TF isotopes measured at IB ($R^2 = 0.88$ with slope 1.02 and $R^2 = 0.71$ with slope 1.06, respectively). Stable isotope data of the stream was verified by regression to the manually-taken, weekly grab samples ($R^2 = 0.69$, also see Figure IV.3c).

Erkensruhr runoff was highly correlated with runoff and *SWC* measured at Wüstebach ($R^2 = 0.88$ and 0.89, respectively). Thus, using Wüstebach *SWC*, the modeling period was split into three distinct modeling periods: a wet state followed by a dry state and a wet state again. They will from now on be referred to as 'Winter_12', 'Summer_13' and 'Winter_13' (Figure IV.3). The precipitation radar data showed that the distributed precipitation amounts over the Erkensruhr catchment amounted on average to 92% of the recorded Schöneseiffen amounts (94% for 2010, 90% for 2011). Thus, Schöneseiffen precipitation amounts were multiplied with a global rescaling factor of 0.92.

Delineation of runoff events during the wet states resulted in five identified events. The four events of Winter_12 surpassed the 97.5% daily hydrograph gradient at the beginning of the rising hydrograph limb. They directly followed each other and thus were modeled as one segment. For the single event of Winter_13 the 97.5% were exceeded at the peak of the rising hydrograph. Due to this, it was not modeled separately. For Summer_13 we used the hourly hydrograph gradient and identified 3 dominant events (Figure IV.5).

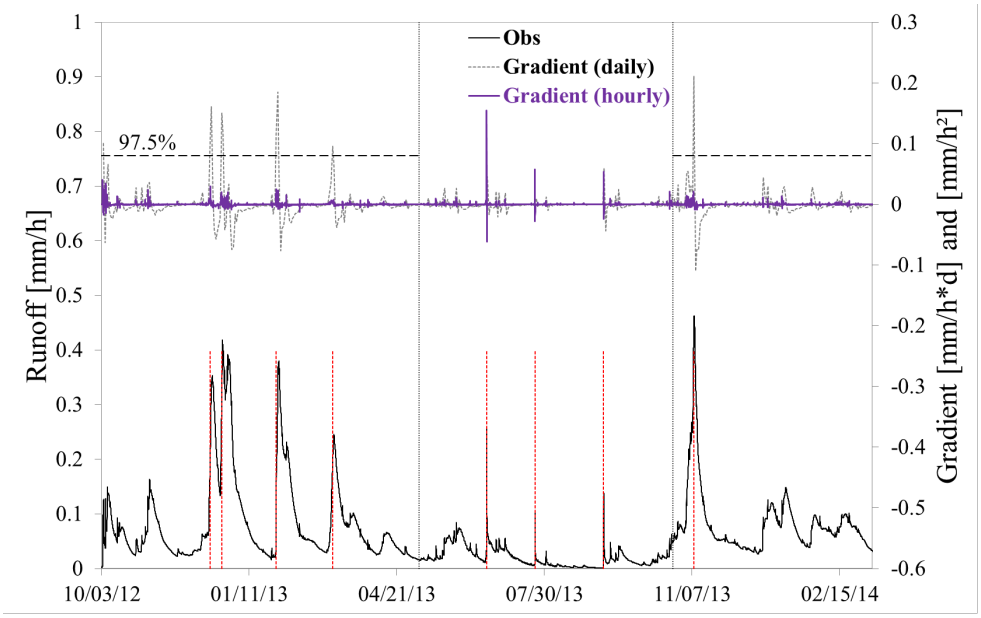

Figure IV.5. Identification of runoff events in the hydrograph (Obs) by using the 97.5% confidence interval of daily hydrograph gradient (Gradient (daily)) during the catchment's wet states. For the dry catchment state the hourly hydrograph gradient was used (Gradient (hourly)). Identified events are marked by dashed, red lines.

Hydrograph simulation results for all modeling periods showed overall good VE values ranging from 0.59 to 0.83 (Figure IV.6a, Figure IV.7 and Table IV.2). Although several runoff events were well modeled, some peak runoff volumes were underestimated. RTDs of Winter_12 and Winter_13 showed a faster response than the RTD of Summer_13, with shorter MRTs of 26 and 13 days compared to 118 days for Summer_13 (Figure IV.8, Table IV.2). With approximately 7 days, the modeled event phase of Winter_12 had an even shorter MRT time than the wet states (Winter_12 and Winter_13). This was reflected in the steep increase of its corresponding RTD (Winter_12 (E) in Figure IV.8). Combining the standard simulation with the event simulation of Winter_12 resulted in a RTD that matched the one of Winter_13 (Winter_12 (C) compared to Winter_13 in Figure IV.8). The RTDs of the drying and wetting-up phase of Summer_13 plot close to the main phase RTD of Summer_13. They

had similar MRTs (54 and 42 days) which were in between the longer MRT of Summer_13 and the shorter MRTs of both winters.

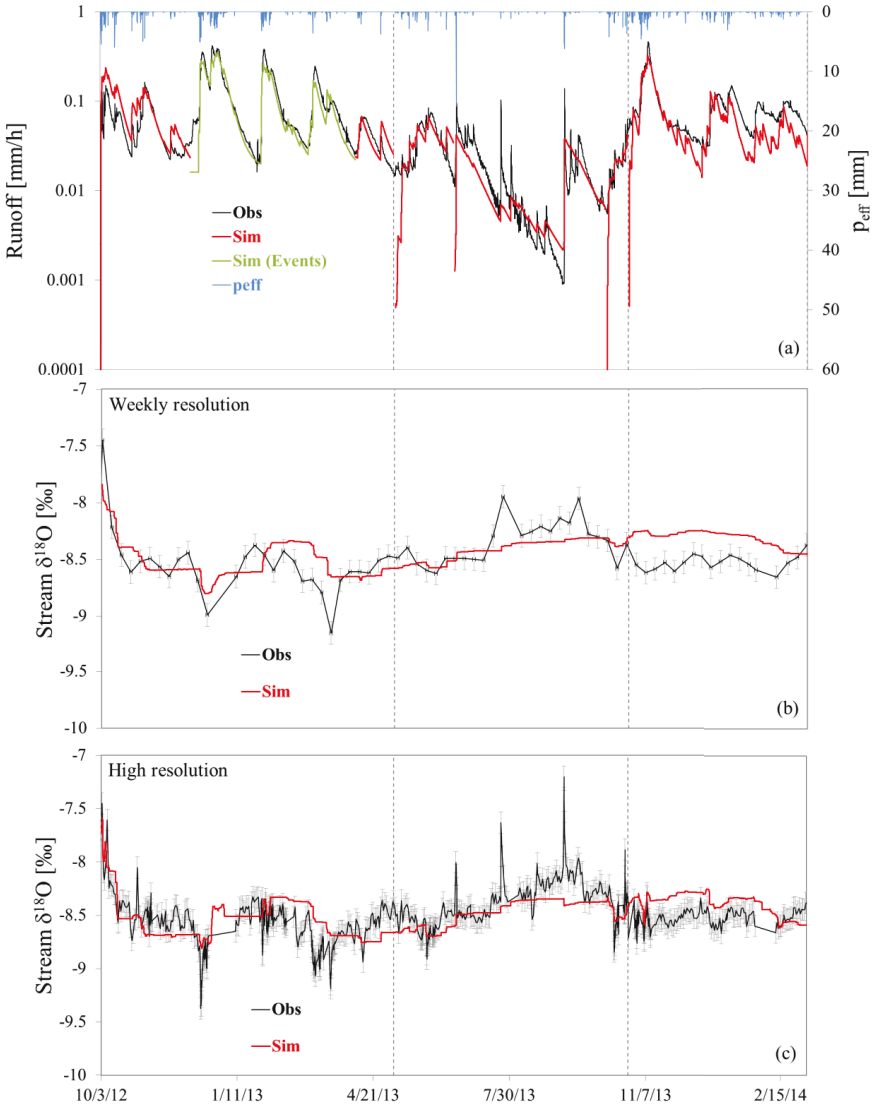

Figure IV.6. (a) Simulated runoff (Sim) with event modeling (Sim (Events)) plotted against observed runoff (Obs). Effective precipitation (p_{eff}) is shown as blue bars from the top. (b) and (c) Stream isotope modeling results (Sim) plotted against observed stream isotopes (Obs) using weekly and high temporal resolution. Vertical, dashed grey lines in all panels denote the three modeling periods.

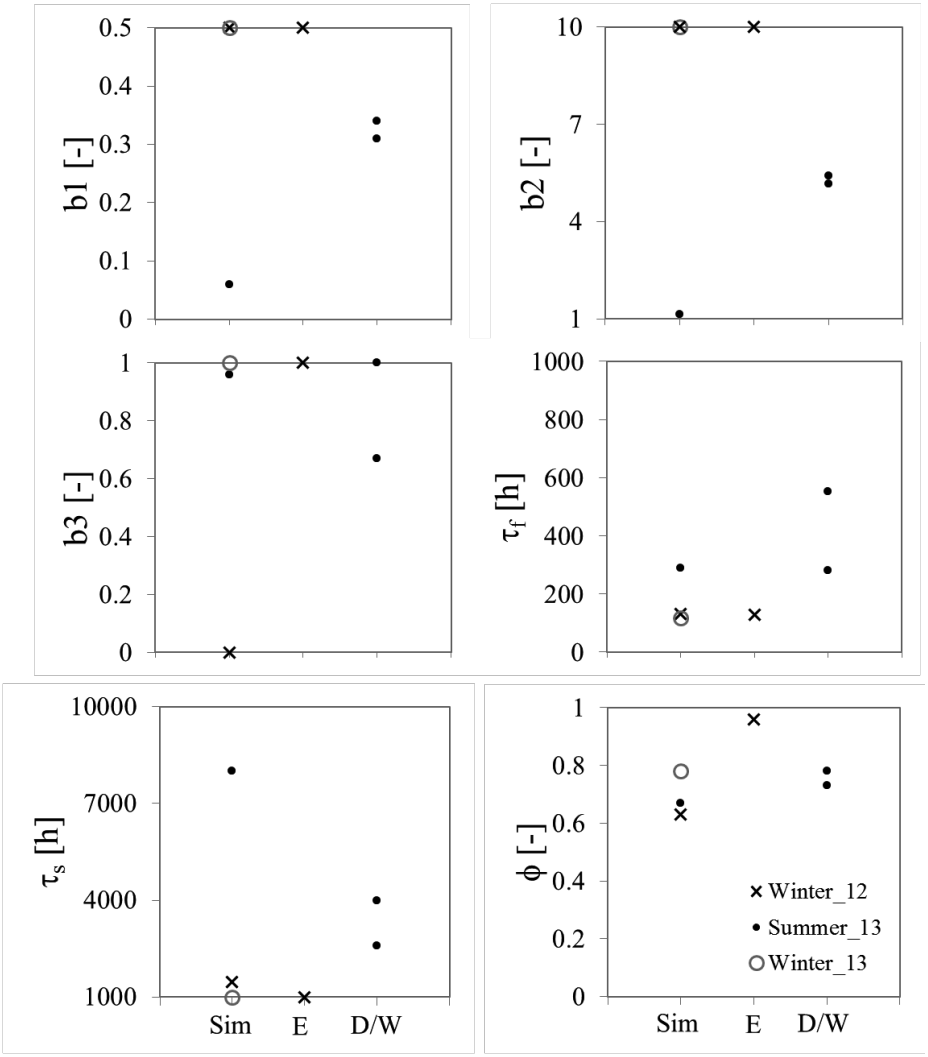

Figure IV.7. Parameter values of the hydrograph simulation with p_{eff} parameters *b1*, *b2* and *b3* and RTD parameters τf, τs and ϕ, displayed for the hydrograph simulation (Sim), the event case (E) and the drying and wetting phase (D/W). Vertical axis limits denote the parameter search boundaries.

Table IV.2. Parameter values of the three modeling periods Winter_12, Summer_13 and Winter_13 for the hydrograph simulation (Sim), the event simulation (E) and the drying (D) and wetting-up (W) phase. Also shown are volumetric efficiency (VE) and the mean response time (MRT).

	Winter_12		**Summer_13**			**Winter_13**
	Sim	**E**	**Sim**	**D**	**W**	**Sim**
b1 [-]	0.5	0.5	0.06	0.34	0.31	0.5
b2 [-]	10	10	1.14	5.18	5.42	10
b3 [-]	0	1	0.96	1	0.67	1
Tf [h]	131	129	289	281	552	118
Ts [h]	1469	1001	8001	3995	2579	1001
phi [-]	0.63	0.96	0.67	0.73	0.78	0.78
VE [-]	0.66	0.77	0.59	0.69	0.83	0.71
MRT [d]	26.1	6.8	118.1	53.5	41.6	13.0

b1, scaling parameter; b2, precipitation weighing parameter; b3, API at t = 0; Tf, fast reservoir mean residence time; Ts, slow reservoir mean residence time; phi, fast reservoir contribution to RTD; VE, volumetric efficiency; MRT, mean response time.

Both winters had similar parameter values, while the main phase Summer_13 parameters differed from the winter ones (e.g., residence time of the slow reservoir of the TPLR model, T_s, Figure IV.7 and Table IV.2). The parameters of the drying and wetting up phase are similar to each other with stronger contrasts in parameter *b3*, which sets the initial wetness conditions of the modeling period. According to *b3*, the catchment was well saturated at the start of the drying phase, while it was more depleted at the start of the wetting-up phase (*b3* = 1 and 0.67 respectively, Figure IV.7 and Table IV.2).

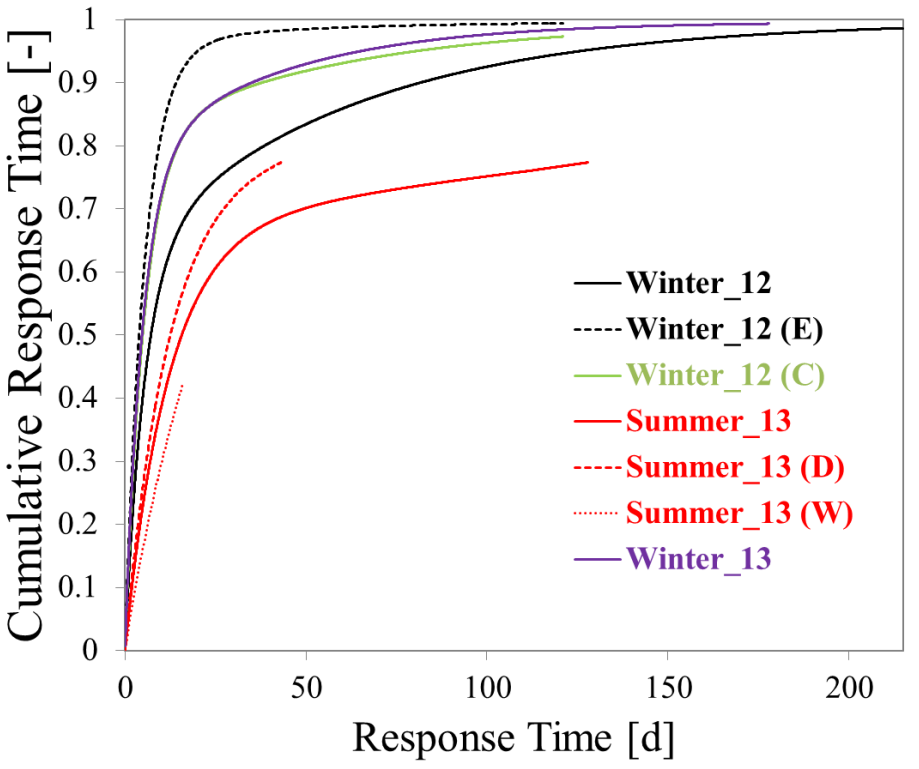

Figure IV.8. Response Time Distributions of the modeling phases. The combination of the Winter_12 simulation with the event simulation resulted in a RTD comparable to Winter_13 (compare to Winter_12 (C)).

Isotope simulation results calculated with high resolution data were better optimized (NSE = 0.34) than results based on weekly resolution (NSE = 0.24) when calculating the high resolution NSE based on only the observed stream isotope values that were also used in the weekly resolution data. Considering all observed values of the high resolution case gave an NSE of 0.22 which is slightly lower than the one of the weekly resolution case. Winter_13 was not well modeled in terms of stream isotopes, with the simulation result overpredicting for both the weekly and the high resolution case. While results based on high resolution data had an NSE of 0.34 when considering all modeling periods before Winter_13, it became -2.01 for Winter_13.

Comparison of the simulated stream isotopes revealed that the high resolution case was able to reproduce short term dynamics with sudden steep changes in isotope values, e.g., at the beginning of 2013 or at the beginning of Winter_13. Comparing this to the weekly resolution results, the beginning of 2013 did not show such a steep increase in stable isotope values, while the decrease in values in Winter_13 is completely missing (Figure IV.6c).

Overall, transit times based on weekly resolution were longer than the ones based on high resolution data, with MTTs of 9.52 and 4.70 years, respectively (Figure IV.9). While the parameters for the residence time of the fast and slow reservoir of the TPLR model were similar in both cases (τ_f = 4931 and 4816, τ_s = 93292 and 86722 for weekly and high resolution, respectively), the parameter for the contribution of the fast reservoir was different (ϕ = 0.11 and 0.56 for weekly and high resolution, respectively). Both TTDs did not fully recover the tracer, with weekly recovering only 35% and high resolution 68%.

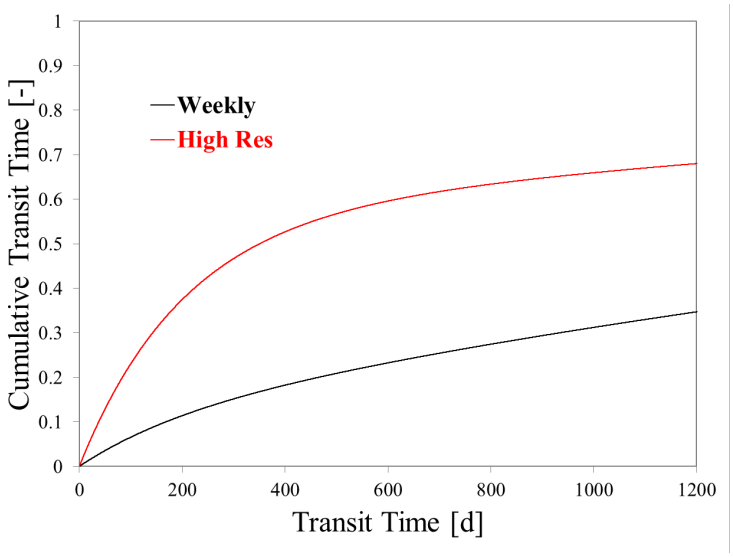

Figure IV.9. Transit Time Distributions based on weekly (Weekly) and high (High Res) resolution of precipitation and stream stable isotope data.

IV.4 Discussion

IV.4.1 Model Input Data

The Wüstebach is a headwater catchment of the Erkensruhr catchment. On the route to the outlet of the Erkensruhr, several further tributaries contribute to the stream flow (Figure IV.2). Despite this, the hydrograph of the Erkensruhr was strongly correlated with the Wüstebach's. *Tetzlaff et al*. [2009a] showed that soils control subcatchment MTTs and thus their water transport characteristics. As the tributaries did not mitigate Wüstebach low flow or dampen peak flow situations in the Erkensruhr hydrograph, it indicates that the subcatchments reacted uniform on average and thus their soils are relatively homogeneous.

Stockinger et al. [2014] have shown that a strong relationship between overall catchment wetness of the Wüstebach and its runoff volumes exists. In their study, the overall catchment wetness was expressed as the spatiotemporal high resolution *SWC* data. Combining this finding with (1) the high correlation between the Wüstebach *SWC* measurements and the Erkensruhr runoff, (2) the similar hydrological reactions of the Erkensruhr and Wüstebach hydrographs expressed in the high correlation of their respective runoff volumes, and (3) the importance of the headwater catchment Wüstebach for the Erkensruhr catchment, indicates that the Wüstebach *SWC* can be used as an appropriate indicator of the overall Erkensruhr catchment wetness conditions. Our assumption is supported by the fact that the use of the Wüstebach *SWC* data enabled the successful splitting of the hydrograph into modeling periods of uniform hydrologic behavior, and the subsequent satisfying simulation of the Erkensruhr hydrograph. This highlights the importance of measuring *SWC* data [*Vereecken et al*., 2008].

The range of calculated weekly OP isotopes is similar to the range of measured weekly OP isotopes reported in *Stockinger et al*. [2015] for the same location. The ranges of OP and TF

isotopes of IB and WU are similar and a high correlation between OP in the south of the catchment and TF of IB in the north of the catchment was found. As TF is reduced in precipitation amount and its stable isotope values are affected by canopy passage in comparison to OP, a direct comparison of OP and TF for the purpose of identifying an isotopic precipitation gradient is complicated. However, both time series plot close to each other (not shown). Thus, precipitation input to the Erkensruhr catchment did at least not show a strong isotopic gradient based on cardinal directions or altitude. However, the similarities of TF and OP only support the assumption of homogeneous above-canopy precipitation isotopes. Canopy passage induces changes in TF isotope values compared to OP that might seem negligible, but are actually important for TTD estimation. *Stockinger et al.* [2015] showed in their study the influence of canopy-induced changes of precipitation isotopes on estimates of TTDs and concluded that TF should not be neglected.

As reported in *Stockinger et al*. [2015], more research on the influence of TF on estimates of TTD is needed. In this study we used a land-use based weighing of three point-measurements, two of which were TF with only a weekly resolution. With this approach we inherently assumed each point-measurement to be representative for the land-use unit it was situated in. Several studies showed the influence of canopy structure on the isotopic composition of TF [*Brodersen et al*., 2000; *Kato et al*., 2013] and problems of TF sampling systems with small precipitation amounts [*Zimmermann and Zimmermann*, 2012]. Although it is not likely that the Erkensruhr coniferous and deciduous forests are uniform in canopy structure throughout the catchment, the NSE value of the Erkensruhr high resolution simulation (0.34, calculated for the weekly observed values only to guarantee comparability to Wüstebach) is virtually equal to the NSE value of the much smaller Wüstebach outlet (0.34, calculated in Chapter II). This supports the assumption of representative TF measurements obtained from the WU and

IB stations, as no drastic drop in NSE can be observed at the Erkensruhr when compared to Wüstebach.

IV.4.2 Hydrograph Simulation Results

IV.4.2.1 Hydrograph Discussion

Results of the hydrograph simulation indicated shorter response times during wet state conditions with decreased MRTs compared to the dry state. A similar behavior was observed by *Birkel et al*. [2012] who observed longer transit times for events with low antecedent wetness. *Heidbüchel et al*. [2012] systematically explained this by differences in storage as well as differences in precipitation and energy input to the catchment. The contrasting behavior to the Wüstebach sub-catchment reported in *Stockinger et al*. [2014], which had shorter response times during dry conditions, can be attributed to the Wüstebach being a special case. The authors argued that the Wüstebach's hillslopes disconnect hydrologically from the runoff-generation process during the dry state, thus disconnecting primarily slow flow paths. This assumption may be valid in small headwater catchments with shallow soil depths, but a complete disconnection of all slow flow paths during dry states should be less likely the more the catchment size increases due to more varied land-use, topography, soil depths, etc., creating buffering effects. Despite the contrasting seasonal response behavior, the runoff of Erkensruhr and Wüstebach was highly correlated ($R^2 = 0.88$), which can be attributed to the extremely low conductivity of the bedrock in the Erkensruhr catchment, leading to similar hydrographs. The different responses during the seasons might have several possible explanations, e.g., the difference in topography, relief energy, land use, and many other factors, which make those two catchments distinct and should be investigated further in future research.

The combined Winter_12 RTDs of the non-event and the event simulation coincided with the Winter_13 RTD. This is indicative of a similar catchment response during wet states. It was already observed in *Stockinger et al*. [2014] that the Wüstebach catchment reacts similar during its two wet states with matching RTDs. Also the Wüstebach's two dry states reacted similar to each other. This could however not be compared to the present study, as the modeling period of the Erkensruhr only comprises one dry state. Contrary to the RTD similarity of both wet states, it could also be argued that only the non-event simulation RTDs should be compared, as the event simulation of Winter_12 can be considered a special case. However, also in this case the wet state RTDs shared more similar parameter values than the dry state RTD and a generally similar catchment response during wet states can be assumed.

IV.4.2.2 Parameter Discussion

The p_{eff} parameters of the drying and wetting-up phase were almost identical and can be physically explained (Figure IV.7, 'D' and 'W' in Table IV.2). The parameter for weighing the effect of past rainfall events on the response of the catchment to current rainfall (*b2*) was approximately 5 for both the D and W phase, indicating medium influence of past rainfall events. Comparing this to the wet states with a value of 10, meaning strong influence of past rainfalls, and to the dry state main phase with approximately 1, indicating negligible influence, makes sense in the context of a filling and emptying subsurface storage. While during wet states the soil water storage is fuller, during drying it empties and reaches a low value in dry state. Depending on rainfall intensity, precipitation events happening during dry state quickly evapotranspirate or discharge and do not have a long term effect on future precipitation events. During wetting-up, the storage increases until it is nearly full again in the wet state and past rainfall events get stored in the soil (compare to the *SWC* of Figure IV.4).

The parameter for setting the initial wetness of the catchment (*b3*) is 1 for the drying phase, indicating a well saturated storage. At the beginning of the dry phase, it decreases to 0.96 while becoming 0.67 at the beginning of the wetting-up phase. Thus, a consistent decrease of storage volume in the catchment was modeled by independent simulation of three individual phases (drying, dry state and wetting-up).

IV.4.3 Isotope Simulation Results

Isotope simulation results of both weekly and high resolution had comparatively low NSE values with respective MTTs of approximately 9.5 and 5 years. The application of stable isotopes with the convolution integral used in TRANSEP reaches its limit for MTTs longer than 4-5 years [*Stewart et al*., 2010]. Thus, the proper simulation of the attenuated streamwater isotopic signal could have been impaired, resulting in the relatively low NSE values. The comparison of the simulation quality of observed stream isotope values that both resolutions share revealed a higher NSE value of the high resolution case (NSE = 0.34). Thus, similar to findings of *Timbe et al*. [2015] using weekly stream isotope data, the high resolution sampling scenario is preferable over the weekly one.

Compared to the simulation result before Winter_13, Winter_13 modeling results were much worse for both data resolution cases (e.g., NSE of Winter_13 = -2.01 for the high resolution case). However, despite the simulation overpredicting the observed stream isotopes, the simulation result based on high resolution data was able to match the temporal dynamics of the observed stable isotope values, e.g., the drop in stream isotopes values near the end of December 2013 and the subsequent rising values. The reason for the sudden mismatch of simulation and observed values at the beginning of Winter_13 or shortly thereafter (depending on the data resolution, see Figures IV.6b and IV.6c) could lie with the model assumptions connected to TRANSEP, e.g., a time-invariant TTD. A model based on time-

variant transit times, e.g., that of *Klaus et al*. [2015], should improve the simulation results. Nonetheless, even results of a simple model such as TRANSEP highlight the potential of higher resolution data in the simulation of stream isotope dynamics.

The importance of using high resolution isotope data was emphasized with the drastic change in TTDs and associated MTTs in this study. The TTD based on weekly data showed a MTT which was twice as long as the one from high resolution data. This finding is corroborated by *Hrachowitz et al*. [2011], who used weekly data and found that MTT errors increase with increasing sampling intervals. Contrary to this, in *Timbe et al*. [2015] the MTTs of the weekly and daily case are almost indistinguishable. This discrepancy can be related to the use of weekly stream isotope data in *Timbe et al*. [2015], while this study used at least daily (and several times 4-hourly) data. At the same time the data resolution of precipitation is higher compared to the former study (0.5 day versus 1 day).

Thus, when estimating TTDs, weekly isotope data misleads our interpretation and concepts of internal catchment processes governing water transport. Our study confirms that high resolution data is needed to avoid this risk and be able to adequately characterize hydrological processes at the catchment scale [*McDonnell and Beven*, 2014].

IV.5 Conclusion

In this study we investigated the influence of sampling frequency on estimates of TTDs and MTTs. We used weekly and high resolution data consisting of at least daily stream and sub-daily precipitation isotopes. The stream isotope simulation result improved when using high resolution data, showing short-term dynamics that were not present in the results based on weekly data. MTTs approximately halved when using high resolution data, with a vastly

different TTD to the one based on weekly data. Our results highlight the importance of sub-weekly isotope data on estimating TTDs.

V. Synopsis

V.1 Summary

TTDs give insights into the internal workings of a catchment regarding water transport. This is important when considering climate change, land use change and pollutant transport. However, they can currently not be verified and their estimates are inherently uncertain. Thus, the aim of this work was to investigate spatiotemporal controls of uncertainties in estimating streamwater TTD.

To achieve this, three hypothesis were tested in two different catchments. Two studies focused on spatial controls of TTDs in the Wüstebach catchment and elucidated the effect of canopy-induced stable isotope tracer changes on TTD estimates. The final study investigated the influence of the temporal sampling interval on the derived TTDs for the Erkensruhr catchment. This summary recaps the three main hypotheses that were investigated, as well as highlights the results. Following this is a synthesis that features a discussion of the study results in context to the overall aim of this work and an outlook on further research needs to be addressed in the future.

(i) A headwater catchment will show heterogeneities in TTDs along its stream network. As most catchment characteristics are homogeneous for the study site, the spatially differing soil types are the source of the varying TTDs.

The MTTs of 15 stream and tributary locations of the small headwater catchment Wüstebach were negatively correlated to the percentage of riparian zone in the respective subcatchments. However, the subcatchment area was not correlated with the MTT and thus had no discernible effect on water transport. In summary, soil types did indeed affect the water transport characteristics. The small headwater catchment showed heterogeneities in TTDs, with the outlet's TTD integrating the different responses.

(ii) The estimates of TTDs of forested catchments are affected by canopy-induced stable isotope tracer changes. Open precipitation or above canopy isotope data is not sufficient to properly characterize these TTDs.

The application of the stable isotope data of OP and TF led to different results for δ^2H and $\delta^{18}O$ concerning estimates of TTDs. Only in the case of using TF data did the TTDs of both isotopes converge. When using OP data, the TTDs spread, thus creating uncertainty. Additionally, modeling of the streamwater isotope tracer signal improved for both stable isotopes in terms of NSE when using TF.

Therefore, OP data used to estimate TTDs of forested catchments is indeed not sufficient and TF data must be used.

(iii) The estimates of TTDs are affected by the temporal resolution of stable isotope data.

Modeling of the streamwater isotope signal of the Erkensruhr catchment with high resolution tracer data improved the NSE when compared to results based on the weekly resolution. The high resolution case captured more dynamics of the observed streamflow isotopes, and its respective TTD was shifted toward shorter transit times.

Thus, the use of stable isotope tracer data with a higher temporal resolution indeed led to changes in the TTD.

V.2 Synthesis

V.2.1 A Global Perspective

Crutzen and Stoermer [2000] termed the current geological epoch the 'Anthropocene'. With this they emphasize the human impact on global storage and circulation patterns of matter and energy. Besides being undeniable, the anthropogenic impact is of yet difficult to model and

thus predict accurately. For example, climate change is now a widely accepted fact, but the exact effects and aftermaths are still under debate. Among these are: endangered animals and plants [*Root et al*., 2003], changes to frequency and intensity of storms [*Emanuel et al*., 2008], changing landscapes [*Allen and Breshears*, 1998], economic impacts [*Tietenberg*, 1997], increase in heat-related diseases [*Khasnis and Nettleman*, 2005; *Pounds et al*., 2006] and increased drought risk [*Dai*, 2011].

In light of this, studying how catchments transport water is not research for the sake of research itself, but for solving global problems. It should be viewed more in terms of human self-preservation. For example, with the ability to produce, unintentionally distribute and eventually introduce potentially toxic substances to the environment, the catchment research question 'How do catchments transport pollutants?' is in reality 'How do we prevent those pollutants from killing us directly or indirectly?'. The first question is just a step to achieving this goal: knowing how water transports the pollutants to the river. This becomes even more important when transport to the groundwater is considered, as half the global population depends on groundwater as a source of drinking supply [*Oki and Kanae*, 2006]. This threat to human health and safety has already reached dimension of poisoning 35 to 77 million people with arsenic-contaminated groundwater in Bangladesh, making it the largest mass poisoning in history [*Smith et al*., 2000]. Similarly, the question 'How does land use change affect the water transport characteristics of a catchment?' really is 'How do we not flood our settlements? How do we protect the eco-system functions we need for our convenience?'. This might seem drastic but when considering the Aral Sea it becomes clear that self-preservation must be considered. *Micklin* [2007] summarizes the effects of the drying of the Aral Sea due to human impact as: negative changes to ecological communities, economic impacts by destruction of fishing grounds, climatic changes around the former shorelines, and dust and salt storms.

According to *Micklin* [2007], the Aral Sea will not be restored in the foreseeable future. Thus, it serves as an example of irreparable damage due to human impact.

Because of this, understanding how catchments transport water and what influences it is an important task. However, as stated in the General Introduction (Chapter I), TTDs as integrative tools to judge a catchment's water transport capabilities cannot be verified. Thus, they and the knowledge gained about catchment water transport are inherently uncertain.

This worked aimed at being a small stepping stone on the way to solving the global problems connected to water.

V.2.2 Spatiotemporal Controls of Streamwater TTD Uncertainty

Understanding the influence of catchment characteristics on the TTD and thus its water transport properties are especially useful in the case of ungauged catchments where e.g., monetary or organizational constraints impair monitoring of hydrologic stores and fluxes. *Hrachowitz et al*. [2013b] analyzed the 'Predictions in Ungauged Basins (PUB)' initiative of the International Association of Hydrological Sciences (IAHS) [*Sivapalan et al*., 2003] and emphasized the fact that our ability to understand, model and predict the water cycle dynamics depend on our ability to understand data uncertainty. Their study lists open research challenges, among which is the question how to achieve reliable predictions in ungauged catchments, as most of the reliable predictions were achieved in gauged ones. The authors note that this impairs the ability of decision makers of e.g., developing countries to sustainably manage water resources. Thus, it is important to ensure that estimates of TTDs are as correct as possible by minimizing uncertainty. However, we can only minimize uncertainty if we know how different factors affect uncertainty in TTD estimates.

The first study of this work investigated how catchment characteristics, namely the riparian zone of the Wüstebach catchment, influence MTTs. The results obtained are useful in the PUB context, as only one location of the catchment was gauged. The other stream and tributary locations were ungauged. However, because of the assumption of a uniform p_{eff} input, the method applied to estimate TTDs for ungauged stream location has the major drawback of being applicable to small, uniformly land covered catchments only. If techniques were developed to estimate p_{eff} without measuring Q then this method could be extended to medium to large catchment. This does however not free us of the necessity of obtaining streamwater and precipitation samples to use as tracers and therefore still poses a problem in remote or hard-to-reach catchments. As was seen in the third study, a higher sampling frequency is preferable, as it influences the TTD. Results ultimately indicate that the uncertainty of the TTD can be limited by referencing it to the distribution of riparian zone to hillslopes, or responsive soils to free draining soils as termed by *Tetzlaff et al*. [2009a].

The second study found that canopy-induced changes of stable isotope tracer values influence TTD estimates in such a way that the uncertainty decreases when interception is considered. The study was conducted in a catchment with a coniferous forest but it can be safely assumed that the results of this study can be extended to deciduous forests too. However, during leaf-less conditions interception is reduced and it could be possible that TTDs derived from TF do not show a difference to OP-derived TTDs. In such a case, the sampling of TF data might be superfluous. It is of yet still unclear if interception must be considered for forested catchments only or if this applies to other land use forms involving vegetation, e.g., agricultural fields or grassland.

The third study investigated the effect of different temporal resolutions on the shape of the TTD and found that a higher resolution leads to a vastly different TTD than for lower

resolution data. In this case it is not possible to straightforwardly say that higher resolution data leads to less uncertainty in TTD estimates, as this is just an assumption. After all, TTDs are no field-measurable quantities and cannot be verified. However, as more information should lead to a better representation of a system, the assumption that higher resolution tracer data improves TTD estimates seems valid. Despite this finding, the practical implementation of the study's result might pose a problem, as many catchments are not easy to reach, and other constraints like time or workforce limitations might impede a high resolution sampling effort. To overcome this challenge, the hydrologic community should aim for automatic on-site sampling systems that are reliable and require low maintenance.

V.3 Outlook

This work highlighted different spatiotemporal controls on TTD estimates which are quickly summarized as: (1) riparian zones foster shorter transit times, (2) interception needs to be considered for forested catchments, and (3) a high temporal resolution of tracer data is preferable.

Future research can benefit from these findings by e.g., designing sampling campaigns that include throughfall. To move forward further, the availability of high resolution data is necessary to increase our knowledge of the water transport in catchments. Currently, there is a lack in easy-to-use and maintain, field-deployable measurement stations that collect tracer data in a high resolution. Ideally, a measurement method would be developed in the future that can actually measure TTD at the catchment scale. Such technology does not currently exist, but it would be a game changer in TTD estimation. With it, TTD estimates could finally be verified or falsified, making it possible to effectively work on model structures and test theories about water transport in catchments. This would also clarify the influence of

catchment characteristics on water transport times without a doubt and could help elucidate other questions like the frequency and occurrence of preferential flow in soils.

VI. References

Abbaspour, K. C., R. Schulin, and M. T. van Genuchten (2001), Estimating unsaturated soil hydraulic parameters using ant colony optimization, Adv Water Resour, 24(8), 827-841.

Allen, C. D., and D. D. Breshears (1998), Drought-induced shift of a forest-woodland ecotone: Rapid landscape response to climate variation, P Natl Acad Sci USA, 95(25), 14839-14842.

Allen, S. T., J. R. Brooks, R. F. Keim, B. J. Bond, and J. J. McDonnell (2013), The role of pre-event canopy storage in throughfall and stemflow by using isotopic tracers, Ecohydrol., doi: 10.1002/eco.1408.

Asano, Y., T. Uchida, and N. Ohte (2002), Residence times and flow paths of water in steep unchannelled catchments, Tanakami, Japan, J Hydrol, 261(1-4), 173-192.

Asano, Y., and T. Uchida (2012), Flow path depth is the main controller of mean base flow transit times in a mountainous catchment, Water Resour Res, 48.

Bachmair, S., M. Weiler, and G. Nutzmann (2009), Controls of land use and soil structure on water movement: Lessons for pollutant transfer through the unsaturated zone, J Hydrol, 369(3-4), 241-252.

Berman, E. S. F., M. Gupta, C. Gabrielli, T. Garland, and J. J. McDonnell (2009), High-frequency field-deployable isotope analyzer for hydrological applications, Water Resour Res, 45.

Beven, K., and J. Freer (2001), A dynamic TOPMODEL, Hydrol Process, 15(10), 1993-2011.

Beven, K. (2009), Environmental modelling: an uncertain future? : an introduction to techniques for uncertainty estimation in environmental prediction, Routledge/Taylor & Francis, London [etc.].

Beven, K. J. (2012), Rainfall-runoff modelling: the primer, 2nd ed., xxix, 457 p. pp., Wiley-Blackwell, Chichester, West Sussex ; Hoboken, NJ.

Beven, K., and P. Germann (2013), Macropores and water flow in soils revisited, Water Resour Res, 49(6), 3071-3092.

Birkel, C., S. M. Dunn, D. Tetzlaff, and C. Soulsby (2010), Assessing the value of high-resolution isotope tracer data in the stepwise development of a lumped conceptual rainfall-runoff model, Hydrol Process, 24(16), 2335-2348.

Birkel, C., C. Soulsby, and D. Tetzlaff (2011a), Modelling catchment-scale water storage dynamics: reconciling dynamic storage with tracer-inferred passive storage, Hydrol Process, 25(25), 3924-3936.

Birkel, C., D. Tetzlaff, S. M. Dunn, and C. Soulsby (2011b), Using lumped conceptual rainfall-runoff models to simulate daily isotope variability with fractionation in a nested mesoscale catchment, Adv Water Resour, 34(3), 383-394.

Birkel, C., C. Soulsby, D. Tetzlaff, S. Dunn, and L. Spezia (2012), High-frequency storm event isotope sampling reveals time-variant transit time distributions and influence of diurnal cycles, Hydrol Process, 26(2), 308-316.

Bishop, K., J. Seibert, S. Koher, and H. Laudon (2004), Resolving the Double Paradox of rapidly mobilized old water with highly variable responses in runoff chemistry, Hydrol Process, 18(1), 185-189.

Bogena, H. R., M. Herbst, J. A. Huisman, U. Rosenbaum, A. Weuthen, and H. Vereecken (2010), Potential of Wireless Sensor Networks for Measuring Soil Water Content Variability, Vadose Zone J, 9(4), 1002-1013.

Bogena, H. R., J. A. Huisman, R. Baatz, H.-J. Hendriks-Franssen, and H. Vereecken (2013), Accuracy of the cosmic-ray soil water content probe in humid forest ecosystems: The worst case scenario, Water Resour Res.

Bogena, H.R., R. Bol, N. Borchard, N. Brüggemann, B. Diekkrüger, C. Drüe, J. Groh, N. Gottselig, S.J. Huisman, A. Lücke, A. Missong, B. Neuwirth, T. Pütz, M. Schmidt, M. Stockinger, W. Tappe, L. Weihermüller, I. Wiekenkamp, and H. Vereecken (2015), A terrestrial observatory approach for the integrated investigation of the effects of deforestation on water, energy, and matter fluxes. Science China: Earth Sciences 58(1): 61-75, doi: 10.1007/s11430-014-4911-7.

Borchardt, H. (2012), Einfluss periglazialer Deckschichten auf Abflusssteuerung am Beispiel des anthropogen überprägten Wüstebaches (Nationalpark Eifel), Dissertation (PhD), Lehrstuhl für Physische Geographie und Geoökologie, Fakultät für Georessourcen und Materialtechnik, Rheinisch-Westfälische Technische Hochschule Aachen, Aaachen, Germany.

Botter, G., E. Bertuzzo, and A. Rinaldo (2011), Catchment residence and travel time distributions: The master equation, Geophys Res Lett, 38.

Brodersen, C., S. Pohl, M. Lindenlaub, C. Leibundgut, and K. von Wilpert (2000), Influence of vegetation structure on isotope content of throughfall and soil water, Hydrol Process, 14(8), 1439-1448.

Brooks, J. R., H. R. Barnard, R. Coulombe, and J. J. McDonnell (2010), Ecohydrologic separation of water between trees and streams in a Mediterranean climate, Nat Geosci, 3(2), 100-104.

Calderon, H., and S. Uhlenbrook (2014), Characterising the climatic water balance dynamics and different runoff components in a poorly gauged tropical forested catchment, Nicaragua, Hydrological Sciences Journal, doi: 10.1080/02626667.2014.964244.

Cappa, C. D., M. B. Hendricks, D. J. DePaolo, and R. C. Cohen (2003), Isotopic fractionation of water during evaporation, J Geophys Res-Atmos, 108(D16).

Celle-Jeanton, H., R. Gonfiantini, Y. Travi, and B. Sol (2004), Oxygen-18 variations of rainwater during precipitation: application of the Rayleigh model to selected rainfalls in Southern France, J Hydrol, 289(1-4), 165-177.

Coenders-Gerrits, A. M. J., R. J. van der Ent, T. A. Bogaard, L. Wang-Erlandsson, M. Hrachowitz, and H. H. G. Savenije (2014), Uncertainties in transpiration estimates, Nature, 506(7487), E1-E2.

Cornelissen, T., B. Diekkrüger, B. and H.R. Bogena (2014), Significance of scale and lower boundary condition in the 3D simulation of hydrological processes and soil moisture variability in a forested headwater catchment, J Hydrol, doi: dx.doi.org/10.1016/j.jhydrol.2014.01.060.

Craig, H. (1961), Isotopic Variations in Meteoric Waters, Science, 133(346), 1702-1703.

Criss, R. E., and W. E. Winston (2008), Do Nash values have value? Discussion and alternate proposals, Hydrol Process, 22(14), 2723-2725.

Crutzen, P. J., and E. F. Stoermer (2000). "The 'Anthropocene'". Global Change Newsletter 41: 17–18.

Dai, A. G. (2011), Drought under global warming: a review, Wires Clim Change, 2(1), 45-65.

Detty, J. M., and K. J. McGuire (2010), Topographic controls on shallow groundwater dynamics: implications of hydrologic connectivity between hillslopes and riparian zones in a till mantled catchment, Hydrol Process, 24(16), 2222-2236.

Dewalle, D. R., and B. R. Swistock (1994), Differences in O-18 Content of Throughfall and Rainfall in Hardwood and Coniferous Forests, Hydrol Process, 8(1), 75-82.

Duffy, C. J. (2010), Dynamical modelling of concentration-age-discharge in watersheds, Hydrol Process, 24(12), 1711-1718.

Dunn, S. M., C. Birkel, D. Tetzlaff, and C. Soulsby (2010), Transit time distributions of a conceptual model: their characteristics and sensitivities, Hydrol Process, 24(12), 1719-1729.

Dunne, T., and R. D. Black (1970), Partial Area Contributions to Storm Runoff in a Small New-England Watershed, Water Resour Res, 6(5), 1296-&.

Emanuel, K., R. Sundararajan, and J. Williams (2008), Hurricanes and global warming - Results from downscaling IPCC AR4 simulations, B Am Meteorol Soc, 89(3), 347-+.

Etmann, M. (2009), Dendrologische Aufnahmen im Wassereinzugsgebiet Oberer Wüstebach anhand verschiedener Mess- und Schätzverfahren, M.S. thesis, Institut für Landschaftsökologie, University of Münster, Münster, Germany.

Evaristo, J., S. Jasechko, and J. J. McDonnell (2015), Global separation of plant transpiration from groundwater and streamflow, Nature, 525(7567), 91-94.

Fraley, C., and A. E. Raftery (2002), Model-based clustering, discriminant analysis, and density estimation, J Am Stat Assoc, 97(458), 611-631.

Garmendia, E., P. Mariel, I. Tamayo, I. Aizpuru, and A. Zabaleta (2012), Assessing the effect of alternative land uses in the provision of water resources: Evidence and policy implications from southern Europe, Land Use Policy, 29(4), 761-770.

Gat, J. (2010), Isotope hydrology : a study of the water cycle, vii, 189 p. pp., : Imperial College Press, London.

Gerrits, A. M. J., and H. H. G. Savenije (2011), 2.04 - Interception, in Treatise on Water Science, edited by P. Wilderer, pp. 89-101, Elsevier, Oxford.

Goderniaux, P., P. Davy, E. Bresciani, J. R. de Dreuzy, and T. Le Borgne (2013), Partitioning a regional groundwater flow system into shallow local and deep regional flow compartments, Water Resour Res, 49(4), 2274-2286.

Gonfiantini, R. (1978), Standards for Stable Isotope Measurements in Natural Compounds, Nature, 271(5645), 534-536.

Gottselig N., Bol R., Nischwitz V., Vereecken H., Amelung W., and Klumpp E.. 2014. Distribution of phosphorus-containing fine colloids and nanoparticles in stream water of a forest catchment. Vadose Zone J. 13. doi:10.2136/vzj2014.01.0005.

Grabs, T., J. Seibert, K. Bishop, and H. Laudon (2009), Modeling spatial patterns of saturated areas: A comparison of the topographic wetness index and a dynamic distributed model, J Hydrol, 373(1-2), 15-23.

Graf, A., H. R. Bogena, C. Drüe, H. Hardelauf, T. Pütz, G. Heinemann, and H. Vereecken (2014), Spatiotemporal relations between water budget components and soil water content in

a forested tributary catchment, Water Resour. Res., 50, 4837–4857, doi:10.1002/2013WR014516.

Grayson, R. B., A. W. Western, F. H. S. Chiew, and G. Bloschl (1997), Preferred states in spatial soil moisture patterns: Local and nonlocal controls, Water Resour Res, 33(12), 2897-2908.

Gupta, M. and E. S. F. Berman (2013), Applications of cavity-enhanced absorption spectrometry for water isotope monitoring in hydrology, medical diagnostics, and wine authentication, Gases & Instrumentation International, Vol. 7, Issue 2, pp. 12-16.

Harman, C. J. (2015), Time-variable transit time distributions and transport: Theory and application to storage-dependent transport of chloride in a watershed, Water Resour Res, 51(1), 1-30.

Heidbüchel, I., P. A. Troch, S. W. Lyon, and M. Weiler (2012), The master transit time distribution of variable flow systems, Water Resour Res, 48.

Herrmann, A., S. Bahls, W. Stichler, F. Gallart, and J. Latron (1999), Isotope hydrological study of mean transit times and related hydrogeological conditions in Pyrenean experimental basins (Vallcebre, Catalonia), Integrated Methods in Catchment Hydrology: Tracer, Remote Sensing and New Hydrometric Techniques(258), 101-109.

Horton, R. E. (1933), The role of infiltration in the hydrologic cycle, Eos T Am Geophys Un, 14, 446-460.

Hrachowitz, M., C. Soulsby, D. Tetzlaff, J. J. C. Dawson, and I. A. Malcolm (2009a), Regionalization of transit time estimates in montane catchments by integrating landscape controls, Water Resour Res, 45.

Hrachowitz, M., C. Soulsby, D. Tetzlaff, J. J. C. Dawson, S. M. Dunn, and I. A. Malcolm (2009b), Using long-term data sets to understand transit times in contrasting headwater catchments, J Hydrol, 367(3-4), 237-248.

Hrachowitz, M., Soulsby, C., Tetzlaff, D. and Malcolm, I. A. (2011), Sensitivity of mean transit time estimates to model conditioning and data availability. Hydrol. Process., 25: 980–990. doi: 10.1002/hyp.7922

Hrachowitz, M., H. Savenije, T. A. Bogaard, D. Tetzlaff, and C. Soulsby (2013a), What can flux tracking teach us about water age distribution patterns and their temporal dynamics?, Hydrol Earth Syst Sc, 17(2), 533-564.

Hrachowitz, M., H. H. G. Savenije, G. Blöschl, J. J. McDonnell, M. Sivapalan, J. W. Pomeroy, B. Arheimer, T. Blume, M. P. Clark, U. Ehret, F. Fenicia, J. E. Freer, A. Gelfan, H. V. Gupta, D. A. Hughes, R. W. Hut, A. Montanari, S. Pande, D. Tetzlaff, P. A. Troch, S. Uhlenbrook, T. Wagener, H. C. Winsemius, R. A. Woods, E. Zehe, and C Cudennec, (2013b), A decade of Predictions in Ungauged Basins (PUB)a review, Hydrolog Sci J, 58(6), 1198-1255.

Inamdar, S. P., and M. J. Mitchell (2007), Contributions of riparian and hillslope waters to storm runoff across multiple catchments and storm events in a glaciated forested watershed, J Hydrol, 341(1-2), 116-130.

Jakeman, A. J., and G. M. Hornberger (1993), How Much Complexity Is Warranted in a Rainfall-Runoff Model, Water Resour Res, 29(8), 2637-2649.

Jasechko, S., Z. D. Sharp, J. J. Gibson, S. J. Birks, Y. Yi, and P. J. Fawcett (2013), Terrestrial water fluxes dominated by transpiration, Nature, 496(7445), 347-+.

Jasechko, S., Z. D. Sharp, J. J. Gibson, S. JeanBirks, Y. Yi, and P. J. Fawcett (2014), Uncertainties in transpiration estimates Reply, Nature, 506(7487), E2-E3.

Jencso, K. G., B. L. McGlynn, M. N. Gooseff, S. M. Wondzell, K. E. Bencala, and L. A. Marshall (2009), Hydrologic connectivity between landscapes and streams: Transferring reach-and plot-scale understanding to the catchment scale, Water Resour Res, 45.

Jencso, K. G., B. L. McGlynn, M. N. Gooseff, K. E. Bencala, and S. M. Wondzell (2010), Hillslope hydrologic connectivity controls riparian groundwater turnover: Implications of catchment structure for riparian buffering and stream water sources, Water Resour Res, 46.

Jenson, S. K., and J. O. Domingue (1988), Extracting Topographic Structure from Digital Elevation Data for Geographic Information-System Analysis, Photogramm Eng Rem S, 54(11), 1593-1600.

Jost, G., H. Schume, and H. Hager (2004), Factors controlling soil water-recharge in a mixed European beech (Fagus sylvatica L.)-Norway spruce [Picea abies (L.) Karst.] stand, Eur J for Res, 123(2), 93-104.

Kato, H., Y. Onda, K. Nanko, T. Gomi, T. Yamanaka, and S. Kawaguchi (2013), Effect of canopy interception on spatial variability and isotopic composition of throughfall in Japanese cypress plantations, J Hydrol, 504, 1-11.

Kendall, C., and J. J. McDonnell (1998), Isotope tracers in catchment hydrology, xxix, 839 p. pp., Elsevier, Amsterdam ; New York.

Khasnis, A. A., and M. D. Nettleman (2005), Global warming and infectious disease, Arch Med Res, 36(6), 689-696.

Kienzler, P. M., and F. Naef (2008), Subsurface storm flow formation at different hillslopes and implications for the 'old water paradox', Hydrol Process, 22(1), 104-116.

Kirchner, J. W., X. H. Feng, and C. Neal (2000), Fractal stream chemistry and its implications for contaminant transport in catchments, Nature, 403(6769), 524-527.

Kirchner, J. W. (2003), A double paradox in catchment hydrology and geochemistry, Hydrol Process, 17(4), 871-874.

Klaus, J., K. P. Chun, K. J. McGuire, and J. J. McDonnell (2015), Temporal dynamics of catchment transit times from stable isotope data, Water Resour Res, 51(6), 4208-4223.

Kubota, T., Tsuboyama, Y., 2003. Intra- and inter-storm oxygen-18 and deuterium variations of rain, throughfall, and stemflow, and two-component hydrograph separation in a small forested catchment in Japan. J. Forest Res. 8 (3), 179–190.

Leibundgut C, J. J. McDonnell, G. Schultz (1999), Integrated Methods in Catchment Hydrology — Tracer, Remote Sensing, and New Hydrometric Techniques, IAHS Publication No. 258, p. 284.

Liu, H., and H. Lin (2015), Frequency and Control of Subsurface Preferential Flow: From Pedon to Catchment Scales, Soil Sci Soc Am J, 79(2), 362-377.

Lyon, S. W., S. L. E. Desilets, and P. A. Troch (2009), A tale of two isotopes: differences in hydrograph separation for a runoff event when using delta D versus delta O-18, Hydrol Process, 23(14), 2095-2101.

Lyon, S. W., H. Laudon, J. Seibert, M. Morth, D. Tetzlaff, and K. H. Bishop (2010), Controls on snowmelt water mean transit times in northern boreal catchments, Hydrol Process, 24(12), 1672-1684.

Maloszewski, P., W. Rauert, P. Trimborn, A. Herrmann, and R. Rau (1992), Isotope Hydrological Study of Mean Transit Times in an Alpine Basin (Wimbachtal, Germany), J Hydrol, 140(1-4), 343-360.

McDonnell, J. J., McGuire, K., Aggarwal, P., Beven, K. J., Biondi, D., Destouni, G., Dunn, S., James, A., Kirchner, J., Kraft, P., Lyon, S., Maloszewski, P., Newman, B., Pfister, L., Rinaldo, A., Rodhe, A., Sayama, T., Seibert, J., Solomon, K., Soulsby, C., Stewart, M., Tetzlaff, D., Tobin, C., Troch, P., Weiler, M., Western, A., Wörman, A. and Wrede, S. (2010), How old is streamwater? Open questions in catchment transit time conceptualization, modelling and analysis. Hydrol. Process., 24: 1745–1754. doi: 10.1002/hyp.7796.

McDonnell, J. J., and K. Beven (2014), Debates-The future of hydrological sciences: A (common) path forward? A call to action aimed at understanding velocities, celerities and residence time distributions of the headwater hydrograph, Water Resour Res, 50(6), 5342-5350.

McGlynn, B. L., and J. Seibert (2003), Distributed assessment of contributing area and riparian buffering along stream networks, Water Resour Res, 39(4).

McGuire, K. J., J. J. McDonnell, M. Weiler, C. Kendall, B. L. McGlynn, J. M. Welker, and J. Seibert (2005), The role of topography on catchment-scale water residence time, Water Resour Res, 41(5).

McGuire, K. J., and J. J. McDonnell (2006), A review and evaluation of catchment transit time modeling, J Hydrol, 330(3-4), 543-563.

McMillan, H., B. Jackson, M. Clark, D. Kavetski, and R. Woods (2011), Rainfall uncertainty in hydrological modelling: An evaluation of multiplicative error models, J Hydrol, 400(1-2), 83-94.

Micklin, P. (2007), The Aral Sea disaster, Annu Rev Earth Pl Sc, 35, 47-72.

Miyata, S., K. Kosugi, T. Gomi, and T. Mizuyama (2009), Effects of forest floor coverage on overland flow and soil erosion on hillslopes in Japanese cypress plantation forests, Water Resour Res, 45.

Nash, J. E., and J. V. Sutcliffe (1970), River flow forecasting through conceptual models: Part I - A discussion of principles, J Hydrol, 10(3), 282 - 290.

Navar, J., D. J. Turton, and E. L. Miller (1995), Estimating Macropore and Matrix Flow Using the Hydrograph Separation Procedure in an Experimental Forest Plot, Hydrol Process, 9(7), 743-753.

Niemi, A. J. (1977), Residence Time Distributions of Variable Flow Processes, Int J Appl Radiat Is, 28(10-1), 855-860.

Oki, T., and S. Kanae (2006), Global hydrological cycles and world water resources, Science, 313(5790), 1068-1072.

Pearce, A. J., M. K. Stewart, and M. G. Sklash (1986), Storm Runoff Generation in Humid Headwater Catchments .1. Where Does the Water Come From, Water Resour Res, 22(8), 1263-1272.

Peng, H. H., C. Y. Zhao, Z. D. Feng, Z. L. Xu, C. Wang, and Y. Zhao (2014), Canopy interception by a spruce forest in the upper reach of Heihe River basin, Northwestern China, Hydrol Process, 28(4), 1734-1741.

Pounds, J. A., M. R. Bustamante, L. A. Coloma, J. A. Consuegra, M. P. L. Fogden, P. N. Foster, E. La Marca, K. L. Masters, A. Merino-Viteri, R. Puschendorf, S. R. Ron, G. A.

Sánchez-Azofeifa, C. J. Still, and B. E. Young, (2006), Widespread amphibian extinctions from epidemic disease driven by global warming, Nature, 439(7073), 161-167.

Ranalli, A. J., and D. L. Macalady (2010), The importance of the riparian zone and in-stream processes in nitrate attenuation in undisturbed and agricultural watersheds - A review of the scientific literature, J Hydrol, 389(3-4), 406-415.

Rank, D., W. Papesch, and R. Tesch (2005), Runoff characteristics of the upper Danube basin: conclusions from long-term environmental isotope records, Geophysical Research Abstracts, 7.

Richter, D. (1995), Ergebnisse methodischer Untersuchungen zur Korrektur des systematischen Meßfehlers des Hellmann-Niederschlagsmessers, 93 S. pp., Selbstverl. des Dt. Wetterdienstes, Offenbach am Main.

Richter, F. (2008), Bodenkarte zur Standorterkundung. Verfahren Quellgebiet Wüstebachtal (Forst), Geologischer Dienst Nordrhein-Westfalen, Krefeld, Germany.

Rinaldo, A., K. J. Beven, E. Bertuzzo, L. Nicotina, J. Davies, A. Fiori, D. Russo, and G. Botter (2011), Catchment travel time distributions and water flow in soils, Water Resour Res, 47.

Roa-Garcia, M. C., and M. Weiler (2010), Integrated response and transit time distributions of watersheds by combining hydrograph separation and long-term transit time modeling, Hydrol Earth Syst Sc, 14(8), 1537-1549.

Rodgers, P., C. Soulsby, S. Waldron, and D. Tetzlaff (2005), Using stable isotope tracers to assess hydrological flow paths, residence times and landscape influences in a nested mesoscale catchment, Hydrol Earth Syst Sc, 9(3), 139-155.

Root, T. L., J. T. Price, K. R. Hall, S. H. Schneider, C. Rosenzweig, and J. A. Pounds (2003), Fingerprints of global warming on wild animals and plants, Nature, 421(6918), 57-60.

Rosenbaum, U., H. R. Bogena, M. Herbst, J. A. Huisman, T. J. Peterson, A. Weuthen, A. W. Western, and H. Vereecken (2012), Seasonal and event dynamics of spatial soil moisture patterns at the small catchment scale, Water Resour Res, 48.

Savenije, H. H. G. (2004), The importance of interception and why we should delete the term evapotranspiration from our vocabulary, Hydrol Process, 18(8), 1507-1511.

Saxena, R. K. (1986), Estimation of Canopy Reservoir Capacity and O-18 Fractionation in Throughfall in a Pine Forest, Nord Hydrol, 17(4-5), 251-260.

Shaman, J., M. Stieglitz, and D. Burns (2004), Are big basins just the sum of small catchments?, Hydrol Process, 18(16), 3195-3206.

Simunek, J., M. T. van Genuchten, and M. Sejna (2008), Development and applications of the HYDRUS and STANMOD software packages and related codes, Vadose Zone J., 7(2), 587–600, doi:10.2136/Vzj2007.0077.

Sivapalan, M., et al. (2003), IAHS decade on Predictions in Ungauged Basins (PUB), 2003-2012: Shaping an exciting future for the hydrological sciences, Hydrolog Sci J, 48(6), 857-880.

Smith, A. H., E. O. Lingas, and M. Rahman (2000), Contamination of drinking-water by arsenic in Bangladesh: a public health emergency, B World Health Organ, 78(9), 1093-1103.

Soulsby, C., D. Tetzlaff, and M. Hrachowitz (2009), Tracers and transit times: windows for viewing catchment scale storage?, Hydrol Process, 23(24), 3503-3507.

Srinivasan, V., E. F. Lambin, S. M. Gorelick, B. H. Thompson, and S. Rozelle (2012), The nature and causes of the global water crisis: Syndromes from a meta-analysis of coupled human-water studies, Water Resour Res, 48.

Stewart, M. K., and B. D. Fahey (2010), Runoff generating processes in adjacent tussock grassland and pine plantation catchments as indicated by mean transit time estimation using tritium, Hydrol Earth Syst Sc, 14(6), 1021-1032.

Stewart, M. K., Morgenstern, U. and McDonnell, J. J. (2010), Truncation of stream residence time: how the use of stable isotopes has skewed our concept of streamwater age and origin. Hydrol. Process., 24: 1646–1659. doi: 10.1002/hyp.7576

Stockinger, M. P., H. R. Bogena, A. Lücke, B. Diekkrüger, M. Weiler, and H. Vereecken (2014), Seasonal soil moisture patterns: Controlling transit time distributions in a forested headwater catchment, Water Resour. Res., 50, 5270–5289, doi:10.1002/2013WR014815.

Stockinger, M. P., A. Lücke, J. J. McDonnell, B. Diekkrüger, H. Vereecken, and H. R. Bogena (2015), Interception effects on stable isotope driven streamwater transit time estimates, Geophys Res Lett, 42(13), 5299-5308.

Stoltidis, I., Krapp, L., 1980. Hydrological map NRW. 1:25.000, sheet 5404. State Agency for Water and Waste of North Rhine-Westfalia, Düsseldorf.

Tetzlaff, D., I. A. Malcolm, and C. Soulsby (2007), Influence of forestry, environmental change and climatic variability on the hydrology, hydrochemistry and residence times of upland catchments, J Hydrol, 346(3-4), 93-111.

Tetzlaff, D., J. J. McDonnell, S. Uhlenbrook, K. J. McGuire, P. W. Bogaart, F. Naef, A. J. Baird, S. M. Dunn, and C. Soulsby (2008), Conceptualizing catchment processes: simply too complex?, Hydrol Process, 22(11), 1727-1730.

Tetzlaff, D., J. Seibert, and C. Soulsby (2009a), Inter-catchment comparison to assess the influence of topography and soils on catchment transit times in a geomorphic province; the Cairngorm mountains, Scotland, Hydrol Process, 23(13), 1874-1886.

Tetzlaff, D., J. Seibert, K. J. McGuire, H. Laudon, D. A. Burn, S. M. Dunn, and C. Soulsby (2009b), How does landscape structure influence catchment transit time across different geomorphic provinces?, Hydrol Process, 23(6), 945-953.

Tietenberg, T. H. (1997), The economics of global warming, xxii, 624 p. pp., E. Elgar Pub., Cheltenham, UK ; Brookfield, Vt., US.

Timbe, E., D. Windhorst, P. Crespo, H. G. Frede, J. Feyen, and L. Breuer (2014), Understanding uncertainties when inferring mean transit times of water trough tracer-based lumped-parameter models in Andean tropical montane cloud forest catchments, Hydrol Earth Syst Sc, 18(4), 1503-1523.

Timbe, E., D. Windhorst, R. Celleri, L. Timbe, P. Crespo, H. G. Frede, J. Feyen, and L. Breuer (2015), Sampling frequency trade-offs in the assessment of mean transit times of tropical montane catchment waters under semi-steady-state conditions, Hydrol Earth Syst Sc, 19(3), 1153-1168.

van Schaik, L., J. Palm, J. Klaus, E. Zehe, and B. Schroder (2014), Linking spatial earthworm distribution to macropore numbers and hydrological effectiveness, Ecohydrology, 7(2), 401-408.

Vereecken, H., J. A. Huisman, H. Bogena, J. Vanderborght, J. A. Vrugt, and J. W. Hopmans (2008), On the value of soil moisture measurements in vadose zone hydrology: A review, Water Resour Res, 44.

Viville, D., B. Ladouche, and T. Bariac (2006), Isotope hydrological study of mean transit time in the granitic Strengbach catchment (Vosges massif, France): application of the FlowPC model with modified input function, Hydrol Process, 20(8), 1737-1751.

Vuurens, S., F. Stagnitti, G. de Rooij, J. Boll, L. Ling, M. LeBlanc, D. Ierodiaconou, V. Versace, and S. Salzman (2005), Quantifying effects of soil heterogeneity on groundwater pollution at four sites in USA, Sci China Ser C, 48, 118-127.

Weiler, M., B. L. McGlynn, K. J. McGuire, and J. J. McDonnell (2003), How does rainfall become runoff? A combined tracer and runoff transfer function approach, Water Resour Res, 39(11).

Williams, A. G., J. F. Dowd, and E. W. Meyles (2002), A new interpretation of kinematic stormflow generation, Hydrol Process, 16(14), 2791-2803.

Windhorst, D., P. Kraft, E. Timbe, H. G. Frede, and L. Breuer (2014), Stable water isotope tracing through hydrological models for disentangling runoff generation processes at the hillslope scale, Hydrol Earth Syst Sc, 18(10), 4113-4127.

World Meteorological Organization (2008), Guide to meteorological instruments and methods of observation. 7th ed. Geneva, Switzerland: World Meteorological Organization.

Yoo, C., J. Kim, and J. Yoon (2012), Uncertainty of areal average rainfall and its effect on runoff simulation: A case study for the Chungju Dam Basin, Korea, Ksce J Civ Eng, 16(6), 1085-1092.

Zacharias, S., H. R. Bogena, L. Samaniego, M. Mauder, R. Fuß, T. Pütz, M. Frenzel, M. Schwank, C. Baessler, K. Butterbach-Bahl, O. Bens, E. Borg, A. Brauer, P. Dietrich, I. Hajnsek, G. Helle, R. Kiese, H. Kunstmann, S. Klotz, J. C. Munch, H. Papen, E. Priesack, H.

P. Schmid, R. Steinbrecher, U. Rosenbaum, G. Teutsch and H. Vereecken (2011), A Network of Terrestrial Environmental Observatories in Germany, Vadose Zone J, 10(3), 955-973.

Zehe, E., H. Elsenbeer, F. Lindenmaier, K. Schulz, and G. Blöschl (2007), Patterns of predictability in hydrological threshold systems, Water Resour Res, 43(7).

Zimmermann, A., and B. Zimmermann (2014), Requirements for throughfall monitoring: The roles of temporal scale and canopy complexity, Agr Forest Meteorol, 189, 125-139.

VII. Appendix

VII.1 Field experiment to test evaporation losses of the sampling system

From 10th October to 7th November 2014 we conducted a field experiment to test for potential evaporative losses and changes in stable isotope composition induced by the design of the precipitation sampling system used in the Wüstebach catchment. For this experiment four samplers were placed outside the institute building in Jülich (Germany) under a plastic tarp. Thus, the samplers were open to ambient air but sheltered from precipitation. To create a worst case scenario, we excluded the table tennis balls in the funnels, meaning that one of our protective measures against evaporation and evaporative isotope enrichment was missing in this experiment. The samplers were filled with 250 ml of water of known isotopic value. Given the dimensions of the sampling bottle (maximum capacity of 6300 ml), this translates to an evaporative surface of 13.5 x 13.5 cm (0.0182 m²) with a water table depth of 2 cm and an air volume with height >20 cm directly above the water table inside the sampling bottle. The water of two samplers was sampled after 1, 2 and 3 weeks (reusing two samplers for the 3 weeks experiment) and isotopically analyzed.

Meteorological conditions (measured in a distance of 200 m to the experiment) are shown in Figure A3. Results of this experiment showed no change in water volume (within measurement accuracy) and only negligible changes in isotopic composition of the used standard waters that are within the uncertainty of the analytical system (0.1‰ for $\delta^{18}O$, Figure A4). This ensures that our measured input data are reliable, even though we are aware that there is room to improve the throughfall sampling strategy.

VII.2 Additional information on the hydrograph modeling

Hydrograph simulation results for the three modeling periods are shown in Figure III.2a of the main text. VE values for Winter 2012, Summer 2013 and Winter 2013 were 0.65, 0.66 and 0.80 respectively. Summer 2013 represented the dry state of the overall catchment wetness, with the hillslopes hydrologically disconnected and only surface-saturated areas generating runoff. In contrast to the reduced runoff-generating area of 5 ha found in *Stockinger et al*. [2014], in this study the precipitation-equivalent runoff volumes based on an area of 5 ha exceeded precipitation volumes. We found the reduced runoff-generating area to be 9.8 ha by closing the gap between precipitation and runoff volumes. This reflects an increase of surface-saturated areas and is best explained by the closure of the transport pipe of the groundwater reservoir. This closure happened after the modeling period considered in *Stockinger et al*. [2014] (5 ha) but prior to this study (9.8 ha). Prior to the closure, fetched groundwater was bypassing the soil matrix and directly routed to the river. We hypothesize that the closure led to backlogged water exfiltrating the pipe and entering the soil matrix. This wet up the soil and increased the surface-saturated areas of the Wüstebach. To test the consistency of the 9.8 ha approach, we additionally simulated runoff for Summer 2012 (dry state, not shown), as it was already influenced by the closure of the transport pipe. We found that best results (VE = 0.59) were also obtained when using a runoff-generating area of 9.8 ha. Nevertheless, further investigations are needed to clarify this hypothesis.

The cumulative RTD for the Winter 2012 period (Appendix Figure A7) showed faster and slower components of hydrologic response (99-quantile at 194 days). Faster components are indicative of water celerities (water pressure waves through the soil), while the slower components represent convective and diffusive water transport [*Rinaldo et al*., 2011]. The Summer 2013 period exhibited only faster components (99-quantile at 58 days). Winter 2013

(99-quantile at 50 days) was similar to Summer 2013 and thus to the catchment's reaction during dry states. The primarily fast reaction of Winter 2013 could be attributed to the partial deforestation in August of the same year, as an additional runoff simulation for Winter 2011 (prior to the study period) also found fast and slow components comparable to Winter 2012. Increased stream water turbidity and strongly reduced chemical loads in the river three months after deforestation point towards fast chemical leaching due to the exposed soil [*Gottselig et al*., 2014].

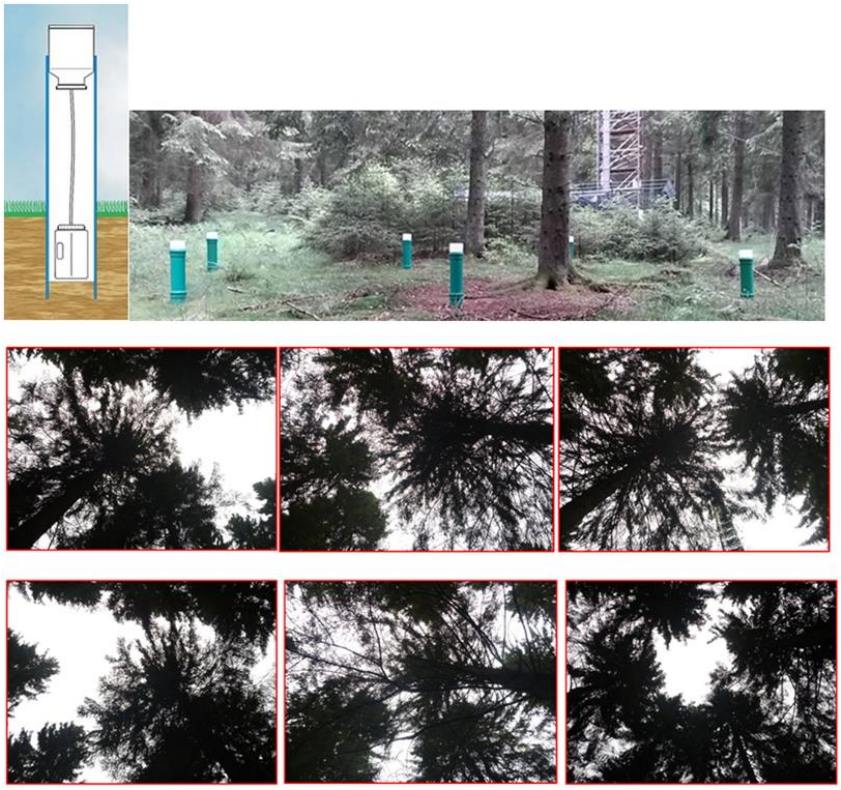

Figure A1. UMS deposition collector RS200 schematic (available at http://www.ums-muc.de) used as funnel TF samplers with upward view, indicating the covered heterogeneity of the canopy structure.

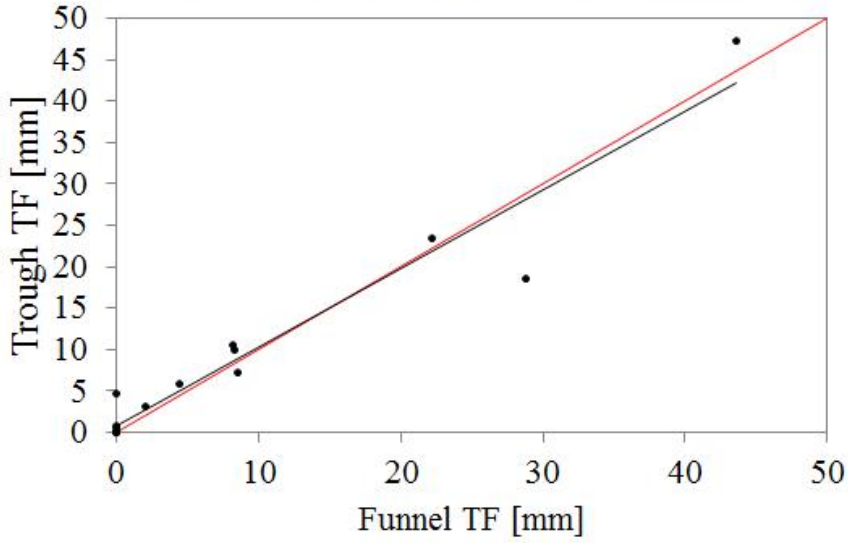

Figure A2. Top: Trough TF sampling system operated by the University of Trier (UoT); Bottom: Regression between collected TF volumes of UoT to volumes of this study. The 1:1 line (red) compared to the regression line (black) with Trough TF = 0.9463 * Funnel TF + 0.8629, an R^2 of 0.94 and 5%-significance $p = 4.2 * 10^{-9}$ shows good agreement.

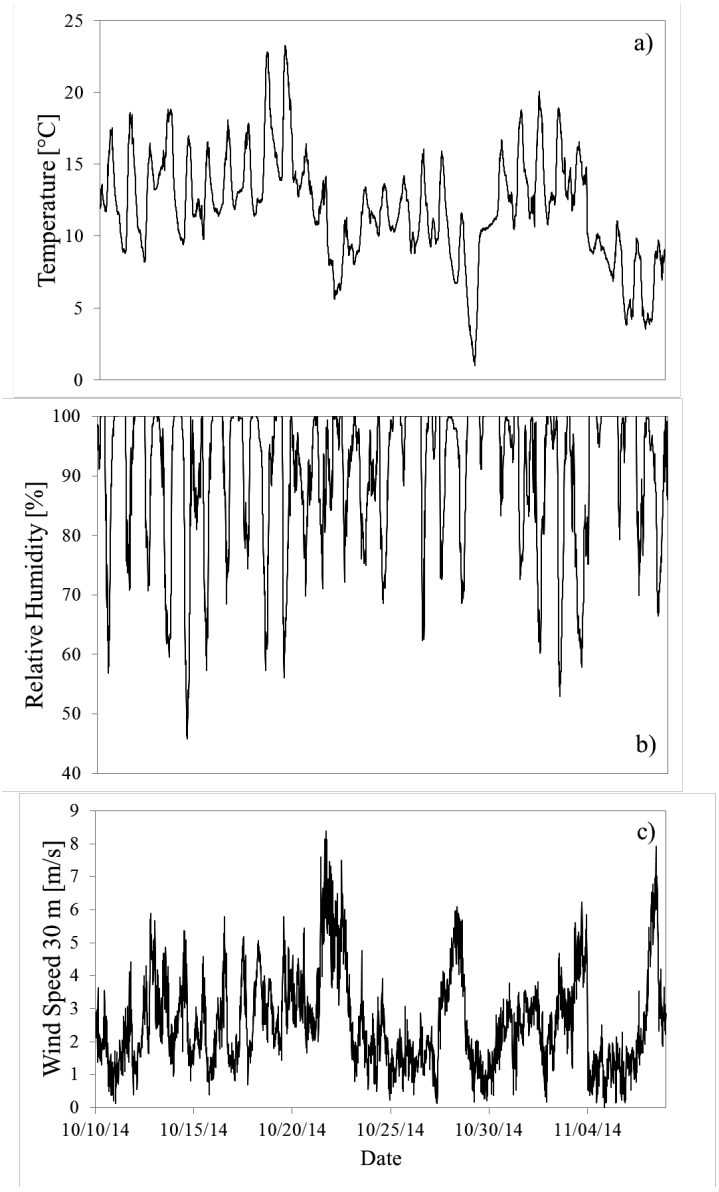

Figure A3. Meteorological conditions during the field experiment to test for evaporative losses of the precipitation sampling system. Time series of (a) temperature, (b) relative humidity and (c) wind speed measured at 30 m above ground (10 m above canopy).

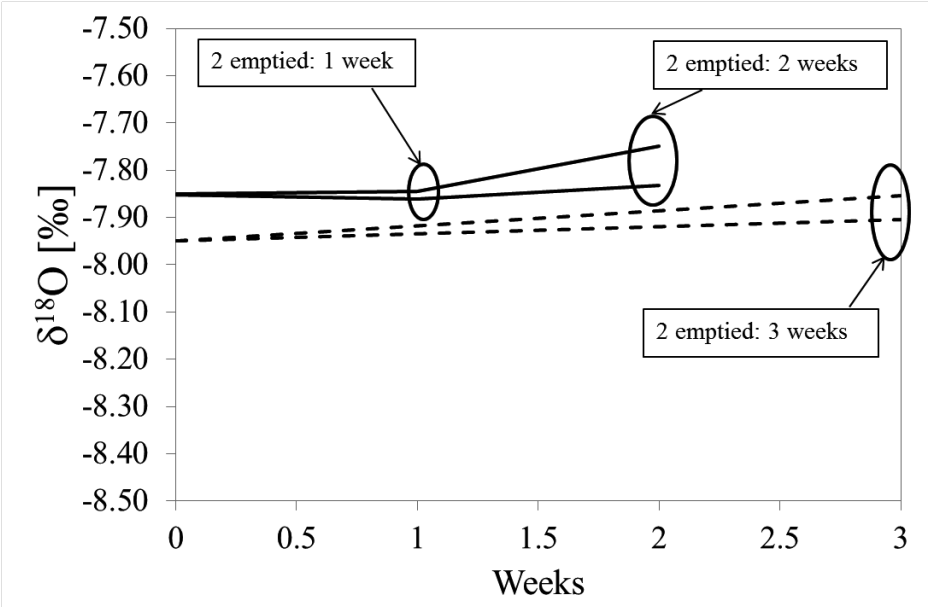

Figure A4. Results of the field experiment to test for evaporative losses of the precipitation sampling system. After 1, 2 and 3 weeks two samplers were emptied. Weeks 1 and 2 used the same reference water with $\delta^{18}O$ = -7.85 ‰, while the 3-week interval used different reference water with $\delta^{18}O$ = -7.95 ‰. The observed changes in isotope values are negligible with respect to the general conclusions we draw from our field data.

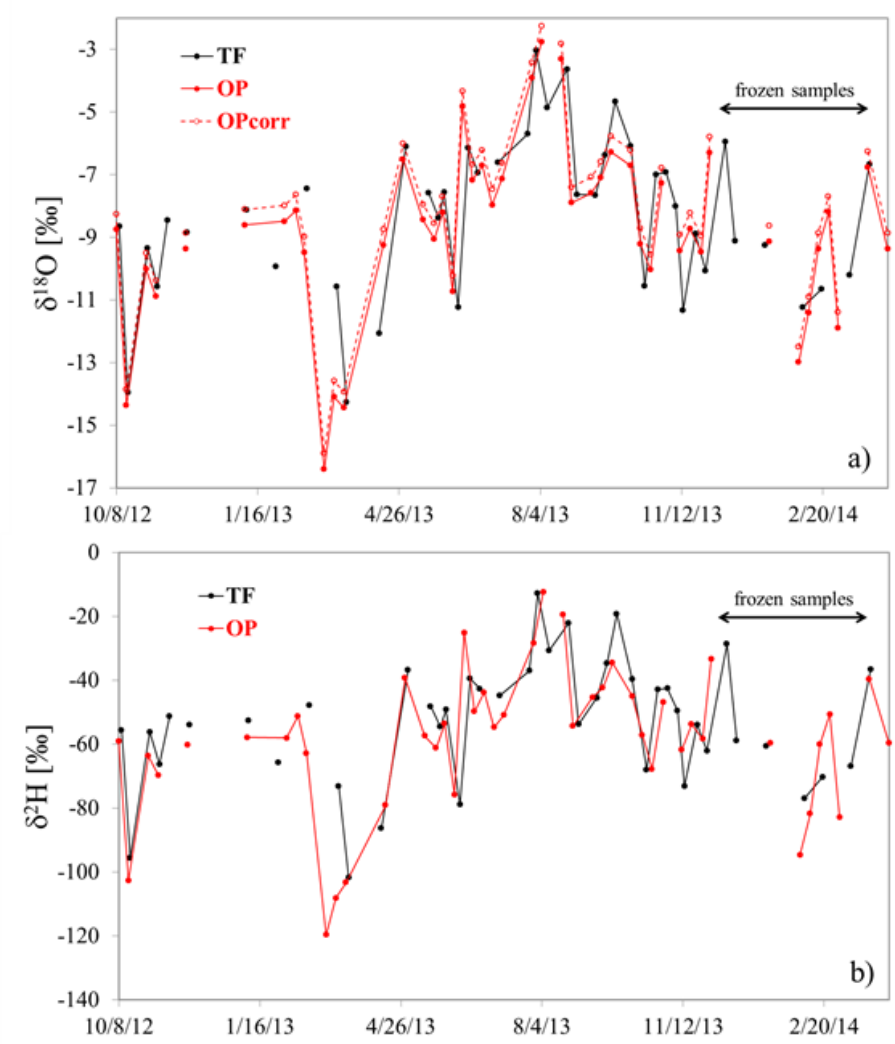

Figure A5. a) $\delta^{18}O$ time series of δTF, δOP and δOPcorr used as precipitation isotope input data for estimating TTDs. b) $\delta^{2}H$ time series of δTF and δOP used as precipitation isotope input data for estimating TTDs. Several times samples were frozen (frozen samples).

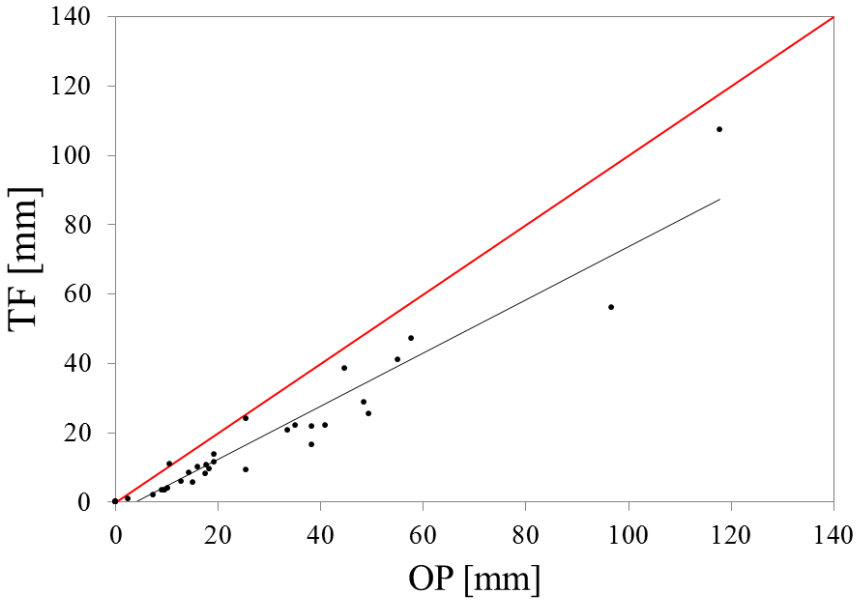

Figure A6. Linear regression line (black, n = 35) of OP and TF volumes with TF = 0.7667 * OP – 2.976, R^2 = 0.92 and p = 1.10 * 10^{-19}. The deviation from the 1:1 line (red) is caused by interception evaporation.

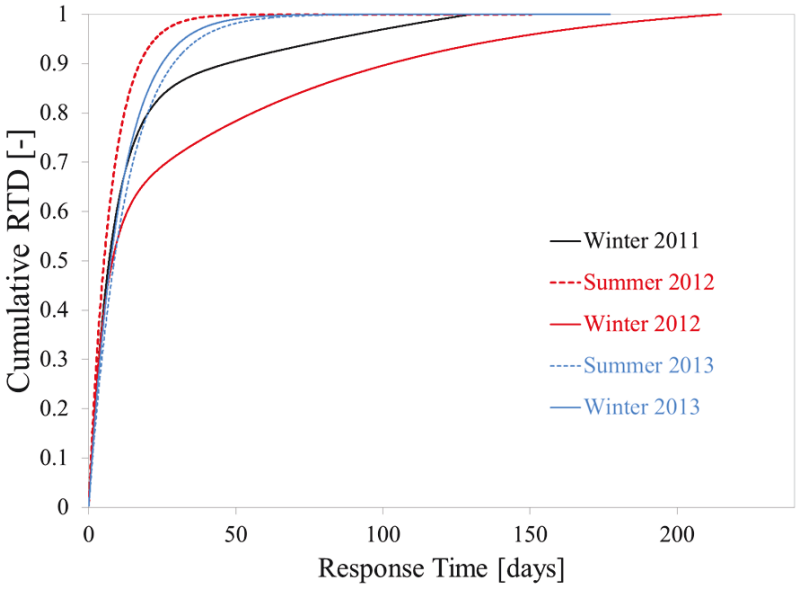

Figure A7. Response Time Distributions of the 3 modeling periods (Winter 2012, Summer 2013 and Winter 2013) and, for reasons of comparison, the year before the modeling period of this study (Winter 2011 and Summer 2012).

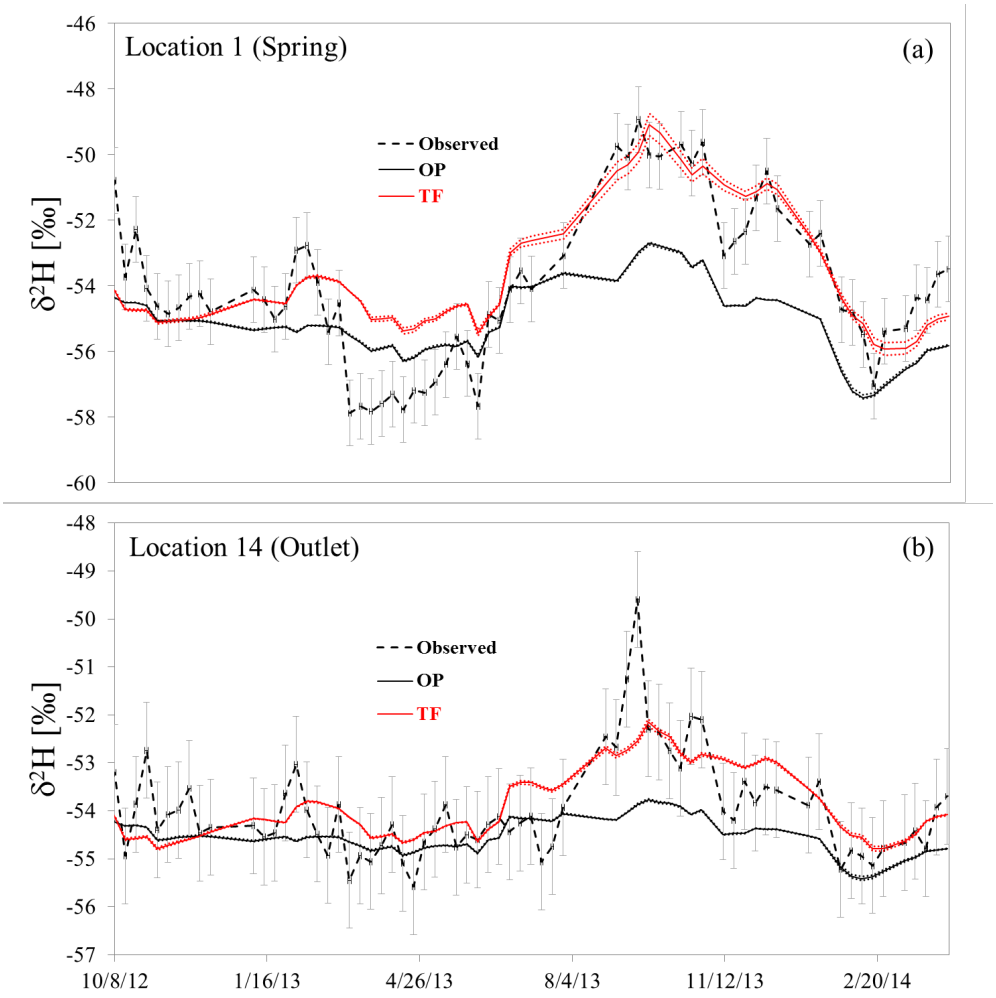

Figure A8. (a) and (b) stream isotope simulation results for location 1 (spring) and location 14 (outlet) based on δ^2H. Observed stream isotopes with grey errors bars compared to simulations using δOP and δTF. Uncertainty boundaries are shown as dashed lines.

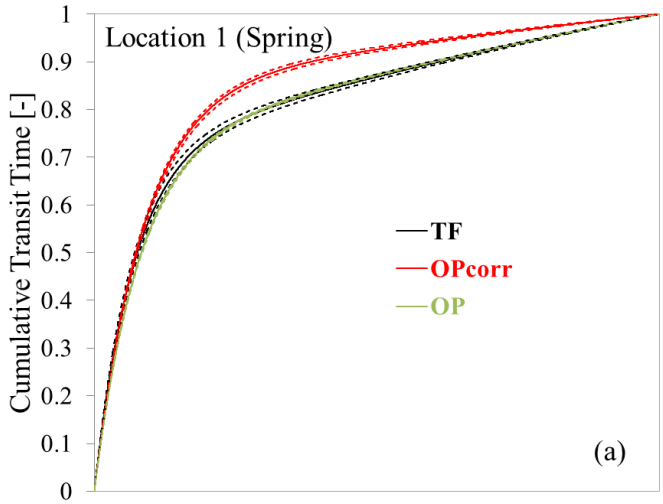
Location 1 (Spring)
Cumulative Transit Time [-]
TF
OPcorr
OP
(a)

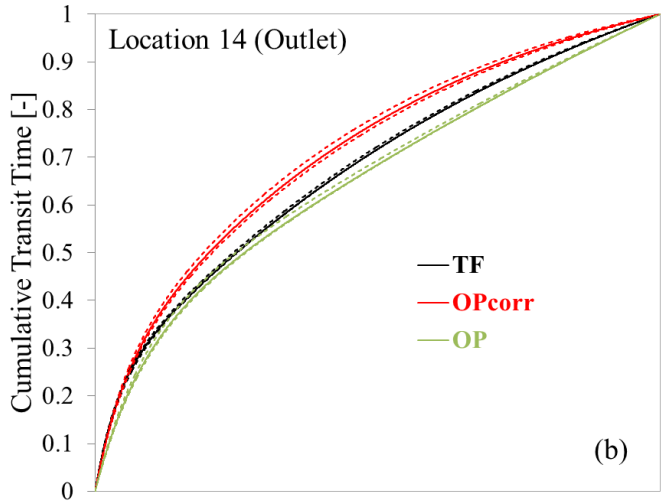
Location 14 (Outlet)
Cumulative Transit Time [-]
TF
OPcorr
OP
(b)

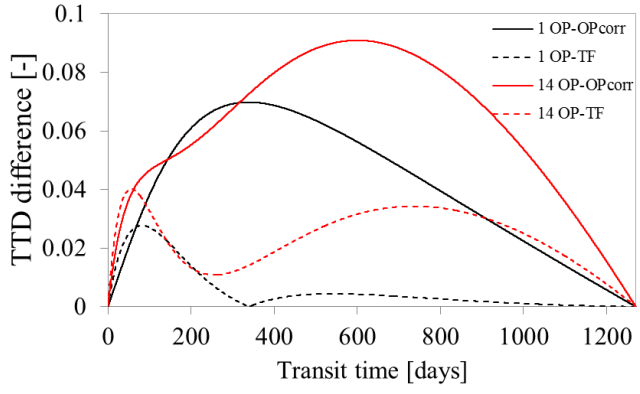
TTD difference [-]
1 OP-OPcorr
1 OP-TF
14 OP-OPcorr
14 OP-TF
Transit time [days]

Figure A9. TTDs derived by using δOP, δOP_{corr} and δTF isotope tracer data of $\delta^{18}O$ for (a) the spring (location 1) and (b) the outlet (location 14). Uncertainty boundaries are shown as dashed lines. Panel (c) shows absolute differences of cumulative TTDs as a function of transit time.

Danksagung

Prof. Dr. Harry Vereecken danke ich für die stetige Unterstützung und anregende Diskussionen in den halbjährlichen Gesprächen und dem PhD-Seminar. Bei Prof. Dr. Wulf Amelung bedanke ich mich für die Übernahme des Korreferats.

Ich möchte mich ganz herzlich bei meinen beiden Betreuern Dr. Andreas Lücke und Dr. Heye Bogena bedanken, die mir immer mit wissenschaftlichem Rat und Tat zur Seite standen und die durch Freude und Witz für die nötige Ausdauer bei Feldarbeiten sorgten; diese konnten nämlich manchmal nahe an den Rand der Verzweiflung bringen!

Außerdem danke ich Prof. Dr. Bernd Diekkrüger für seine Ratschläge bei hydrologischen Diskussionen und Thomas Cornelissen für unseren Gedankenaustausch über die Hydrologie der gemeinsam untersuchten Einzugsgebiete.

Für ihre nie enden wollende Arbeitskraft danke ich dem „Feld-Team“ des IBG-3, das sich immer um meine Messgeräte als auch um die Probenahmen gekümmert hat: Ferdinand Engels, Werner Küpper, Phillip Meulendick, Leander Fürst, Willi Benders und Rainer Harms. Für erheiternde Gespräche beim Probenumfüllen sei Sirgit Kummer herzlich gedankt!

Ein besonderer Dank geht an Holger Wissel, der stets den Überblick und die Kontrolle in den IBG-3 Laboren behält und mehrere tausend Wasserproben für meine Arbeit auf Isotopen analysiert hat.

A very special thanks goes out to Saskatoon, the Paris of the Prairies, and Prof. Jeffrey McDonnell for having me as a scientific guest at the Global Institute of Water Security for 3 months. He opened my eyes on how to aim for high impact journals and how to work most efficiently. The weekly group discussions, the paper club, and private invitations as well as seeing the band Queen live together, improved my scientific and social life in Canada. All my colleagues and friends there a big thank you for awesome social activities and scientific discussions: Willemijn Appels, Sun Chun, Scott Jasechko, Zhaiyk Yerikuly, Jaivime Evaristo, Anna Coles, Dawn Keim, Kim Janzen and Marijn Piet.

Danke für lustige, schräge, irrwitzige, anregende und kuriose Gespräche in der Mittagsrunde als auch im sozialen Leben: Sebastian Gebler (na na na Hammer to Fall), Kathrina Rötzer (Was soil denn das?), Maria Wolff (Kabelbruch ahoi!), Markus Duschl (scheinbar mit einer Lizenz für Stocki-Witze ☺), Wei Qu (you can drive a car now, cool!), Inge Wiekenkamp (Amazing harp player and very nice cat sitter!), Anne Klosterhalfen (cookie monster), Anne Röseler (super PhD representative!), Anja Klotzsche (Preisträgerin im Nerd-Test), Jing Wei (I hope that all your dreams come true), Shurong Liu (Deutschmeisterin), Jannis Heil (Meister-DJ), Maria Quade (15 Uhr Gymnastik ist genial!), Roland Baatz (das gemeinsame Zocken war toll!), Dorina Walther (mit einem genialen Gedächtnis!), Gaochao Cai (awesome acoustic guitar show at Christmas!), Nina Siebers (was wäre die Rurtalbahn nur ohne dich?), Katrin Huber (vui zvui gfui), Laura Gangi (Tatort-Abende…so genial!), Magdalena Landl (Passt!), Asta Kunkl (immer so happy! Weiter so!), Jannis Groh (danke auch für Katzen sitten ;)) und Youri Rothfuss (danke für den Tipp mit ArtistWorks!).

Außerdem ein herzlicher Dank an The Slaves, die IBG-3 Band, bei der ich zuerst als Bassist und dann als Gitarrist Musik machen durfte und weiterhin werde.

Band / Volume 300
Strom- und Gasmarktdesign zur Versorgung des deutschen Straßenverkehrs mit Wasserstoff
M. Robinius (2015), VI, 255 pp
ISBN: 978-3-95806-110-1

Band / Volume 301
Alterung von Vakuum-plasmagespritzten MCrAlY-Schutzschichten und ihre Wechselwirkung mit Nickel- und Cobalt-basierten γ/γ'-Superlegierungen
P. J. Terberger (2015), IX, 149 pp
ISBN: 978-3-95806-113-2

Band / Volume 302
Verbundvorhaben ELFA Effiziente Luftfahrzeuge
Brennstoffzellensysteme zur Energieerzeugung BREZEN – Teilprojekt: Kerosinaufbereitung
R. Peters, J. Meißner, J. Pasel, R. C. Samsun, D. Stolten
(2016), viii, 84 pp
ISBN: 978-3-95806-114-9

Band / Volume 303
Cavity-Ringdown-Spektroskopie zur Untersuchung der Rolle höherer Stickoxide für den nächtlichen Schadstoffabbau in der unteren Atmosphäre
S. Schrade (2016), II, 118 pp
ISBN: 978-3-95806-116-3

Band / Volume 304
Thermo-mechanical Properties of Mixed Ionic-Electronic Conducting Membranes for Gas Separation
V. K. Stournari (2016), 167 pp
ISBN: 978-3-95806-117-0

Band / Volume 305
Untersuchungen zu suspensionsplasmagespritzten Wärmedämmschichtsystemen
N. Schlegel (2016), X, 136 pp
ISBN: 978-3-95806-118-7

Band / Volume 306
Laser processing for the integrated series connection of thin-film silicon solar cells
B. Turan (2016), xii, 188 pp
ISBN: 978-3-95806-119-4

Band / Volume 307
Development and Application of a Multiscale Model for the magnetic Fusion Edge Plasma Region
F. Hasenbeck (2016), 190 pp
ISBN: 978-3-95806-120-0

Band / Volume 308
Emissions of Biogenic Volatile Organic Compounds and Ozone Balance under Future Climate Conditions
C. Wu (2016), VI, 105 pp
ISBN: 978-3-95806-121-7

Band / Volume 309
Computerunterstützte Auslegung eines Brennstoffzellen-Batterie-Hybridsystems für die Bordstromversorgung
C. Krupp (2016), iii, 207 pp
ISBN: 978-3-95806-124-8

Band / Volume 310
Influence of H_2O, HCl and H_2S on the Release and Condensation of Trace Metals in Gasification
M. Benito Abascal (2016), XIX, 172 pp
ISBN: 978-3-95806-125-5

Band / Volume 311
Mechanical and Thermochemical Properties of Nano-structured Membranes for Gas Separation in Fossil-fired Power Plants
J. Zhang (2016), II, 134 pp
ISBN: 978-3-95806-126-2

Band / Volume 312
Development of Embedded Thermocouple Sensors for Thermal Barrier Coatings (TBCs) by a Laser Cladding Process
Y. Zhang (2016), II, 108 pp
ISBN: 978-3-95806-129-3

Band / Volume 313
Streamwater transit time distributions at the catchment scale: constraining uncertainties through identification of spatio-temporal controls
M. Stockinger (2016), XIX, 161 pp
ISBN: 978-3-95806-131-6

Energie & Umwelt /
Energy & Environment
Band / Volume 313
ISBN 978-3-95806-131-6